Proteomics of Downstream Responses to Growth Signals in Proliferating Cells

by

John Patrick Murphy

Submitted in partial fulfilment of the requirements
for the degree of Doctor of Philosophy

at

Dalhousie University
Halifax, Nova Scotia
April 2011

DALHOUSIE UNIVERSITY

DEPARTMENT OF BIOLOGY

The undersigned hereby certify that they have read and recommend to the Faculty of Graduate Studies for acceptance a thesis entitled “Proteomics of Downstream Responses to Growth Signals in Proliferating Cells” by John Patrick Murphy in partial fulfilment of the requirements for the degree of Doctor of Philosophy.

Dated: April 19, 2011

External Examiner: _____

Research Supervisor: _____

Examining Committee: _____

_____

Departmental Representative: _____

DALHOUSIE UNIVERSITY

DATE: April 19, 2011

AUTHOR: John Patrick Murphy

TITLE: Proteomics of Downstream Responses to Growth Signals in Proliferating Cells

DEPARTMENT OR SCHOOL: Department of Biology

DEGREE: PhD CONVOCATION: October YEAR: 2011

_____

Signature of Author

Table of Contents

List of Tables

List of Figures

Abstract

Some of the most profound changes elicited by cell growth stimuli influence dramatic rewiring of metabolism. Intriguingly, rapidly dividing cells with aberrant growth factor signalling, such as cancer cells, tend to rely on glycolysis to generate an adequate supply of building blocks required for cell proliferation and invasion. In this study, we observed that in response to stimulation with insulin-like growth factor 1 (IGF-1), MCF-7 breast adenocarcinoma cells show increased levels of the key glycolysis proteins pyruvate kinase M2 and lactate dehydrogenase A. We then developed targeted multiple reaction monitoring (MRM) mass spectrometry assays to conduct quantitative analysis of glycolysis proteins and heterogeneous nuclear ribonucleoproteins (hnRNPs), the latter implicated in pyruvate kinase splicing and many other aspects of cell proliferation. Application of the glycolysis MRM assay to examine IGF-1 stimulated MCF-7 cells revealed increased levels of all sequential proteins from phosphoglycerate mutase 1 to lactate dehydrogenase A in the glycolysis pathway. An extension of this study to cell lines of varying invasiveness, suggest a relation between glycolysis and metastasis. The clinical applicability of glycolysis MRM assay was also shown by its successful application to lung cancer biopsy analysis. Success with the targeted analysis of glycolysis proteins led to a similar approach for the hnRNP family. Our results showed evidence that a poorly characterized hnRNP (A/B) may be regulated by the c-Myc transcription factor but does not evidently influence pyruvate kinase splicing.

Our approach using MRM to examine small subsets of proteins downstream of cellular growth signals is relatively novel. Our results demonstrate the potential for such targeted MS strategies because of their high selectivity and multiplexing capabilities. Further, the findings from our analyses provide novel insights into the downstream changes elicited by growth signals such as IGF-1 and c-Myc.

List of Abbreviations Used

Akt, protein kinase B
ALDO, aldolase
AMPK, AMP-activated protein kinase
ANT, adenine nucleotide transporter
ANXA6, annexin A6
APOBEC, apolipoprotein B mRNA editing enzyme, catalytic polypeptide-like
ATP, adenosine triphosphate
BLAST, basic local assignment search tool
CALR, calreticulin
CAPZA1, F-actin capping protein subunit alpha-1
CE, collision energy
COPE, coatomer protein complex epsilon subunit
CSRP1, cysteine and glycine-rich protein
CTSD, cathepsin D
DDA, data directed analysis
EDGE, extraction and analysis of differential gene expression
EGFR, epidermal growth factor receptor
EIF3B, eukaryotic translation initiation factor 3 subunit B
ELISA, enzyme-linked immunosorbant assay
ENO, enolase
FASN, fatty acid synthase
FBP, fructose 1,6-bisphosphatase
^{18}FDG-PET, [18F] fluoro-2-deoxyglucose positron emission tomography
G6PD, glucose 6-phosphate dehydrogenase
GAPDH, glyceraldehyde 3-phosphate dehydrogenase
GDI1, guanine dissociation inhibitor 1
GLUT, glucose transporter
GO, gene ontology
GPM, global proteome machine
HIF, hypoxia inducible factor
HK, hexokinase
hnRNP, heterogeneous nuclear ribonucleoprotein
HSPA1L, heat shock protein 1L
HSPA8, heat shock cognate 70 protein A8
IDH2, isocitrate dehyrogenase 2
IGF-1, insulin-like growth factor-1
IGF-1R, insulin-like growth factor-1 receptor
ILF3, interleukin enhancer-binding factor 3
IKK, IκB kinase
IQGAP1, Ras GTPase activating protein
KMC, k-means clustering
KNN, k nearest neighbour
LASP1, LIM and SH3 domain protein 1

LC, liquid chromatography
LDHA, lactate dehydrogenase A
LMNB1, lamin B1
LOD, log-odds
MAPK, mitogen-activated protein kinase
MAX, myc-associated factor X
MCT, monocarboxylate transporter
MDH1, malate dehydrogenase 1
MDM2, mouse double minute 2
MEV, multi-experiment viewer
MIDAS, MRM-initiated detection and sequencing
MMTS, methyl methane-thiosulfate
MRM, multiple reaction monitoring
MS, mass spectrometry
mTOR, mammalian target of rapamycin
NACA, nascent polypeptide-associated complex subunit alpha
NAD, nicotinamide adenine nucleotide
NADPH, nicotinamide adenine dinucelotide phosphate (reduced)
NF-κB, nuclear factor κ-light-chain-enhancer of activated B cells
OGT, O-GlcNAc transferase
PDK, pyruvate dehydrogenase kinase
PEP, phosphoenolpyruvate
PFKFB, 6-phosphofructo-2-kinase/fructose 2,6-bisphosphatase
PFKP, phosphofructokinase C
PGAM, phosphoglycerate mutase
PI3K, phosphoinositide 3-kinase
PKM2, pyruvate kinase M1/M2
PPIA, Peptidyl-prolyl cis-trans isomerase A
PRIDE, PRoteomics IDEntification database
ProSAPiP1, Uncharacterized protein KIAA0552
PTB1, polypyrimidine tract binding protein
PTEN, phosphatase and tensin homologue
RHEB, Ras homologue enriched in brain
RLPL0, 60S ribosomal protein
ROS, reactive oxygen species
RTK, receptor tyrosine kinase
RT, retention time
RTK, receptor tyrosine kinase
SISCAPA, stable isotope standards with capture by antipeptide antibodies
SCO, synthesis of cytochrome c oxidase
SCX, strong cation exchange
SUV, specific glucose uptake value
TEAB, tri-ethyl ammonium bicarbonate
TIGAR, TP53-induced glycolysis and apoptosis regulator
TKT, transketolase
TPI, triosephosphate isomerase

TSC, tuberous sclerosis protein
VAPB, vesicle associated membrane protein
VEGF, vascular epithelial growth factor
VDAC, voltage dependent anion channel
VHL, von Hippel Landau tumour suppressor
TXNDC5, thioredoxin domain-containing protein 5

Chapter 1: Introduction[1]

Abstract

Cancer cells dramatically alter their metabolism in order to increase the production rate of intermediates required for nucleic and fatty acid biosynthesis in rapidly proliferating cells. While not well understood, dysregulation of oncogenes and tumour suppressors found in growth factor signal transduction pathways results in the altered expression of specific isoforms of glycolysis proteins. A full understanding of glycolytic alterations in cancer through a systems biology approach requires tools to observe changes in the set of proteins that make up the glycolytic proteome. We propose that a targeted proteomics approach employing multiple reaction monitoring (MRM) is an excellent strategy to quantitatively monitor sets of proteins, such as those making up the glycolytic proteome. MRM is particularly well suited to proteins of glycolysis as they are of moderate to high abundance. Such systems-based efforts provide a means to understand the mechanisms for an altered glycolytic proteome in cancer, perhaps leading to novel therapeutic targets and metabolic signatures for use in cancer prognosis.

[1] Published; J. Patrick Murphy, Patrice D. Côté, and Devanand M. Pinto. 2010. *Current Proteomics*; In Press. JPM, PDC, and DMP are affiliated with Dalhousie Biology, Halifax, NS and JPM and DMP are affiliated with the National Research Council Institute for Marine Biosciences, Halifax, NS. Text has been slightly modified from its published format.

1.1 Altered Glucose Metabolism in Cancer and the Warburg Effect

A consistent feature of tumour cells is an altered glucose metabolism, first observed by biochemist Otto Warburg in the 1920's and now given the namesake "the Warburg Effect" [1]. Warburg's observations remain relevant as demonstrated by the now common usage of radio-labelled glucose uptake in tumour imaging. At the transcript level, mRNAs encoding glycolysis proteins make up significant portions of transcriptome signatures representing various different types of malignancies [2]. Genes encoding glycolysis proteins are over-expressed in 70% of human cancers [3]. At the protein level, proteomic analyses using two dimensional gel electrophoresis techniques have shown elevated expression of glycolytic proteins in colorectal[4] and renal cell carcinomas [5].

The altered metabolism of tumours is generally believed to result from the selective pressures of the hypoxic tumour micro-environment, under which metabolic fitness advantages are conferred[6]. Others, however, have shown that proliferative cancer cells may already be metabolically reprogrammed before encountering hypoxic conditions[7]. Such reprogramming may occur through mutations in oncogenes and tumour suppressors resulting in altered growth factor signalling and changes in metabolism. Regardless of its origin, there are multiple benefits of the altered glycolytic phenotype to proliferating cells (Fig. 1.1). At first glance increasing glycolysis seems inefficient since it only produces a fraction of the ATP (2 moles/mole glucose) that can be produced using oxidative phosphorylation (36 moles ATP/mole glucose). However, by regulating glycolysis, cells can redirect metabolites towards the nucleotide and fatty acid synthesis pathways needed for proliferation[8]. Glycolysis does not require oxygen, so is especially advantageous for cell survival and proliferation inside solid tumours where cells are frequently over 100 μm from the nearest blood vessel and therefore reside in a hypoxic (low oxygen) environment[9]. A better understanding of the glycolytic differences between quiescent and proliferating cells may uncover novel targets for cancer therapies.

The first part of this introductory chapter provides an overview of current knowledge of the regulation of metabolism in cancer cells. The second part aims to demonstrate the benefits of targeted proteomics using multiple reaction monitoring as a

powerful tool in studying metabolic systems in proliferating cells, which is applied in later chapters.

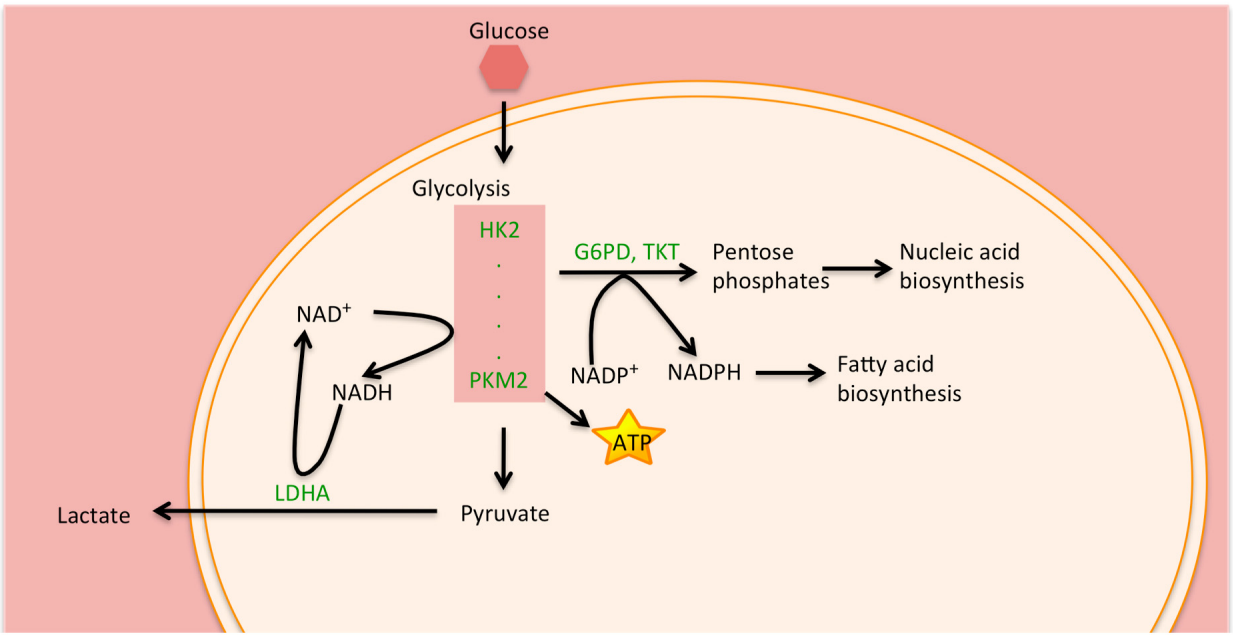

Figure 1.1. Depiction of Proposed Survival Advantages Conferred by Altered Glucose Metabolism. Proliferating cells, such as cancer cells, redirect carbon flux to fuel nucleic and fatty acid biosynthesis, and increase low-oxygen production of ATP. A redirected metabolism may therefore provide nucleic acids and fatty acids for rapid turnover of daughter cells in proliferative tumours. Acidification of the micro-environment by the production of lactate further enhances breakdown of surrounding normal tissues, aiding in tumour invasion.

1.2 Glycolytic Protein Isoforms in Tumour Metabolism

A notable difference between proliferating cancer cells and their normal counterparts is the expression of different glycolytic protein isoforms. Protein isoforms are produced by related genes, or arise from alternatively spliced pre-mRNA from the same gene. Alternate splice variants of several proteins (such as p53, vascular epithelial growth factor, and CD44) are commonly over-expressed in cancer [10]. Protein isoforms thus revise our view of glycolysis as that of a simple, static pathway. As a result of gene duplication events, several isoforms of glycolytic enzymes have evolved with different kinetic properties and, through the altered expression of these isoforms, the pathway can be regulated based on the glycolytic requirements of the cell [11]. Glucose metabolism might therefore follow any number of pathways (Fig. 1.2), with some favouring tumour growth. Much of the understanding of cancer metabolism may come from how specific isoforms or splice variants are regulated in cancer cells[12]. Hexokinase 2 and pyruvate kinase M2 are perhaps the best-known proliferation-enhanced proteins of glycolysis.

1.2.1 Hexokinase 2

There are 4 main isoforms and several splice variants of hexokinase – HK1, HK2, HK3, and HK4 (also called GCK)[13]. Over-expression of HK2 is observed in tumour cells[14], where it is associated with the outer mitochondrial membrane through a voltage-dependent anion channel (VDAC)[15]. By this mitochondrial association, HK2, along with VDAC and the adenine nucleotide transporters (ANT1-3), use newly synthesized ATP from the inner mitochondrial membrane in the priming stage of glycolysis, phosphorylating glucose and generating glucose-6-phosphate at high rates[13]. In addition to priming glycolysis, the HK2-VDAC interaction at the outer mitochondrial membrane inhibits binding of Bad and Bax to VDAC, thereby inhibiting caspase-mediated apoptosis[16], further promoting cell proliferation.

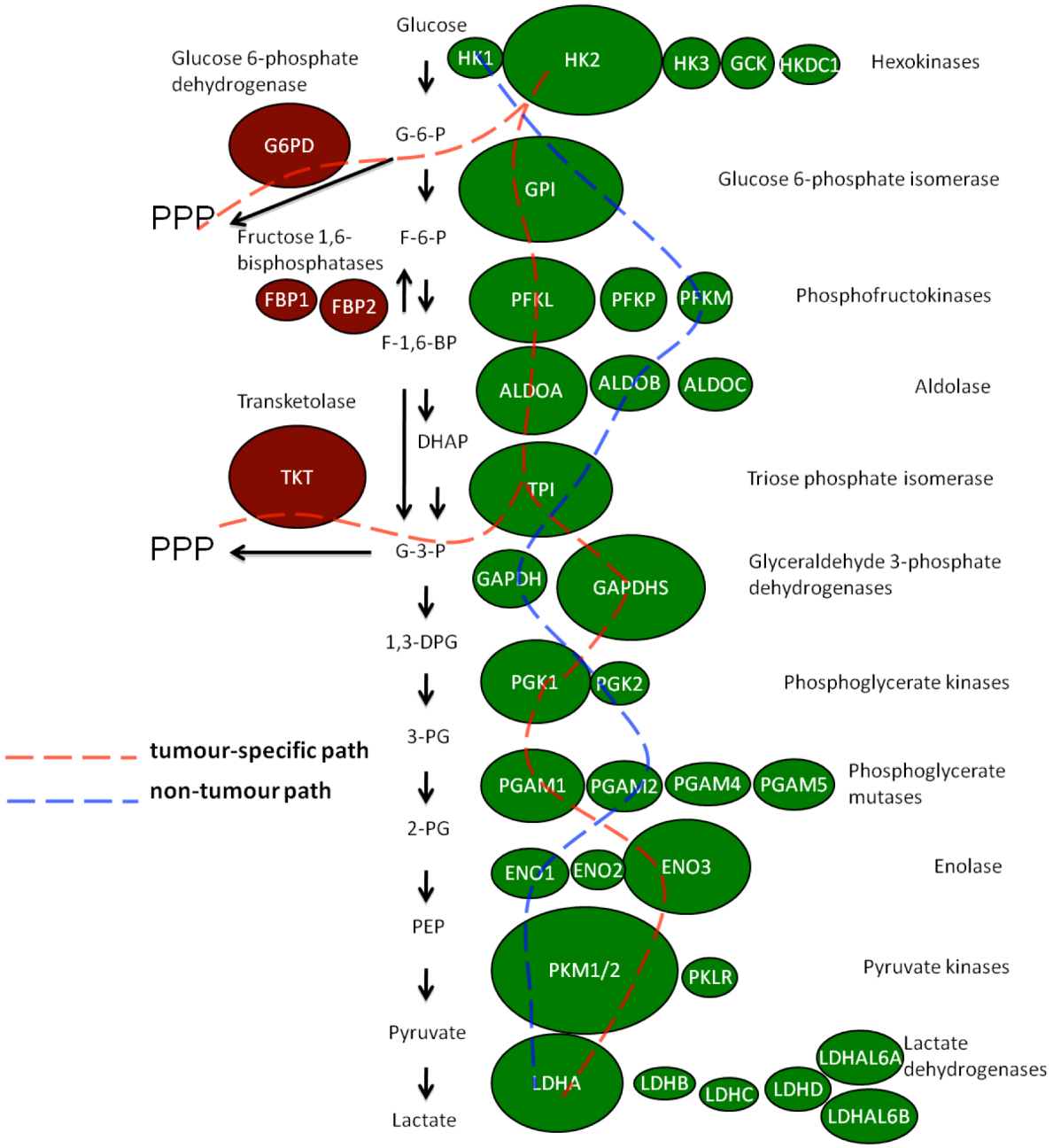

Figure 1.2. Putative Isoform-specific Paths of Glucose Metabolism Through the Glycolysis Pathway. Shown for each of the main proteins of glycolysis are the currently known isoforms. Based on the over-expression of specific isoforms, exemplified here by the size of each circle, the reactions of glycolysis could follow different paths in tumour cells (red lines), than in normal cells (blue line). Isoforms depicted here are expressed by single genes and an even greater number of paths are possible if splice variants are included (e.g. PKM2). (green = traditionally forward glycolysis directing, red = traditionally glycolysis redirecting).

1.2.2 Pyruvate Kinase M2

Pyruvate kinase is a key glycolytic enzyme that catalyses the dephosphorylation of phosphoenolpyruvate (PEP) to form pyruvate and is consistently shown to be important in cancer biology. There are two pyruvate kinase isoforms (PKLR, and PKM1/M2) and each isoform has two known splice variants. Expression of the L and R variants of PKLR, are expressed in liver and red blood cells respectively, but the expression of M1 and M2 variants of PKM1/M2 depends on the developmental stage[17]. The M1 variant is expressed in most adult tissues and the M2 variant is normally expressed during embryonic development. Intriguingly the M2 variant is also highly expressed in proliferating cancer cells[18]. Recent work has shown that exchanging the embryonic M2 variant for the M1 variant, reverses the Warburg effect in cultured cell lines[19], suggesting a key role for the M2 splice variant in tumourigenesis.

Enzymatically, the M2 variant is less efficient than the M1 variant at converting PEP to pyruvate and metabolites are believed to assimilate upstream and enter biomass synthesis pathways[18, 19]. PKM2 thus seemingly lowers pyruvate accumulation, which contradicts the consistent finding of high lactate (of which pyruvate is a precursor) levels in cancer cells. However, it has recently been shown that the phosphate from PEP is transferred to phosphoglycerate mutase (PGAM1) leaving pyruvate as a product[20]. Pyruvate and lactate accumulation also can occur through glutamine metabolism in cancer cells, a process which further supplements proliferating cells with NADPH for lipid biosynthesis [21].

Interestingly, in direct relation to growth factor signalling, PKM2 binds directly to phosphotyrosines, such as those of receptor tyrosine kinases (RTKs), which interferes with the normal allosteric activation of PKM2 by the upstream glycolysis intermediate fructose-1,6-bisphosphate[22]. The observation that a reduction in mitochondrial ATP production under hypoxic conditions coordinates a PKM2-mediated effect on glycolysis, provides a link between tumour hypoxia and PKM2 expression[23]. Conflicting with the commonly held view that the M2 variant of pyruvate kinase is only expressed in embryonic or tumour tissue, PKM2 has been detected at similar levels between normal and carcinogenic breast, lung, and oesophageal tissues, suggesting that some tissues already possess the M2 variant prior

to malignant transformation[24]. The promotion of tumour growth by PKM2 is further complicated by the fact that it has been shown to trans-locate to the nucleus to induce cell death in response cell exposure to apoptotic agents[25]. The role of the PKM2 splice variant in cancer biology is therefore important but complex. As a result of its exclusive expression in proliferating cells, PKM2 and the regulation thereof demands further attention as a therapeutic target for cancer.

1.2.3 Emerging Roles for Other Metabolic Proteins

In addition to specific isoforms of glycolytic enzymes, the existence of other glycolysis related proteins, such as those of the pentose phosphate shunt, can alter the direction of glucose metabolism. In the pentose phosphate shunt, glucose-6-phosphate dehydrogenase (G6PD), catalyzes the reaction of glucose-6-phosphate to 6-phosphoglucono-δ-lactone, producing NADPH and ribose sugars for nucleic and fatty acid biosynthesis[26]. G6PD was shown to be necessary for increasing ATP production in cells detached from the extra-cellular matrix – a key event in metastasis[27]. Recent work has shown another group of proteins, the 6-phosphofructo-2-kinase/fructose 2,6-bisphosphatases (PFKFBs) also alter glycolysis[28]. PFKFBs promote glycolysis by regulating cellular levels of fructose-2,6-bisphosphate, a positive allosteric activator of phosphofructokinase-1 (PFK-1). They also inhibit gluconeogenesis (regeneration of glucose) by inhibiting fructose 1,6,-bisphosphatases, enzymes which catalyze the formation of fructose-6-phosphate from fructose 1,6-bisphosphate[29]. Interestingly, expression of PFKFB mRNA was found to be under the control of MAPK signalling downstream of growth factor activation in mouse fibroblasts. Of the four known isoforms, PFKFB4 was specifically found to be over-expressed in MCF-7 breast cancer cells under hypoxic conditions and expression of PFKFB3 has been shown to be regulated by hypoxia *in vivo*[30].

Another well known metabolic enzyme, lactate dehydrogenase (LDH) contributes to the excretion of lactate into the tumour micro-environment – a key process involved in matrix degradation, invasion, and metastasis[31]. Lactate dehydrogenase converts pyruvate, the normal end-product of glycolysis, to lactate, regenerating NAD^+ for continuous rounds of glycolysis[32]. Lactate is released into the extra-cellular environment by a monocarboxylate transporter (MCT) channel protein, of which MCT4 isoform expression is

enhanced in cancer cells[33]. Several LDH isoforms are known (Fig 1.2), the most well-characterized isoform being lactate dehydrogenase A (LDHA), which appears to be required for cell proliferation under hypoxic conditions [32]. Pyruvate conversion is further enhanced in proliferating cells by increased expression of pyruvate dehydrogenase kinase-1 (PDK1), which inhibits the pyruvate conversion to acetyl-CoA by pyruvate dehydrogenase, thus inhibiting pyruvate entry into oxidative phosphorylation in the mitochondria [34]. It is clear then, that altered expression of glycolytic proteins (canonical and isoform-specific) is advantageous to tumour growth and contributes to the Warburg effect.

1.3 Genetic Regulation of Tumour Metabolism

If the altered metabolism of cancer cells is manifested by aberrant expression of multiple glycolytic proteins and isoforms thereof, how does the metabolic system become reprogrammed? A prevailing view is that the glycolytic proteome is regulated by a multitude of proteins, several of which are well known oncogenes or tumor suppressors (Table 1) [35]. In recent years, HIF-1α, c-Myc, and p53 have emerged as key regulators of the glycolytic proteome[36]. In addition, the immune response regulator, nuclear factor kappa-light-chain-enhancer of activated B cells, (NF-kB) has recently emerged as an important regulator of glycolysis. NF-kB and p53 both regulate cell physiology in response to stressors, but do so in diametrically opposing ways where the former promotes cell division and the latter initiates senescence and apoptosis [37]. The regulation of these mutually antagonistic signalling pathways is of central importance to cancer metabolism. The majority of literature in this area has not focused on isoform-specific regulation, perhaps due to a lack of appropriate tools for isoform study, but a clearer picture is taking shape in regards to the general routes to reprogrammed metabolism.

Table 1.1. Genetic Regulators of Glycolysis

Protein name *Aliases*	**Activated by** *Inactivated by*	**Activates** *Inactivates*	**Observation(s)**
TSC-2 *FLJ43106, LAM, TSC4*	p53, AMPK *AKT-1*	*Rheb*[38]	Tumor suppressor GTPase. Negative regulator of the G protein Rheb.
HIF-1a	cMyc *PHD*[39] *VHL*[40]	Glut1[41] Glycolytic enzymes[41] LDH, PDK1[41], p53 [42], MXI1 *cMyc*[39]	Transcription factor. Major regulator of the Crabtree effect [43, 44]. Activates glucose transport and glycolysys, and downregulates mitochondrial oxygen consumption[41]. Antagonizes repressive c-Myc activity for gene activation[39]. Prolyl hydroxylases (PHD), which lead to the degradation of HIF-1 with VHL, are active in the presence of high O_2 levels and require α-ketoglutarate as a substrate[26].
AMPK *AAK-2* (*C. elegans*)	high AMP[45], AMPK kinase sestrins[46], cytochrome c oxydase[47, 48], LKB-1, p53	FOXO[49, 50] p53[51], TSC-2[38], GLUT4	Energy sensor: activated in the presence of high AMP and low glucose [52]. Enhances glucose uptake, fatty acid oxydation (FAO), and activates aerobic glycolysis [53].
c-Myc *MRTL, bHLHe39*	HectH9/ARF-BP1 *HIF-1a* *MXI1*	*Glycolytic enzymes*	Oncogene. Transcription factor: controls the expression of several glycolytic enzymes[39, 54-61].
IKK	TNF receptor pathway *p53*	NF-kB *p53*	Important node in p53 and NF-kB regulation. Phosphorylates IkB, an inhibitory subunit of NF-kB, in response to an extrinsic stressor (eg. infectious disease). This leads to the degradation of IkB and activation of NF-kB. Directly serine-phosphorylates p53 marking it for ubiquitination and degradation by b-TrCP-1 [62].
NF-kB *EBP-1, KBF1, p105, NFKB-p50, p105, p50*	IKK, *Sirtuin proteins* *IkB*[63]	>200 protein targets GLUT3 [27], IkB[63]	Oncogene. Post translationally regulated transcription factor. Responds to >100 types of mediators (bacterial or viral infections, cytokines, other stresses)[64]. Upon activation by IKK, moves to the nucleus and activates genes containing NF-kB response elements. Leads to cell proliferation.
p53 *TP53 (human gene)*	HIF-1[42] *MDM2/MDM4*	>100 protein targets MDM-2/MDM-4, IGF-BP3[65,] PTEN [38], AMPK, TIGAR[66], PGAM[67], TSC-2 [38], SCO-2 [68], sestrins [46] *IKK, AKT-1, PI3K, GLUT1/4* [69]	Tumor suppressor. Post-translationally regulated transcription factor. Once stabilized, moves to the nucleus to activate genes containing the p53 response element. Leads to apoptosis, cell cycle arrest or senescence. Represses the glucose transporters GLUT 1 and 4[69], represses glycolysis via TIGAR[66], and activates SCO-2 to enhance oxydative phosphorylation[68], Loss or dysregulation is a key inducer of the Warburg effect[52]

Table 1.1 (continued)

Protein name ***Aliases***	**Activated by** ***Inactivated by***	**Activates** ***Inactivates***	**Observation(s)**
PTEN *BZS; DEC; GLM2; MHAM; TEP1; MMAC1;*	p53	*PIP3*[38]	Tumor suppressor. Lipid phosphatase that eliminates PIP3 and thus blocks AKT-1 activation.
IGF-1	*IGF-BP3*	IGF-1 receptor/PI3K	Potent activator of the AKT-1 pathway.
mTOR *FRAP*	Rheb *TSC-1/2*	HIF-1α[40]	Activator of growth and glycolysis. Represses autophagy.
AKT-1 *PKB*		IKK, MDM-2, IkB *p53, TSC-2, Bad* *FOXO*	Oncogene. Kinase that acts on many targets to prevent apoptosis.
FOXO	*AKT-1*	TSC-1	Tumor suppressor. Transcription factor for TSC-1, an inhibitor of mTOR[46].
TIGAR	p53	*PFK-1* [70]	Represses glycolysis in response to p53 activation by reducing F-2,6-P levels, an activator of PFK-1. Reduces ROS levels.
MDM-2	p53 *ATM* *ARF* *CHK1/2*	*p53* *MDM4* *MDM2* *HIF-1a*	Ubiquitin ligase. Cornerstone of several autoregulatory loops with p53, MDM4 and with itself. Is inhibited by ATM and CHK1/2 upon detection of DNA damage.
Rheb		mTOR[38]	G protein. Positive regulator of mTOR.
IGF-BP3 *BP-53, IBP3*	p53	*IGF-1*[65]	Prevents activation of the IGF-1 pathway.
ARF *p14ARF*	cMyc	ATR *MDM-2*	Tumor suppressor. Inhibits MDM-2 (promotes p53) and inhibits NF-kB via ATR/CHK1.
OGT	activated by *O*-Glc-NAc from the hexosamine biosynthetic pathway	NF-kB IKK p53	*O*-Glc-NAc transferase. Activates NF-kB, IKK, and p53 by *O*-Glc-NAc glycosylation [71].
VHL *HRCA1, RCA1*		*HIF-1a*[40]	Tumor suppressor. Oxygen sensor: contained within E3 ubiquitinases, the von Hippel Lindau protein binds directly to prolyl hydroxyl moieties added to HIF-1a in normoxic conditions by prolyl hydroxylases (PHD).

1.3.1 HIF-1

The tumour micro-environment is characterized by low oxygen levels (hypoxia) and increased interstitial pressure as a result of a disorganized microvasculature [72, 73]. The discovery that hypoxia inducible factor-1 (HIF-1), is a regulator of metabolic changes under hypoxia[74], has led to further work demonstrating the importance of this protein for tumour formation [75]. Notably, HIF-1 alters the gene expression of multiple metabolic proteins (Fig. 1.3) including ENO1, PKM2 and LDHA[35, 76-78]. HIF-1α -/- embryonic stem cells grown under hypoxic conditions display severely reduced levels of glucose transporters, glycolytic enzymes, tumour growth, and vascularisation[75].

The active HIF-1 transcription factor is a complex of HIF-1α and HIF-1β, the latter being ubiquitously expressed. Under normoxic conditions, HIF-1α is rapidly degraded in a two step process where HIF-1α is initially prolyl hydroxylated by oxygen-dependent hydroxylases. This modification subsequently allows HIF-1α to be recognized by the von Hippel Lindau (VHL) tumour suppressor in complex with ubiquitin ligases, marking it for degradation (Fig. 1.3)[40]. Under hypoxic conditions, reactive oxygen species released by the mitochondria inhibit the prolyl hydroxylation, stabilizing HIF-1α, and permitting the HIF-1α and β complex to enhance transcription factor activity of glycolytic proteins[79, 80]. In some tumours, inactivating mutations in VHL prevent degradation of HIF-1α rendering HIF-1 transcriptional effects upon metabolism constitutive [81]. The HIF-1 mechanism can also be affected by mutations in genes encoding succinate dehydrogenase and fumarate hydratase. Such mutations result in the accumulation of fumarate and succinate which inhibit prolyl hydroxylases from marking HIF-1α for degradation [82]. An additional link between HIF-1α and metabolism is the requirement of the citric acid cycle intermediate, α-ketoglutarate, as a substrate for prolyl hydroxylases [83]. HIF-1α activity is also influenced by cellular metabolic state, where under conditions of glucose deprivation, an increased level of AMP activates AMP-activated protein kinase (AMPK) (Fig. 3) [84], which has been shown to increase HIF-1α expression in pancreatic and prostate cancer cells [85]. Perhaps as a feed forward mechanism, the glycolysis end products pyruvate and lactate have been shown to alter the levels of glycolytic enzymes by preventing the oxygen-induced degradation of HIF-1α[7]. Most of the HIF-1 transcriptional effects are thought to occur through interaction with

hypoxia response elements in the genome. For example, the gene for HK2 has been shown to contain response elements for HIF-1 [81, 86].

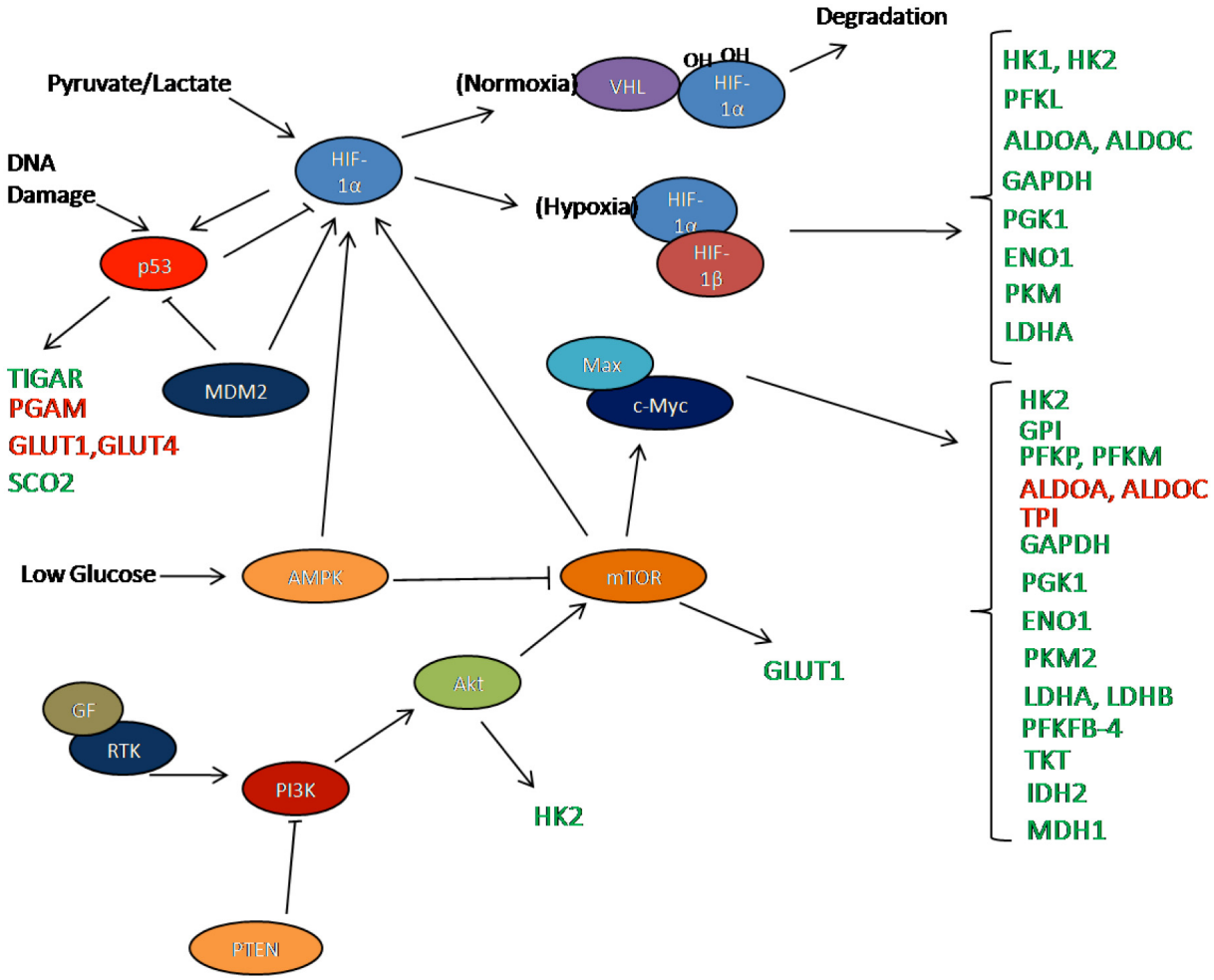

Figure 1.3. An Overview of HIF-1, c-Myc, p53 and Growth Factor Signalling in Regulation of Proteins Involved in Glucose Metabolism. The activation of signal transduction components and transcription factors upstream of glycolytic protein expression is effected by hypoxia, pyruvate/lactate concentration, activation of p53 by DNA damage, low glucose, and growth factor signalling. Shown are glycolytic proteins upregulated (green) by c-Myc, HIF-1 or p53 and those downregulated (red). Abbreviations besides those already indicated in Fig. 3 are; VHL (von Hippel Landau tumour suppressor), HIF-1 (hypoxia inducible factor-1), p53 (tumour suppressor p53), MDM2 (human homologue of mouse double minute 2), c-Myc (human homologue of avian myelocytomatosis virus oncogene), Max (myc-associated factor X), AMPK (AMP-activated protein kinase), mTOR (mammalian target of rapamycin), Akt (protein kinase B), GF (growth factor), RTK (receptor tyrosine kinase), PI3K (phosphotidylinositol-3-kinase), PTEN (phosphatase and tensin homologue), GLUT (glucose transporter), SCO2 (synthesis of cytochrome c oxidase 2).

1.3.2 c-Myc

The c-Myc transcription factor is upregulated in ~30% of human cancers and controls the expression of several glycolysis proteins (Fig. 1.3) [54]. Dysregulated expression of c-Myc often occurs in cancers as a result of chromosomal translocations [59]. Expression of c-Myc is believed to be mainly controlled downstream of β-catenin signalling, in which mutations in any of the various components might be sufficient to alter metabolism through c-Myc. Interestingly, the genes for TPI, ALDOA, and ALDOC have also been shown in rats to be downregulated by c-Myc [54]. In two recent publications, three ribonucleoproteins, hnRNPI, hnRNPA1, and hnRNPA2, under the control of c-Myc, were shown to facilitate the mRNA splicing to form the M2 variant in some cell lines[60,61]. There is considerable interplay between HIF-1α and c-Myc as they both act on similar transcriptional response elements, including those for glycolytic genes [39]. In a seemingly opposing effect, HIF-1α inhibits c-Myc activity by interaction with the c-Myc transcriptional co-activator, myc-associated factor X (MAX), repressing c-Myc responsive genes (Fig. 3) [87]. Over-expression of c-Myc, however, can overcome the inhibitive effect of HIF-1α [88], thereby collaborating with the HIF-1α transcription of metabolic genes [87] .

1.3.3 p53

Also playing a major role in metabolic reprogramming leading to the Warburg effect is the tumour suppressor p53 - one of the most frequently mutated proteins in cancer. p53 is usually subject to rapid turnover (6 to 30 minute half-life depending on the cell type) but in response to DNA damage and oxidative stress, p53 is stabilized (half-life increases to hours) and moves to the nucleus where it increases transcription of genes for cell cycle arrest and apoptosis [89, 90]. p53 is also stabilized by HIF-1α under hypoxic conditions in normal cells but also represses HIF-1 complex transcription [42]. Mouse double minute 2 homologue (MDM2), a ubiquitin ligase regulates p53 by degradation but increases the expression of HIF-1α under hypoxic conditions, albeit in a p53-independent manner (Fig. 1.3) [91, 92]. p53 contributes to changes in the cancer cell metabolism by activating TP53-induced glycolysis and apoptosis regulator (TIGAR), a protein that suppresses glycolysis by decreasing levels of fructose-2,6 bisphosphate (an allosteric activator of PFK-1 [66]). p53 also

suppresses glycolysis by ubiquitination of phosphoglycerate mutase (PGAM), and loss of p53 has been shown to increase PGAM activity, thereby promoting glycolysis [67]. Moreover, p53 suppresses membrane glucose transporters, GLUT1 and GLUT4, decreasing glucose uptake [69]. In relation to mitochondrial respiration, loss of p53 activity prevents the expression of the gene encoding the synthesis of cytochrome c oxidase 2 (SCO2) protein [68], a key enzyme of oxidative phosphorylation. The interplay between p53, c-Myc, and HIF-1 thus plays a key role in alteration of metabolic protein expression.

1.3.4 NF-κB

Whereas the tumor suppressor p53 responds to cellular stressors such as, for example, DNA damage and hypoxia by "shutting down" through cell cycle arrest and apoptosis, NF-κB will instead respond to the stress caused by infectious disease by mobilizing the immune system and activating cell proliferation (this division-promoting activity of NF-κB makes it a possible oncogene). NF-κB activation results in enhancement of aerobic glycolysis through increased transcription of the glucose transporter GLUT 3, which in turn results in increased levels of pyruvate. The increased glucose levels also promote the pentose phosphate shunt. These two pathways produce the substrates required for the synthesis of lipids, nucleic acids, and amino acids, and for the production of NADPH to counter oxidative stress, all of which are necessary for cell proliferation. Although they both respond to stress, the opposing functions of p53 and NF-κB make their simultaneous activation detrimental to the cell. An elaborate reciprocal regulation network consisting of several nodes that allow crosstalk between the p53 and NF-κB pathways is therefore in place to prevent this from occurring. For example, upon activation, protein kinase B (Akt) phosphorylates MDM2 which accelerates the degradation rate of p53 [93] and simultaneously, Akt phosphorylates the IκB kinase (IKK) protein which in turn activates NF-κB [94]. Several other proteins such as the tumor suppressor gene product p14ARF, IκB, the histone acetyl-transferase enzymes p300/CBP are involved in counterbalancing the activities of the p53 and NF-κB pathways [37]. Interestingly, not all regulatory systems have opposing effects on these pathways. A portion of the elevated levels of glucose inside the cell is fed into the hexosamine pathway and the UDP-GlcNAc produced as a result is used as a substrate for protein glycosylation by the enzyme *O*-GlcNAc transferase (OGT). *O*-GlcNAc

is added to both p53 and NF-κB by OGT and thus appears to enhance both p53 and NF-κB simultaneously. In such a situation, p53 seems to dominate by repressing the expression of the glucose transporters GLUT-1 and 3 [95].

1.3.5 PI3K/Akt/mTOR

Dysregulated growth factor signalling has long been implicated in oncogenesis and is increasingly being investigated for links to regulating metabolism. Specifically, receptor tyrosine kinases (RTKs) have been shown to promote the expression of glycolytic genes by initiating the PI3K/Akt/mTor pathway [96, 97]. Many cancers contain activating mutations in PI3K, RTK's, or inactivating mutations of the negative regulator of PI3K, phosphatase and tensin homologue (PTEN) [98]. Changes in the expression of metabolic proteins by PI3K is facilitated through the activation of Akt, which has been shown to bring about a glycolytic switch in glioblastomas[99]. Akt also increases glucose uptake through up-regulation of GLUT1 expression [100-102] via downstream activation of the mammalian target of rapamycin (mTOR) (Fig. 1.3) [103, 104]. Additionally, Akt accentuates glycolysis by activating HK2 (Fig. 1.3) and increasing its association with the mitochondrial outer membrane [105, 106]. Downstream of Akt is mTOR, a serine/threonine kinase, and a crossroads protein in regulating nutrient uptake, energy metabolism, cell growth, proliferation, and cell survival[107, 108]. Besides activation by Akt in response to growth signals, mTOR is regulated by metabolic state, where it is inhibited by the cellular energy sensing protein AMPK under high AMP (low glucose) levels[109]. Moreover, induction of glycolysis proteins by mTOR, accompanies the activation of HIF-1 [110, 111] and c-Myc expression (Fig. 1.3)[112].

Briefly, HIF-1, c-Myc, p53, NF-kB and components of PI3K/Akt/mTOR pathways form an intricate network to coordinate glycolysis in cells. It is therefore conceivable, that frequently observed mutations in cancer-related genes such as p53 or PTEN, constitutively alter expression of glycolytic proteins, resulting in metabolism suited to cell proliferation. However, even after a long history of biochemical studies of metabolism, glycolytic protein expression in cells is not well characterized.

1.4 Targeted Proteomics of Tumour Metabolism

A greater understanding of the Warburg effect and how it relates to cell proliferation might be best achieved through systems-wide approaches, where metabolism can be modeled under various conditions. Such approaches require methodologies to observe changes in the glycolytic proteome. Traditionally, measurements of changes in sets of proteins have been accomplished using affinity-based approaches such as Western blots or ELISA, but development of such methods is expensive and time consuming[113]. Alternatively, "shotgun" quantitative proteomics platforms based on 2D-LC-MS/MS can quantify thousands of proteins in a single experiment[114]. In "shotgun"-type analyses, peptides are chosen for MS/MS based on their intensity; therefore, "shotgun" proteomics is inherently biased towards the analysis of moderate to high abundant peptides[115]. Interpretation is also complicated by variations in chromatographic behaviour, which result in incompletely overlapping lists of peptide spectra acquired between biological replicates (Fig. 1.4) [116]. Proteins of low abundance can be detected through enrichment/depletion strategies, or more extensive 2-dimensional liquid chromatography (2D-LC) or even 3D-LC fractionation, but at the expense of throughput[117]. These limitations restrict current proteomics analysis to small numbers of samples. As a result, thousands of proteins can be confidently identified using "shotgun" proteomics, however protein quantification is not precise and needs to be verified in larger sample sizes because of typically high false discovery rates[118].

While shotgun proteomics is a powerful approach capable of measuring the expression of thousands of proteins in a given sample, it tends to be hypothesis generating. In addition, the incomplete overlap between replicates further compounds the difficulty in using quantitative proteomics to test a specific biological hypothesis. Recently, there has been interest in the hypothesis-driven, targeted proteomic approach, as this method is amenable to quantification, in a reproducible manner, of a limited subset of the proteome (Fig. 1.4)[119]. Targeted proteomics is often used for verification of potential biomarker panels, signalling cascades, or other data sets resulting from global proteomics experiments. Targeted proteomic methods offer higher throughput than global methods since they are amenable to one-dimensional chromatographic analysis unlike the extensive

two and three-dimensional separations usually performed in global proteomic analyses. Metabolic proteins, such as those of glycolysis, are mostly of moderate to high abundance and are among the most frequently identified group of proteins in global proteomics experiments. Because of their abundance, glycolytic proteins can be targeted using robust proteomic approaches, usually in an isoform-specific manner without multiple sample fractionation steps. Multiple opportunities therefore exist for using targeted proteomics to interrogate the mechanisms of sustained metabolic reprogramming of tumours.

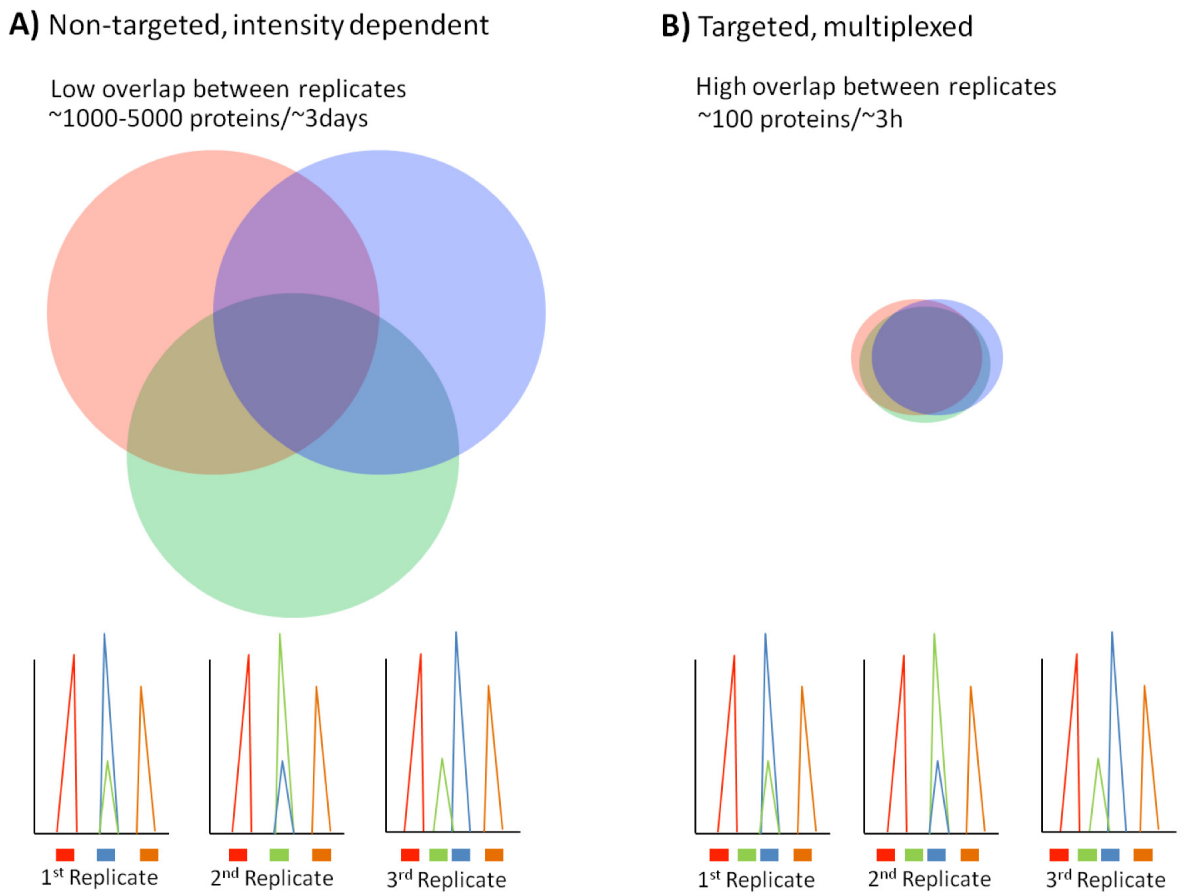

Figure 1.4. Intensity-dependent Versus Targeted Proteomics. Peptides selected for tandem MS analysis (colored squares on the bottom chromatograms) overlap less between replicates in the intensity dependent approach (A) than in the targeted, MRM-based approach (B) where specific precursor and product ion pairs are targeted for prior-determined peptides. Although more proteins are detected by the intensity-dependent approach, the targeted approach provides much greater throughput.

1.4.1 MRM for Targeting Isoform-specific Proteomic Subsets

The key MS technique for targeted proteomics is the use of one dimensional liquid chromatography (1D-LC) and multiple reaction monitoring (MRM) mass spectrometry. Due to its increased throughput, overlap, sensitivity, and amenability for multiplexing, LC-MRM has become a key tool for targeting sets of proteins [120]. In an LC-MRM experiment, the sample is separated by a simple 1D-LC separation and the mass spectrometer is set to briefly monitor selected pairs of parent peptides and peptide fragments, termed transitions[121]. Monitoring multiple transitions per peptide ensures high selectivity and

monitoring hundreds of transitions a single LC-MRM-MS analysis provides highly multiplexed peptide quantification.

The choice of peptides and transitions to monitor requires knowledge of the most proteotypic peptides – those identified consistently by MS - and their most reliably monitored product ions. Transitions can be predicted *in silico* but the most reliable transitions are those selected from empirically obtained product ion spectra[122]. Databases of empirical peptide product ion spectra are available for transition selection, such as Peptide Atlas (http://www.peptideatlas.org) the Global Proteome Machine (the GPM) (http://www.thegpm.org) and the PRoteomics IDEntifications (PRIDE) database (http://www.ebi.ac.uk/pride). However, spectra from these databases, may be specific to a particular instrument, sample preparation method or tissue and, therefore, might not suit all users. Optionally, peptide MS/MS spectra from given sets of proteins, can be generated by targeted fragmentation. In this process, an *in silico* predicted MRM transition is monitored and used to trigger the collection of an MS/MS spectrum for many peptides. The process is termed MIDAS (for MRM-initiated detection and sequencing) [123] and alleviates the bias resulting from intensity-dependent collection of product ion spectra.

The use of peptide LC-MRM analysis may also be tailored towards protein isoforms. However, in practice this process is challenging. Arguably, the greatest challenge occurs as a result of the high sequence similarity between isoforms, resulting in only small stretches of unique, isoform-specific sequences. These small isoform-specific positions may therefore contain few or no proteotypic peptides while LC-MRM analysis requires at least one, preferably several, proteotypic peptides for quantifying the isoform. Additionally, not all isoforms may be known for a given set of proteins [124]. These challenges aside, there are still multiple opportunities for targeting subsets of proteins, with isoform-specificity, using LC-MRM to understand the metabolism of cells.

1.4.2 The Potential of LC-MRM Analysis of the Warburg Effect

Many disease-related proteins of low-abundance have been aggressively targeted by sophisticated fractionation strategies followed by MRM. Directly targeting high to moderately abundant modulators of cell growth, far downstream of growth signals has been overlooked even though many of these proteins they are commonly identified in

global proteomic experiments. For example, through a recent survey study, glycolytic proteins (more specifically ENO, PK, TPI, and GAPDH) are among those frequently identified differentially expressed proteins in proteomics [125]. Glycolytic proteins mostly reside in the cytosol except for occasional cases when proteins are bound to, or located in sub-cellular compartments. As such, most glycolytic proteins are soluble in mild, detergent free buffers that are compatible with MS analysis. The first example of a proteomic targeting of a metabolic protein set has recently been conducted in *Saccharomyces cerevisiae*[119]. Using MRM, and incorporating internal standards, absolute quantification (in copies per cell) of 45 proteins of the carbon metabolism network were monitored in a time-course transition from glucose-rich to fermentative metabolism. LC-MRM analysis of each time-point took less than 1 hour and provided high accuracy of quantification (mean of ~15% CV). A clear metabolic shift was observed towards induction of glyoxylate cycle proteins.

The suitability of LC-MRM towards glycolytic proteins creates many opportunities for a system-wide view of metabolism in cancer. For example, this small, manageable, proteome subset could be assayed in response to stimulation by many growth factors and combinations thereof, knockdown or small molecule inhibition of signal transduction components, medium-throughput screens of small molecule or peptide libraries, or simulated tumour micro-environment conditions. Cell line perturbation, followed by measurement of changes in key cellular metabolites, has been conducted using progressively transformed fibroblast cell lines, where lactate dehydrogenase, hexokinase, mitochondrial ATP synthase, PI3K, or mTOR were inhibited with small molecules, revealing metabolite changes congruent with the Warburg effect [126]. Also in this study, more progressively transformed cell lines showed a 6-fold induction of lactate production, glucose uptake, and ribose-5-phosphate (for nucleotide biosynthesis), compared to a control cell line. LC-MRM methodologies, as part of a broader strategy, may answer important questions about glycolytic proteins in cell proliferation. Moreover, such an approach will enhance our understanding of the roles of oncogene and tumour suppressor mutations and the selective pressures of the tumour landscape, in altering metabolism[127].

1.5 New Opportunities for Prognosis Using Targeted Proteomics

Whether the Warburg effect is necessary for tumour formation or not, the altered glucose metabolism of proliferating cells has proven prognostic utility. The specific glucose uptake value (SUV), resulting from ^{18}FDG-PET scans, is negatively correlated with patient survival[128], where sensitivity ranges from 84-87%, and specificity ranges from 88-93%, depending on the cancer[129]. Not surprisingly, patient SUV has been shown to correlate with many of the Warburg-related proteins such as GLUT-1 and HIF-1α expression in pancreatic cancer[130], increased HK2 expression in gastric carcinomas [131] as well as more direct indicators such as tumour cells/volume and proliferation rates in breast cancer[132].

Use of metabolic indicators as biomarkers has been explored in cancer in other forms than ^{18}FDG-PET. For example, a combined analysis of protein and mRNA data revealed 11 components of glucose metabolism that were associated with poor survival of patients with lung adenocarcinoma[133]. In an analysis of a large cohort of samples from heterogeneous tumour-types, altered metabolic protein signatures were observed in more than 95% of the tumours[134]. In another recent example, a study using enzyme-linked immune-sorbent assays (ELISAs) towards a bio-energetic signature consisting of PKM2, GAPDH, Hsp60, and β-F1-ATPase was used to distinguish normal and cancerous cell-types in 3 tissues (from breast, lung, and oesophagus)[24]. Thus, metabolic signatures are useful for diverse types of cancer.

LC-MRM directed at the glycolytic proteome has enormous potential for increased accuracy in cancer staging [135] by high-throughput analysis of samples from large cohorts of patients[136]. This approach might be more successful than shotgun proteomics approaches which have not yet led to widespread use of clinical protein biomarkers - mainly because of the time and cost to measure an adequate number of samples to exclude false positive results [137]. In fact, less than 10 protein biomarkers have been approved by the US Food and Drug administration in the last 5 years[138]. MRM may reveal effective protein biomarker signatures, perhaps augmenting information from ^{18}FDG-PET scans for patient-specific cancer prognosis and staging, and reducing the clinical requirements for ^{18}F.

Until now LC-MRM biomarker signatures have been targeted using MRM of plasma proteins for which rapid, accurate, and repeatable quantification of many samples is

needed. However, many plasma protein biomarkers of current clinical importance, such as prostate specific antigen and carcinoembryonic antigen are typically present in the pg to ng/mL of plasma range, below the typical MRM-detectable range of ~1-10 ug/mL of plasma[138]. To facilitate their analysis by LC-MRM, multiple fractionation or enrichment steps are often employed. For example, immuno-affinity depletion of the top 6 highly abundant proteins, preceding peptide MRM analysis, was necessary for successful quantification of 47 high/intermediate-abundance human plasma proteins (at <1ug/mL) [120]. Other novel enrichment techniques have recently been introduced, including an approach called stable isotope standards with capture by antipeptide antibodies (SISCAPA), where peptides of interest are specifically immuno-affinity captured alongside stable isotope labelled internal peptide standards followed by absolute quantification by MRM[117, 139, 140]. While the SISCAPA approach does not offer significant improvement in cost or throughput when compared to ELISA, the coupling of affinity to MRM achieves much greater level of multiplexing, specificity, and quantitative accuracy [141]. In most cases, fractionation and enrichment steps prior to MRM, allow for reasonable quantification variability (CV's of 10-20%)[117, 139, 142], but limit throughput, for biomarker verification. As opposed to current protein biomarkers, the glycolytic proteome is typically highly abundant and exhaustive separation is not required for LC-MRM analysis.

Taken together with the constitutive alteration of glycolysis in proliferating cells, LC-MRM of glycolysis proteins has potentially enormous prognostic potential in cancer. Given the relevance of the glycolytic proteome, analysis of patterns in glycolysis protein expression might be useful in selecting patients that will respond to metabolism-based therapies. Members of the glycolysis proteome are emerging as important targets for therapeutic intervention. There are no approved cancer therapies directed at the Warburg effect, however, drugs such as metformin used to treat metabolic disorders are being tested as anticancer agents [143]. Other inhibitors of cancer-related metabolic proteins are currently being assessed for therapeutic potential including hexokinase inhibitors such as, 3-bromopyruvic acid[144], and 2-deoxyglucose[145], a transketolase and pyruvate dehydrogenase inhibitor, oxythiamine [146], and a glucose-6-phosphate inhibitor, 6-aminonicotinamide [146]. Inhibitors of the upstream modulators of glycolytic protein expression are also in various stages of evaluation, including therapeutic agents for mTOR (RAD001, CCI-779, and

AP23573) and HIF-1α (topotecan, NSC 644221, YC-1, and PX-478) which have shown efficacy for inhibiting tumour growth[146-151]. A more detailed portrait of glycolysis in proliferating cells will facilitate the development of novel metabolism-based anticancer drugs.

1.6 Conclusion

An altered metabolism of tumour cell populations resulting in the Warburg effect, occurs in nearly all types of cancer and mounting evidence is showing its regulation by oncogenic growth signals. The glycolytic proteome consists of proteins of moderate to high abundance such that they can be measured using LC-MRM without sample enrichment. We suggest use of targeted LC-MRM of the glycolytic proteome and other subsets of important high-abundance proteins should be pursued to investigate the oncogenic origins of the Warburg effect to reveal cancer therapies. Future work using LC-MRM of the glycolytic proteome will need to assess whether the technique is applicable to clinical samples to be used in the detection of metabolic biomarker signatures. Finally, if metabolically-related cancer therapies are validated, assessing the glycolytic proteome of tumours may be extremely useful in directing patient-specific treatment.

Chapter 2: Temporal Proteomic Analysis of IGF-1R Signalling in MCF-7 Breast Adenocarcinoma Cells[2]

Abstract

Dysregulation of the insulin-like growth factor receptor (IGF-1R) signalling network is implicated in tumour growth and resistance to chemotherapy. We explored proteomic changes resulting from IGF-1 stimulation of MCF-7 adenocarcinoma cells as a function of time. Quantitative analysis using iTRAQ™ reagents, and 2D-LC-MS/MS analysis of 3 biological replicates resulted in the identification of 899 proteins ($p \leq 0.05$) with an estimated mean false positive rate of 2.6%. Quantitative protein expression was obtained from 681 proteins. Further analysis by supervised k-means clustering (KMC) identified five temporal clusters, which were submitted to the FuncAssociate server to assign over-represented gene ontology (GO) terms. Proteins associated with vesicle transport were significantly over-represented. We further analyzed our dataset for proteins showing temporal significance using the software, EDGE, resulting in 20 significantly and temporally changing proteins ($p \leq 0.1$). These significant proteins play roles in, among others, altered glucose metabolism (lactate dehydrogenase A (LDHA) and pyruvate kinase M1/M2 (PKM2)) and cellular stress (nascent polypeptide-associated complex subunit α (NACA) and heat shock (HSC70) proteins). We used multiple reaction monitoring (MRM) to validate these interesting proteins and have revealed several differences in relative peptide expression corresponding to protein isoforms and variants.

[2] Published; J. Patrick Murphy and Devanand M. Pinto. 2010. *Proteomics*; 10 (9) 1847-1860. JPM and DPM are affiliated with Dalhousie Biology, Halifax, NS and the National Research Council Institute for Marine Biosciences, Halifax, NS.

2.1 Introduction

Signalling networks regulate key biological processes and, when perturbed, often result in unregulated cell proliferation, differentiation, or motility [152]. These cellular abnormalities are involved in a multitude of pathogenic processes, including cancer. An increased understanding of protein dynamics in signalling networks will be tremendously useful to design effective therapies [153]. Efforts to use quantitative proteomics to understand cellular signalling networks have focused on the epidermal growth factor receptor (EGFR), the first receptor tyrosine kinase (RTK) to be characterized in relation to cancer [116, 154, 155]. The insulin like growth factor 1 receptor (IGF-1R) is another RTK that is receiving attention as a putative therapeutic target for various types of cancers [156]. IGF-1R is a cell surface RTK that, through downstream interactions with signalling partners, regulates cell proliferation, motility, and inhibition of apoptosis [157], contributing to tumour growth, metastasis, and resistance to chemotherapy [158, 159].

The route of signal transduction through IGF-1R is initiated by the binding of insulin-like growth factor-1 (IGF-1) to the receptor causing a homo-dimerization and trans-phosphorylation, which in turn activates several adapter proteins, subsequently triggering mitogen activated protein kinase, phosphoinositide 3-kinase (PI3K) and Akt cascades [157]. Growth factor-induced signalling is also known to alter glucose metabolism for enhanced cell growth and survival in cancer progression [160]. In addition, IGF-1R signalling has further been implicated in cancer through promoting the activation of the vascular epithelial growth factor (VEGF) [161], interaction with the tumour suppressor p53 [162], and cross talk with estrogen receptor signalling[163, 164]. Propagation of IGF-1R signal transduction is tightly regulated by, for example, IGF-1 binding proteins [165], internalization of the receptor [166], and regulation of downstream cascades.

As part of a broader strategy to detail the mechanisms relating activation of IGF-1R to changes in specific cellular abnormalities in cancer, we monitored the temporal relative protein expression changes in IGF-1 stimulated breast cancer cells using shotgun proteomics [167]. Our approach used an initial discovery phase to identify proteins whose expression is altered following IGF-1 stimulation, followed by a verification phase, where a subset of these proteins were quantified in a targeted manner using multiple reaction

monitoring (MRM). These experiments were enabled using iTRAQ quantitative proteomics in the discovery phase [167], and an orthogonal dimethyl labelling technique for the targeted MRM phase[168]. As a model, we used the well-characterized MCF-7 breast cancer cell line, which has been shown to express IGF-1R [163], making it an excellent model for IGF-1R signalling. Temporal relative expression profiles generated from iTRAQ quantitative analysis revealed a number of proteins and biological themes changing over time in response to IGF-1 stimulation.

2.2 Experimental Procedures

2.2.1 Cell Growth and Stimulation

MCF-7 cells were obtained from the American Type Culture Collection (Manassas, VA) and maintained in DMEM (Invitrogen, Carlsbad, CA), containing 10% FBS, at 5% CO_2 until 80% confluency was reached. Cells were then washed with PBS and serum-starved (no FBS) for 48 h. Three separate cultures were stimulated with 100 ng/mL IGF-1 for 0 (no IGF-1), 6, 12, or 24 h (Fig. 2.1). Following IGF-1 stimulation, cells were washed with PBS and trypsinized with 1.5 mL of 0.25% Trypsin/EDTA (Invitrogen). Detached cells were transferred to a 50 mL tube, centrifuged at 2,000 x g for 5 mins, supernatants were discarded, and pellets were washed twice with PBS. In a similar manner, two additional cultures (3.0×10^6 cells per flask) were grown, serum-starved, and one was stimulated with IGF-1 for 24 h (for optimization of MRM validation experiments).

2.2.2 Cell Lysis and Protein Extraction

Cell pellets were immersed in 1 mL of 50 mM tri-ethyl ammonium bicarbonate (TEAB) buffer (Sigma-Aldrich, St. Louis, MO) and lysed by passage through a 21 G 1.5 needle 20 times. Each mixture was transferred to 3 mL centrifuge tubes, centrifuged at 110,000 x g for 1 h, and the supernatant (cytosolic proteins) was collected. Total protein concentration of the cytosolic fraction was estimated using a Bradford assay [169] with BSA as a standard.

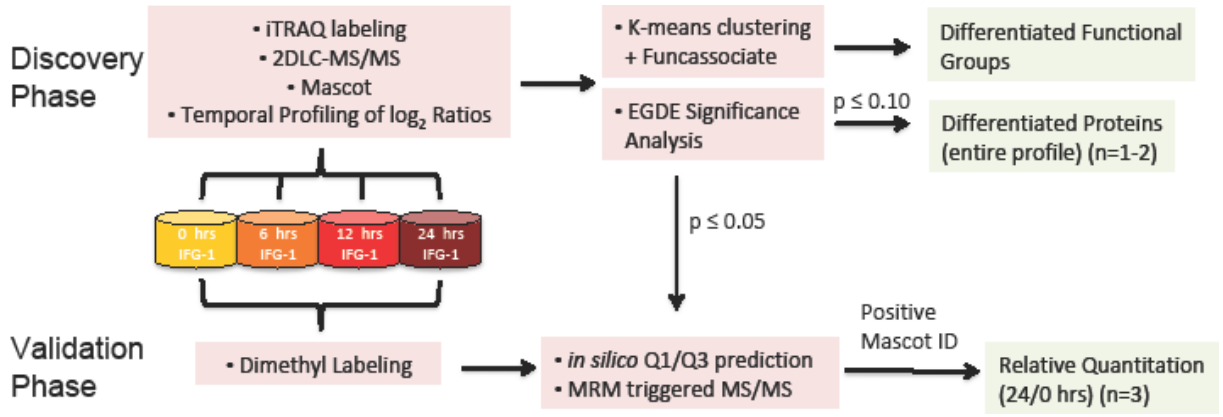

Figure 2.1. Workflow for Discovery and Validation Phases. MCF-7 cells were stimulated for 24 h and iTRAQ analysis was employed to generate temporal profiles. Lists of proteins with similar temporal expression profiles were formed using K-means clustering and submitted to FuncAssociate to identify differentially regulated functional groups. Proteins that showed EDGE significance ($p \leq 0.05$) were targeted for validation using MRM. Dimethyl labelled peptide Q1/Q3 masses for significant proteins were predicted *in silico*, where the y_{n-1} ion was selected for Q3. These predictions were used for MRM triggered MS/MS of, dimethyl-labelled, 24 and 0 h samples. Transitions with positive Mascot identifications were used for relative quantitation between the 24 and 0 h time-points.

2.2.3 iTRAQ Labelling and Offline SCX

Aliquots of 500 mL (~500 mg protein) from each time-point were dried in a vacuum centrifuge and the pellet was re-immersed in 40 mL of iTRAQ dissolution buffer (AB Sciex, Foster City, CA). For the remaining steps of reduction and blocking of cysteine residues, protein digestion and peptide labelling, the iTRAQ manufacturer's (AB Sciex) protocol was followed, except all reagent quantities were doubled. Samples were labelled with iTRAQ reagents as follows: 114 – no IGF-1, 115 – 6 h after IGF-1 addition, 116 – 12 h after IGF-1 addition, and 117 – 24 h after IGF-1 addition. Peptides were separated by strong cation exchange (SCX) chromatography using a 2.1 x 100 mm polysulfoethyl A SCX column (PolyLC, Columbia MD), at a flow rate of 0.2 mL/min. A linear gradient of 100% A (A = 10 mM ammonium formate, 25% ACN, pH 2.8) to 60% B (B = 600 mM ammonium formate, 25% ACN, pH 2.8) over 40 mins was applied, followed by a hold at 60% B for 5 mins, and re-equilibration at 100% A for 15 mins. Fractions (200 µL) were collected every min from 20 to 50 mins and dried in a vacuum concentrator.

2.2.4 Data-directed Acquisition and Protein Identification

LC-MS/MS was performed using a NanoAcquity UPLC system with an Atlantis 1.7 mm particle size, 100 mm x 100 mm bridged ethyl hybrid C_{18} reversed phase column (Waters, Milford, MA), coupled to a QTOF Premier mass spectrometer (Waters) equipped with a nano-electrospray source. Fractions from SCX were resuspended in 30 µL of 5% ACN, 0.1% formic acid, and 1 µL of each sample was injected at flow rate of 500 nL/min. Online reversed phase separation was conducted using a linear gradient of 5% ACN, 0.1% formic acid to 85% ACN, 0.1% formic acid over 65 mins. For data-directed analysis (DDA) acquisition, MS scans were 1 s and MS/MS was conducted on the 4 most intense peaks with charge states of 2 or 3 in the MS spectra, also for 1 s each. The lockspray option was enabled using a constant flow of 2 µL/min of 200 fmol/mL Glu-Fibrinogen B (Sigma-Aldrich), scanning every 20 s. To gain additional protein coverage, three technical replicates were performed for each fraction. The third replicate was analyzed using an exclusion list consisting of all MS peaks selected for fragmentation in the first two replicates. Proteinlynx software package (Waters) was used to process the raw data into peak lists with the following parameters for MS and MS/MS: normal MS background subtract, 10% background threshold, background polynomial = 2, no smoothing, no deisotoping, 6 channel minimum peak width, top 80% centroided, TOF resolution = 10000, NP multiplier = 0.7. Once exported, processed peak lists from all SCX fractions, including those collected from re-injected samples, were combined to 1 peak list per biological replicate using a short Python script. Mascot [170] was used to search the combined peak lists against the IPI human (v.3.50) protein database, and generate ratios from iTRAQ reporter ion intensities. Identification criteria used were as follows; 0.5 Da MS tolerance, 0.4 Da MS/MS tolerance, MMTS as a fixed modification, pT, pS, pY as variable modifications, p-value = 0.05, minimum 2 peptides per protein, and ion score expect cutoff = 15. iTRAQ peptide ratios were average normalized and the protein ratios were calculated using the weighted average calculated by Mascot.

2.2.5 Analysis of iTRAQ Relative Quantitative Data

Individual iTRAQ ratios, generated by Mascot (115/114, 116/114, and 117/114) were first $\log_2$ transformed, and the ratio for each protein was averaged across the 3

replicates. Missing values in the dataset were imputed using the k nearest neighbour (KNN) impute algorithm [171] implemented through the EDGE software package [172], accepting 50% (2/4 time-points) of the values per protein as missing, and imputing based on the 10 nearest neighbours. This dataset (including imputed values) was used as input for k-means clustering (KMC) [173] implemented through the multi-experiment viewer (MeV) gene expression analysis package [174]. KMC was conducted in a supervised manner specifying 5 clusters and 20 iterations, using a Euclidian distance metric. Over-represented GO terms in each KMC cluster were assigned using FuncAssociate [175] with a p-value ≤ 0.05. Significance analysis of time course $\log_2$ data was conducted with the software package EDGE: Extraction and Analysis of Differential Gene Expression [172], using a natural cubic spline.

2.2.6 Selection of MRM Transitions for Validation

Proteins from EDGE analysis with a p-value ≤ 0.05 were selected for targeted MRM validation of the 0 and 24 h time-points. For validation, a labelling method orthogonal to iTRAQ, using dimethyl peptide labelling with isotopically coded formaldehydes [168], was employed. For the EDGE -selected proteins, lists of peptide MRM transitions of the light and heavy dimethylated parent ions and the highest mass y-ion were assembled. For simplicity we refer to this as the y_{n-1} fragment ion, where n is the number of residues in the tryptic peptide. In order to increase the sequence coverage, additional peptides for differentially regulated proteins were assembled using a searchable database of *in silico* predicted of MRM properties (http://rita.imb.nrc.ca/~spenny/mrm/mrm_predict.php). The database contains parent → a_1/y_{n-1} MRM transitions for all doubly charged human dimethyl-labelled tryptic peptides in the IPI human database (v3.50). Peptides were ranked based on the probability of being observed in an electrospray experiment (derived from empirical data and amino acid physical properties). For each of the EGDE-selected proteins, parent → a_1/y_{n-1} transitions were generated including the 10 most predictably observable peptides (7-16 amino acids long) from the database, as well as peptides identified empirically in the iTRAQ experiment.

2.2.7 Differential Labelling by Reductive Methylation

Aliquots of 500 µL (~500 µg protein) were reduced with 5 mM DTT, alkylated with 12 mM iodoacetamide, and digested overnight with 10 µg of sequencing grade trypsin (Promega, Madison, WI) at 37°C. To each sample, 89 µL of 7M CH_2O (0 h samples) or 7M CD_2O (24 h samples) was added, and after 5 mins, an equimolar amount of 6M $NaCNBH_3$ was added. After 2 h, samples within each replicate from the 0 (light-labelled) and 24 h (heavy-labelled) time-points were mixed and acidified with 10 µL TFA. Each of these samples were then desalted using C18 SepPak Light™ cartridges (Waters), separately for each replicate sample, dried in a vacuum centrifuge, and resuspended in 200 µL of 5% ACN, 0.1% formic acid.

2.2.8 MRM and MRM-triggered MS/MS

LC-MS/MS for verification was conducted using an Agilent 1100 capillary HPLC (Agilent, Santa Clara, CA) coupled to a 4000 QTrap mass spectrometer equipped with a nano-electrospray source (AB Sciex). Online reversed phase chromatography was conducted using two monolithic C_{18} 100 mm x 150 mm columns (EMD Biosciences, San Diego, CA) connected in series, an injection volume of 3 mL, flow rate of 2 mL/min and a gradient of 5% ACN (0.1% formic acid) to 30% ACN (0.1% formic acid) in 25 mins, then to 90% ACN (0.1% formic acid) at 35 mins. For MRM acquisition, dwell time was 50 ms and collision energy (CE (eV)) used was calculated by dividing the parent $[M+2H]^{2+}$ m/z by 20. For MRM triggered MS/MS acquisition, the MRM dwell time was 100 ms, and the 2 most intense peaks exceeding 1000 counts were selected for MS/MS, using a rolling CE.

2.2.9 Optimization and Verification of Selected MRM Transitions

Suitable MRM transitions were selected through analysis of additional MCF-7 cell cultures, where 0 and 24 h IGF-1 stimulation samples were selected. To increase throughput, LC-MRM analyses were performed using a 1D-LC separation, as opposed to the 2D-LC separation used in the initial discovery experiments. Initial LC-MRM analysis was conducted in batches of 40 MRM transitions (10 peptides x 4 transitions per peptide), following which a transition was used in a subsequent MRM triggered MS/MS experiment if light and heavy parent → a_1/y_{n-1} peaks were observed at identical retention times (RTs)

and S/N was greater than 10. Resulting MS/MS were submitted to Mascot and searched against the IPI Human database (v.3.50). Identification criteria used were as follows; 0.5 Da MS tolerance, 0.4 Da MS/MS tolerance, carbamidomethyl C as a fixed modification, dimethyl labelling (both light and heavy) as variable modifications, p-value = 0.05, and ion score expect cutoff = 10. For positively identified peptides, MRM transitions (parent → y_{n-1} only) were compiled into a single MRM method, and the Mascot RT was used to match peaks to verified peptides. A summary of these procedures is illustrated in the lower portion of Fig. 2.1.

2.2.10 Analysis of Relative Quantitative MRM

The compiled MRM method (above) was used to perform LC-MRM on the 3 biological replicate samples, with 3 injections per sample. MultiQuant™ v1.1 (AB Sciex) was used to integrate peak areas of MRM chromatograms using the following parameters; smoothing width = 1 point, RT half window = 30 s, minimum peak width = 3 points, minimum peak height = 0, noise% = 40, baseline subtract = 2 mins, and peak splitting = 1. Where more than 1 MRM chromatographic peak was present, the RT reported in the previous verification analysis by Mascot, plus matching retention times for both heavy and light labels were used to indicate the correct peak for integration. If the selection criteria were met, the MRM chromatogram area of the heavy to light parent → y_{n-1} transitions were used to generate relative peptide ratios between the 0 and 24 h replicate time-points. To examine uniqueness of the peptides we chose, each peptide sequence was submitted as a BLAST search against the UniProtKB Human database (http://www.uniprot.org/blast/) with a threshold of 10, PAM30 matrix, no filtering, and no gapped alignments.

2.3 Results

2.3.1 Protein Identification and iTRAQ Relative Quantitation

Proteomic analysis of IGF-1 stimulated MCF-7 cells resulted in the identification of 899 proteins ($\propto$ = 0.05, minimum ionscore = 15, minimum 2 peptides per protein). The data has been converted using PRIDE converter [176] (http://code.google.com/p/pride-

converter) and is available in the PRIDE database [177] (www.ebi.ac.uk/pride) under accession numbers 10885 - 10887. As shown by the Venn diagram in Fig. 2.2, a semi-distinct list of proteins was identified for each of the 3 biological replicates, with limited overlap (606 in rep 1, 335 in rep 2, and 523 in rep 3, totalling 899 unique proteins). We suspect the identification of markedly fewer proteins in replicate 2 is due to a slight SCX RT shift resulting in elution of some peptides outside the fraction collection period. This problem was alleviated by increasing column equilibration before SCX chromatography of replicate 3. As estimated by the decoy database search in Mascot, false discovery rates were 2.8%, 3.3%, and 2.0% in replicates 1, 2, and 3 respectively. Using Mascot, relative expression ratios were generated for 681 of the 899 identified proteins, again with similarly few overlapping proteins as in Fig. 2.2. To relate the $\log_2$ ratios to iTRAQ 114, a value of "0" was set to each protein for the 0 h IGF-1 time-point, while the $\log_2$(iTRAQ 115/114), $\log_2$(iTRAQ 116/114), and $\log_2$(iTRAQ 117/114) values represented the relative expression (to 0 IGF-1) at the 6, 12, and 24 h time-points, respectively. This resulted in a dataset of 681 proteins x 3 replicates x 4 time-points, however, 37.4% of the points within this dataset had missing values, caused by the limited overlap between replicates. The high proportion of missing data would have excluded many proteins from statistical analysis. Therefore, the mean $\log_2$ ratio was used for each time-point, which reduced the missing values to 8.04%. This reduction allowed the remaining missing values to be imputed using the KNN impute algorithm [171], implemented through the EDGE statistical package [172].

The overall profiles of the $\log_2$ ratios in each replicate (Fig. 2.3) indicate a slight change in relative protein expression after 6 h, which was consistent between replicates, and much greater changes after 12 and 24 h, as shown by the much larger vertical spread of the data at the 12 and 24 h time-points in Fig. 2.3. To varying degrees, the same trend was followed for all 3 biological replicates as shown by the solid lines (mean $\log_2$ ratios) in Fig. 2.3.

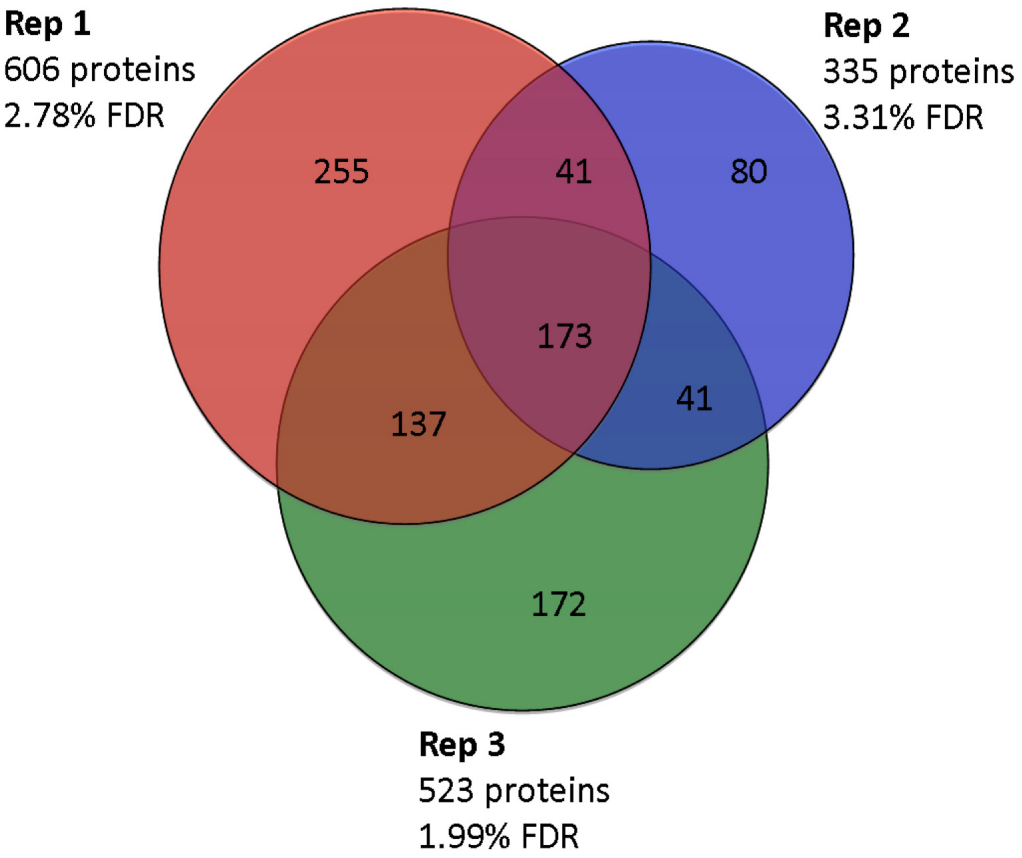

Figure 2.2. Overlapping protein identification between biological replicates. From a total of 899 unique proteins identified, 173 are identified in 3 replicates.

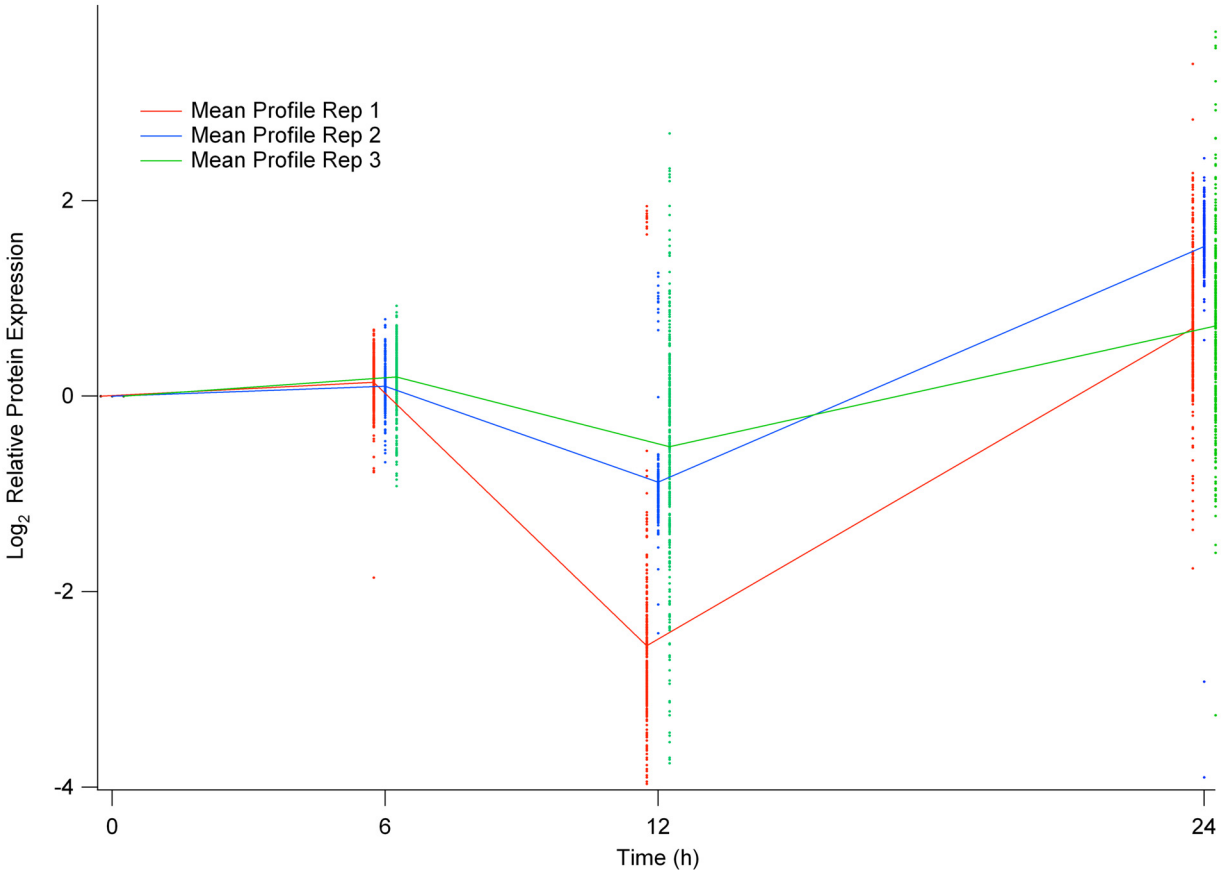

Figure 2.3. Individual Log_2 Ratios for Each Biological Replicate. Coloured dots represent log_2 ratios at each time-point (offset by 0.5 h for clarity). Solid coloured lines connect the mean overall protein ratios over time for each biological replicate. Common to each replicate are overall minor changes after 6 h, decreases after 12 h, followed by increases after 24 h.

2.3.2 K-means Clustering and GO Annotation of Temporal Profiles

A number of clustering techniques can be used to highlight important biological trends in time course gene expression studies including hierarchical clustering [178], sorting organizational maps [179], and KMC [173]. For gene expression, all of these clustering methods partition expression changes of a large set of gene expression measurements into smaller subsets based on their means [178]. Since KMC has been shown to perform well for time course data [173] we have employed supervised KMC of the mean log_2 profiles (including imputed values). Following KMC, we identified over-represented GO terms within each cluster, which allowed construction of temporal profiles of overall cellular processes in response to IGF-1R signalling. A number of preliminary KMC analyses enabled estimation of the number of clusters where diversity increases minimally to be 5. From the 5 clusters

formed, the majority of proteins were grouped in clusters 3, 4, and 5 (Fig. 2.4) showing similar relative expression profiles: minimal change after 6 h, decrease after 12 h and increase after 24 h. The unique differences between clusters 3, 4, and 5, are the degree to which the expression profiles decreased after 12 h (cluster 4 decreased the greatest) and the degree to which they increased after 24 h (cluster 3 increased the greatest) as shown in Fig. 2.4. The profile of KMC-1 showed an increasing relative expression over time, with no decrease after 12 h. Conversely, the profile of KMC-2 showed an initial increase followed by a decrease after 24 h and profiles grouped within it are more heterogeneous.

To expose biological trends in the relative quantitative data, the list of proteins assigned to each cluster was submitted to the FuncAssociate server [175], and the resulting GO terms hit were used to profile cellular functions over time following IGF-1 stimulation. GO terms with a p-value ≤ 0.05 were sorted by decreasing log-odds (LOD) values – based on, for a given GO term, the number of *observed* associated proteins in the list of N, compared to the number of *expected* associated proteins in a random in a list of N human proteins. The GO term descriptions with the 10 highest LOD values for each cluster are shown to the right of the cluster profiles in Fig. 2.4. KMC-1 (Fig. 2.4), which increased temporally without a major decrease at any time-point, showed over-representation of GO terms such as “GTPase activity”, “coated vesicle”, and “protein localization”. This cluster of 48 proteins contains proteins such as Rab proteins and guanine dissociation inhibitors, cortactin, a vesicle associated membrane protein (VAPB), and coatomer protein complex epsilon subunit (COPE). Among proteins in the Rab group, several peptides which are conserved among the Rab family were used for quantitation by Mascot, which may have affected the clustering of these proteins. For example, the peptide LQIWDTAGQER is highly conserved among the Rab family and, therefore, contributed to the temporal profile of each member of the family. KMC analysis did not result in the grouping of all Rab proteins in the same cluster because some peptides were unique to certain family members since, other than a few conserved regions, Rab proteins show high sequence heterogeneity [180]. While not known for their involvement in vesicle trafficking, also grouped within KMC-1 were a number of proteins associated with glycolysis; PKM2, phosphofructokinase C (PFKP), and LDHA.

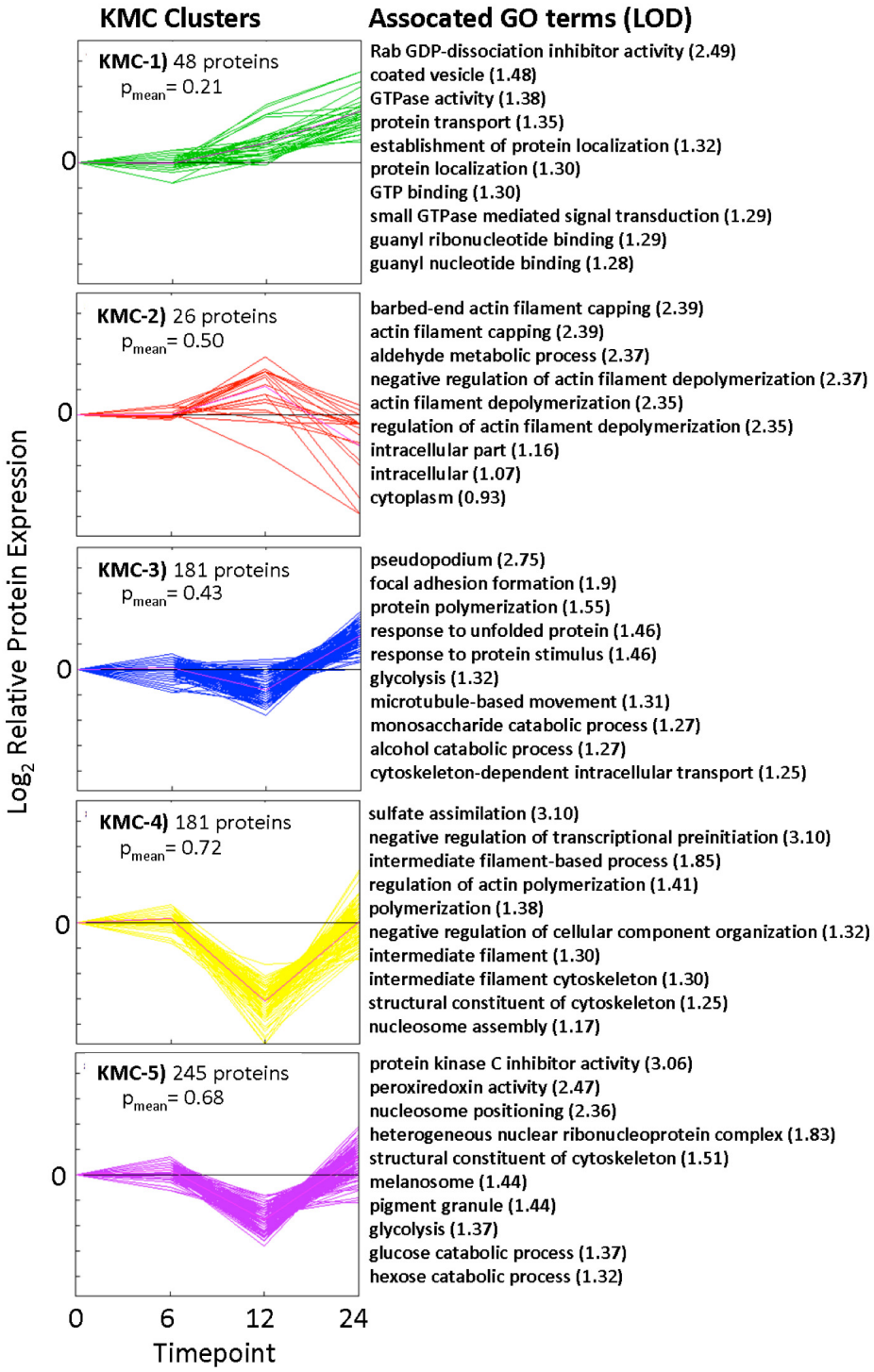

Figure 2.4. K-means Clusters of Time Course Profiles with Associated Over-represented GO Terms. Shown adjacent to each cluster (1-5) are the top 10 over-represented GO terms (FuncAssociate p-value < 0.05) and associated log-odds (LOD), over-represented in the list of proteins for that specific time-point. The number of proteins and mean EDGE p-values (p_{meaAn}) are shown for the proteins in each cluster.

2.3.3 Significance Analysis of Temporal Relative Expression Profiles

In addition to KMC, which does not directly detect significantly different temporal protein profiles, EDGE software [181] was used to analyze the temporal profiles for significance. The algorithms within EDGE run on the R statistical package (http://www.R-project.org) and use spline based curves to model the temporal expression profiles. The technique essentially determines significance by fitting the $\log_2$ time course profiles to either a null (H_o) or alternative (H_a) hypothesis. In this model, H_o is a straight line with a slope of 0 (no change in expression) that minimizes the sum of squares difference across all flat lines, while H_a is a solid curve that minimizes the sum of squares difference across a set of curves (natural spline based used here). Proteins that do not change in response to IGF-1 stimulation will likely fit the null hypothesis. However, this method may also miss proteins that change in response to IGF-1 stimulation but only briefly for a single time point. For a more detailed explanation of the algorithms used and splines in general, see [172, 182]. The spline-based method can be used for a single biological group and therefore was valuable in analyzing our averaged $\log_2$ ratios. Using a p-value cutoff of 0.10 from the expression analysis in EDGE, temporal expression profiles of 20 proteins showed significance. Proteins with ambiguous descriptions, such as two heat shock proteins that showed significance, are herein described as HSPA8 and HSPA1L –the gene symbol notations of the closest homologue from a UniprotKB BLAST result sharing the same group of peptides (for all IPI accession numbers, gene symbol notations used, and $\log_2$ values, including those imputed, see the supporting material). Mean $\log_2$ profiles of the 20 EDGE-significant proteins are individually plotted in Fig. 2.5, along with their representative p-values, and the k-means cluster they appeared in (designated by line color).

While means were used for constructing profiles and assessing temporal significance, only the SEM of proteins with successful relative expression in ≥ 2 replicates (9/20 proteins) was retrieved (error bars, Fig. 2.5). SEM at individual time-points varied depending on the protein, but the majority of the means, where SEM could be calculated, showed significantly different expression after 24 h. For example, the mean $\log_2$ ratio at 24 h among the EDGE-significant proteins was 1.44 with a SEM of 0.30. Some proteins showed very clear temporal changes, such as CSRP1, LDHA, and CTSD, with low SEM at all time-

points (Fig. 2.5). It is also worth noting that 19/20 EDGE-significant proteins showed an upward trend, most increasing the greatest from 12 to 24 h, with GDI1 and CTSD having shown a near linear increase. The exception to the temporally increasing trend was IDH2, which initially increased, then showed an overall steep downward trend after 24 h. All of the significant profiles were different from the general profile shapes in Fig. 2.2, which indicates the spline-based method selected proteins with relative expression different from the mean temporal profiles. The spline-based method also showed promise for selecting proteins that fit a continuous curve function, which is an appropriate model for proteins that showed real expression changes, rather than those that changed non-continuously, by being modified, re-localized, or exported. For example, some proteins in our dataset, like the Rab proteins grouped in KMC-1 (Fig. 2.4), showed a sharp increase between 6 and 12 h, yet EDGE analysis did not show their significance ($p \leq 0.1$). This may be a result of these specific Rab expression profiles fitting poorly to the spline-based, alternative hypothesis curve because the observed differential expression may have been an artifact of a sub-cellular re-localization. Rab profiles showed a variable change between 6 and 12 h, but otherwise the profiles are flatter, perhaps fitting better to the null (flat) hypothesis than the alternate (spline based curve). Proteins showing EDGE significance are likely to have changed in expression if they display a consistent temporal change and, consequently, a better fit to the alternate hypothesis. The mean EDGE p-values (p_{mean}) for the proteins in each cluster are shown in Fig. 2.4 and they imply that proteins in KMC-1, on average, were closest to approaching EDGE-significance.

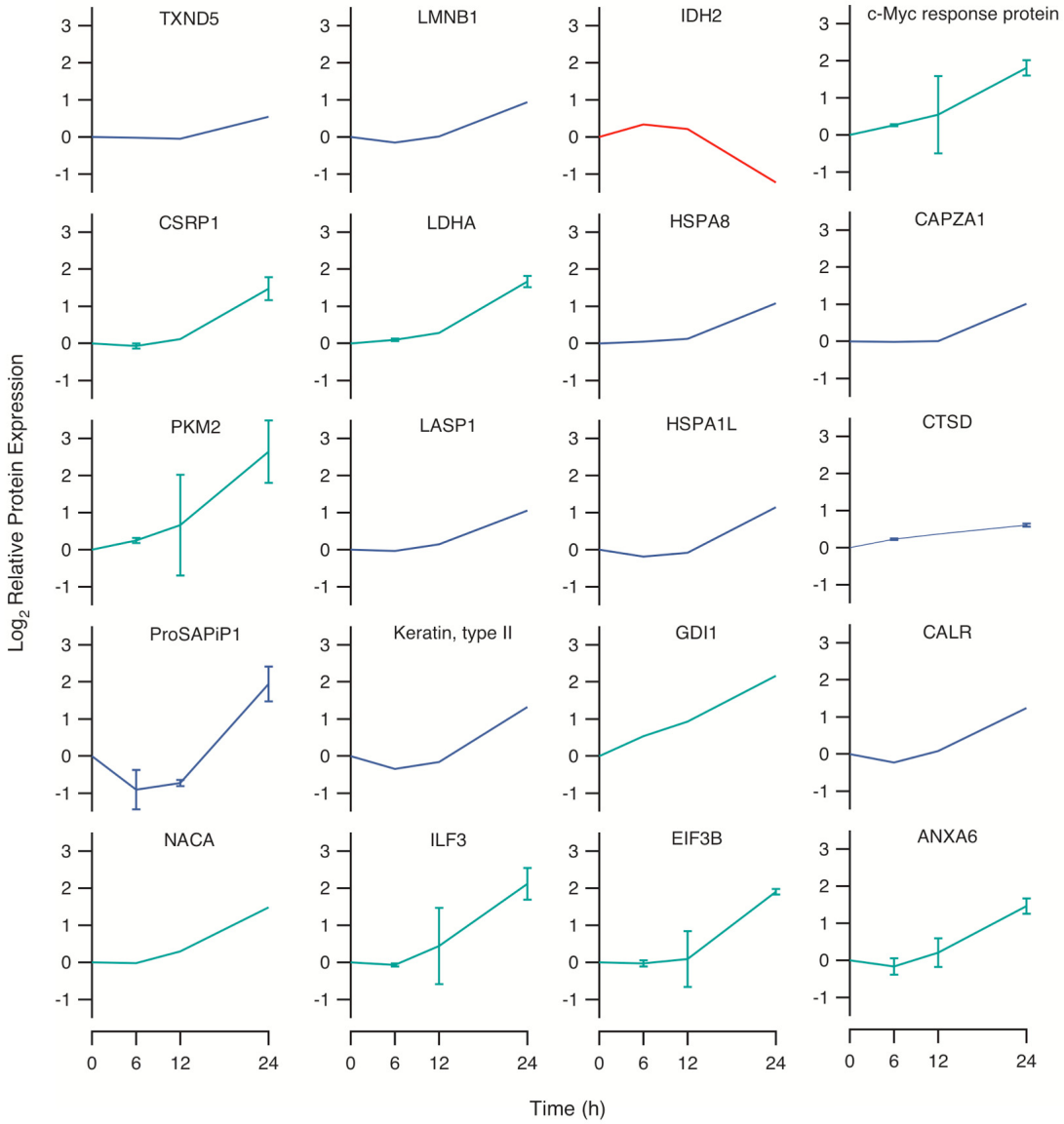

Figure 2.5. Temporal Profiles of EDGE Significant Proteins. Twenty profiles showing significance ($p \leq 0.1$) with EDGE are shown versus time. Error bars are shown for the 9/20 proteins where SEM could be retrieved, while those without error bars were quantified in only one biological replicate. Most profiles increased after 24 h, with the exception of IDH2. (TXNDC5 - thioredoxin domain-containing protein 5, LMNB1 – lamin B1, IDH2 – isocitrate dehydogenase II, CSRP1 – cysteine and glycine-rich protein, LDHA – lactate dehydrogenase A, HSPA8 – heat shock cognate 70 protein A8, CAPZA1 - F-actin capping protein subunit alpha-1, PKM2 – pyruvate kinase M1/M2, LASP1 – LIM and SH3 domain protein 1, HSPA1L – Heat shock protein 1L, CTSD – cathepsin D, ProSAPiP1 - Uncharacterized protein KIAA0552, GDI1 - guanine dissociation inhibitor I, CALR – calreticulin, NACA – nascent polypeptide-associated complex subunit alpha, ILF3 - interleukin enhancer-binding factor 3, EIF3B - eukaryotic translation initiation factor 3 subunit B, ANXA6 – annexin A6). Line

colors represent the k-means cluster that the protein was grouped in (green = KMC-1, red = KMC-2, blue = KMC-3).

2.3.4 Validation of EDGE Significant Proteins by Quantitative MRM

As mentioned above, when using a shotgun proteomics approach, incomplete overlap between replicates complicates quantification. Therefore, we used an MRM approach to improve the reproducibility. MRM also provided more precise measurements, which facilitated measurement of more subtle changes in protein expression. High specificity was also achieved since MRM is a tandem MS measurement allowing for the use of 1D-LC instead of 2D-LC, thus improving throughput. To validate significantly changing proteins (in 3 replicates) and develop a rapid assay for future IGF-1R network perturbation experiments, we employed MRM with one dimension of LC separation in combination with isotopic dimethyl labelling [183]. The advantage of the dimethyl labelling technique for our purposes is the presence of intense and predictable a_1 and y_{n-1} fragment ions [184]. To narrow our list of candidates, proteins with EDGE p-values ≤ 0.05 (rather than 0.1) were selected for further validation. MRM analysis of calculated dimethyl labelled (parent → a_1/y_{n-1}) transitions for *in silico* predicted, as well as empirically derived, peptides for these 12 proteins, resulted in dimethyl labelled transitions generating acceptable peaks (S/N > 10 and equal RT for both transitions) for 62 peptides. Peaks were verified as true peptides through the use of MRM initiated MS/MS, where 22 of the 62 transitions were positively identified as peptides with Mascot, representing 8/12 proteins (6 proteins ≥ 2 peptides). In a single MRM method, the successful peptide transitions (along with their expected retention times) provided accurate relative quantitation for 6 of the EDGE-significant proteins with at least 2 peptides. Our MRM method, optimized for the 6 successfully verified proteins was then used to compare 24 and 0 IGF-1 treatments in the original iTRAQ discovery experiment. The resulting $\log_2$ ratios (24h:0h) of integrated MRM chromatogram peak areas are plotted in Fig. 2.6. The MRM approach provided improved precision (mean SEM of 0.1) compared to iTRAQ analysis (mean SEM of 0.6). Peptide $\log_2$ ratios within four of these proteins – HSPA8, LDHA, NACA, and CTSD – were consistent, however $\log_2$ ratios from HSPA1L protein and PKM2 varied considerably (Fig. 2.6). The mean peptide ratios for these four proteins also agreed well with the iTRAQ ratios from the

discovery phase (Fig. 2.6), with the exception of HSPA8, which may have been different as a result of it being reported from a single biological replicate in the discovery phase.

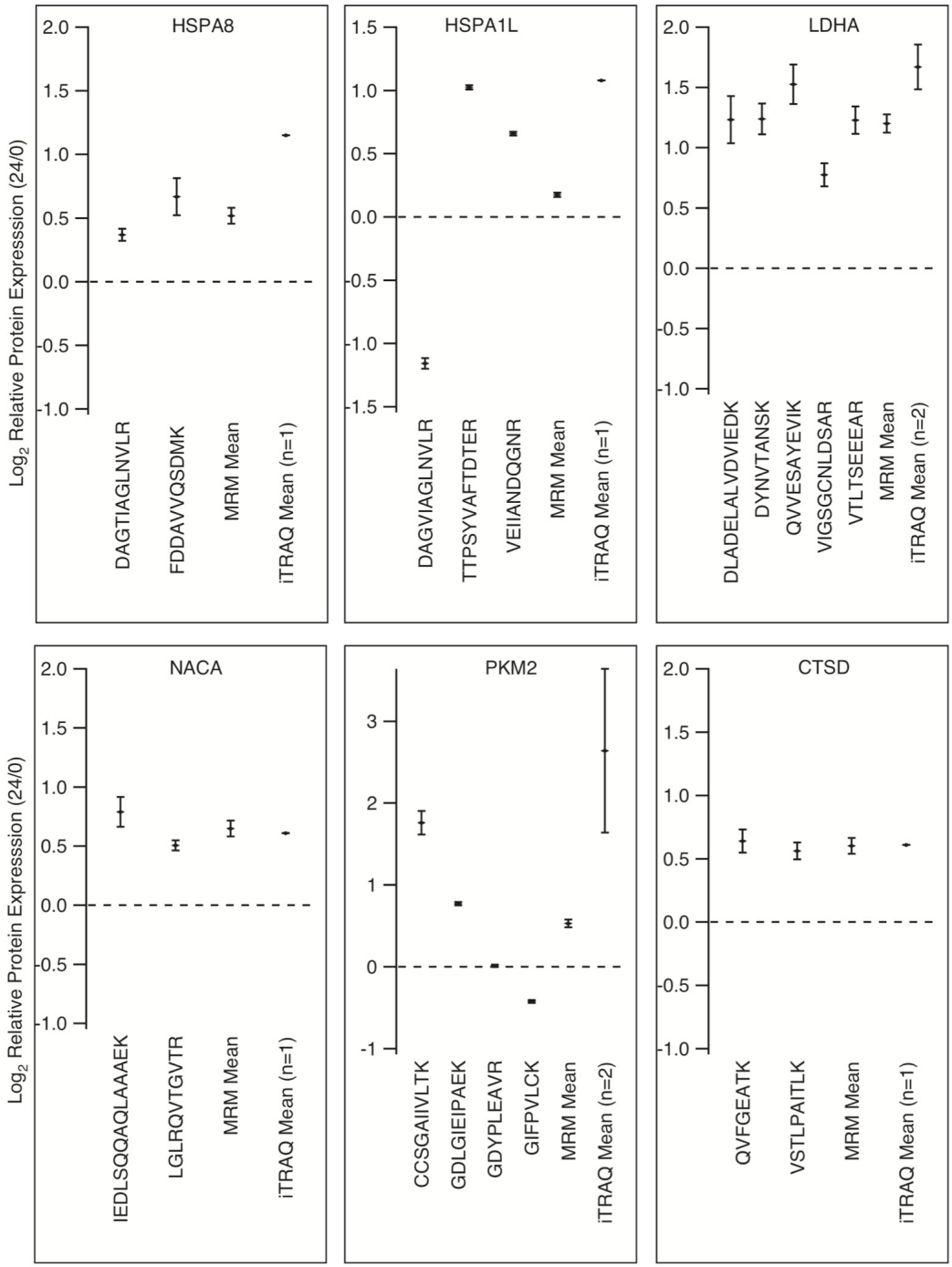

Figure 2.6. Peptides from EDGE Significant Proteins Successfully Assayed Using LC-MRM. Shown for each peptide are the $\log_2$ ratios (±SEM) of the 24/0 h time periods (n=3). Protein means calculated from these peptides are shown in the right of each pane adjacent to the original mean from the iTRAQ analysis. (LDHA – lactate dehydrogenase A, HSPA8 – heat shock cognate 70 protein A8, HSPA1L – Heat shock protein 1L, PKM2 – pyruvate

kinase M1/M2, CTSD – cathepsin D, NACA – nascent polypeptide-associated complex subunit alpha).

2.4 Discussion

Time course measurement of relative protein expression, followed by two separate data analysis methods (KMC and EDGE) has revealed changes in various functional groups of proteins after stimulation of MCF-7 cells with IGF-1. These changes include proteins involved in Rab GTPase activity, coated vesicle trafficking, glycolysis, and cell stress, functions with previously demonstrated involvement with cancer cell proliferation [166, 185, 186]. Our work suggests that these processes are modulated through activation of the IGF-1R network in MCF-7 cells and we have designed MRM assays to follow these changes in a high-throughput manner following perturbation of various IGF-1R network nodes.

2.4.1 Increased Vesicle Trafficking Regulation

The GO terms associated with the group of proteins in KMC-1 (Fig. 2.4) suggest an increase in proteins involved in GTPase regulated trafficking of coated vesicles. Proteins in the cluster that contribute to these resulting over-represented GO terms include 12 Rab proteins, as well as guanine dissociation inhibitors (GDI1 and GDI2), IQGAP1, COPE, and VAPB. Rab proteins are a group of proteins that are activated by exchanging GDP for GTP, a process that is regulated by GDI and GAP proteins (GDI1, GDI2, and IQGAP1 here) [187]. COPE and VAPB are both associated with vesicle transport between the ER and Golgi apparatus [188]: with VAPB mutations commonly linked to motor-neural diseases [189]. Since cycling of regulatory proteins by vesicle trafficking occurs between membrane, ER, and cytosolic compartments [190], our observed increase in trafficking activity may be the result of vesicle associated proteins returning to the cytosol. It is therefore difficult to elucidate whether the change in abundance is due to changes in protein expression or sub-cellular re-localization, both of which may be important. Several members of the Rab group of proteins identified in our dataset do not follow this increasing trend over time and are distributed between KMC-4 and KMC-5 (Fig. 2.4). This observation suggests specific Rab proteins may regulate vesicle trafficking in response to IGF-1R and perhaps RTKs in general, while others, such as

those in KMC-4 and KMC-5, do not. This observation agrees with previous work showing high functional specificity among Rab family members[191,192]. Increased regulation of trafficking downstream of IGF-1R activation suggests the possibility that cell surface receptors were internalized over time. Internalization of surface receptors, can act as a feedback mechanism to attenuate signalling, or to facilitate signal transduction from endosomes [193, 194]. While not directly observed in our experiments, internalization of IGF-1R, has been shown to be essential for activation of the MAPK pathway [195].

2.4.2 Altered Metabolic and Cell Stress Proteins

Since part of the functions of growth factors are to regulate metabolism[196] it is not surprising that of the 20 proteins called significant with EDGE (Fig. 2.5), three (IDH2, PKM2, and LDHA), with respective mean $\log_2$ ratios of -1.2, 2.6, and 1.7 after 24 h stimulation, are metabolic proteins. IDH2 has metabolic functions localized to the mitochondria and such localization changes over time may explain our observed decreases in relative expression observed in our cytosolic samples after IGF-1 stimulation. Levels of glycolytic proteins, such as PKM2, are often increased in tumours, where they are involved in the metabolic switch to preferential use of aerobic glycolysis [197], and are under the control of Ras pathways[198]. Paradoxically, PKM2 can also cause apoptosis upon translocation to the nucleus[25]. LDHA is normally constitutively expressed, catalyzing the inter-conversion of pyruvate and lactate, but has been shown to be over-expressed in highly proliferative cancer cells, where it generates NAD+ for subsequent cycles of glycolysis, producing lactic acid in the process [199]. Specifically in MCF-7 cells, LDHA activity has shown induction by estradiol, an effect that is inhibited by the cancer drug, tamoxifen [200]. Glycolytic proteins are of considerable relevance in therapeutic target design and as prognostic indicators, as tumours resulting from oncogenic mutations show enhanced glycolytic phenotypes [201].

Stress response proteins such as heat shock proteins are commonly over-expressed in perturbed cellular systems [202], and here we have found HSPA8, HSPA1L, and CTSD (respective mean $\log_2$ ratios of 1.2, 1.1, and 0.6 after 24 h stimulation) to be increasing over 24 h of IGF-1 stimulation. Heat shock proteins are associated with proper protein folding [203, 204], are involved in mitotic/spindle formation, and accumulate in large amounts in

cancer cells [205, 206]. CTSD is an aspartic protease involved in stress response, has recently shown to be a mitogen in pro-apoptotic in cancer cells [207], and therefore shows potential as a breast cancer biomarker[208].

2.4.3 Other EDGE-significant Proteins

Transcription and translation are typically increased in response to growth factor stimulation, and, in our case, the transcription/translation related proteins NACA, EIF3B, ILF3, and c-Myc response protein Rcl, all showed increased relative expression (respective mean $\log_2$ ratios of 1.5, 1.9, 2.1, and 1.8) after 24 h stimulation. NACA has been shown to interact with newly formed polypeptides, contribute to transcriptional co-activation [209, 210], and interact with c-Jun transcription factors, to stimulate protein import [211]. Through involvement in protein import, NACA exerts an effect on proliferation and apoptosis [212]. EIF3B, a component of cellular translational machinery, contributes to increased cell growth, facilitating a parallel increase in protein synthesis and is often present at high levels in breast cancer cells [213]. ILF3 is a double-stranded RNA binding protein, which has been shown to regulate the transcription of genes involved in cell cycle inhibition - genes that, if expressed, lead to increased cell proliferation and inhibition of apoptosis [214]. c-Myc transcription factors regulate expression of proteins (in our case, c-Myc response protein Rcl) which may then be involved in cell proliferation, differentiation, and apoptosis leading to increased tumour growth [215].

A number of EDGE-significant proteins (Fig. 2.5) are associated with cell morphology or structure; TXNDC5, CAPZA1, type II Keratin, LASP1, and LMNB1 (respective mean $\log_2$ ratios of 0.6, 1.0, 1.3, 1.1, and 0.9 after 24 h stimulation). TXNDC5, a suspected structural protein, has been shown to be significantly up-regulated in colorectal [216] and hepatocellular carcinoma [217] while CAPZA1, is involved in actin filament regulation, thereby exerting effects on cell structure [218]. Type II keratin is a major constituent of intermediate filaments, which make up the cytoskeletal structure and LASP1 is an actin-binding protein involved in focal adhesion and cell migration [219]. LMNB1 is responsible for the integrity of the nuclear lamina, a nuclear structural component that of which degradation is correlated with apoptosis [220]. The observed increase in LMNB1 in our experiments suggests its involvement with, IGF-1R directed, anti-apoptotic activity.

The levels of several scaffolding and signalling proteins, likely related to IGF-1R signalling or part of cross-talk between pathways, were also shown be significantly increased in our experiments: ProSAPiP1, CSRP1, CALR, ANXA6, and GDI1 (respective mean $\log_2$ ratios of 1.9, 1.5, 1.2, 1.5, and 2.2 after 24 h stimulation). ProSAPiP1 is a poorly characterized, putative interaction partner of a major scaffolding protein ProSAP – a protein mainly thought to be involved in linking RAP-GAP proteins to scaffolding proteins in brain synapses [221]. To our knowledge, expression of ProSAP in breast cancer cells has not before been reported, but may serve a similar scaffolding purpose in IGF-1R related signalling in MCF-7 cells as those involved in synaptic signalling. CSRP1, which increased temporally with IGF-1 stimulation, is a member of the LIM domain family, and has been shown to be a key component of Wnt signalling, controlling cell morphology and other dynamic cell behaviours [222]. CALR is involved in Ca^{2+} homeostasis [223] and Ca^{2+} is involved in signalling related to such processes as apoptosis and cell death [224] - a possible link between our observed increased CALR expression with IGF-1R signalling and apoptosis. ANXA6, which increased, also shows a connection to CALR since ANXA6 activity is Ca^{2+}-dependent. ANXA6 is a GTP-binding protein involved in Ras protein inactivation through recruitment of p120 Ras GTPase activating protein to the membrane, and ANXA6 expression is negatively correlated with cell cycle progression [225]. GDI1, is involved in escorting and cycling Rab proteins (involved in vesicular trafficking) through intracellular locations [226].

2.4.4 Verified Proteins by MRM

In a 1D-LC-MRM assay, with peptide retention times derived from an initial MRM-triggered MS/MS experiment, we were able to verify and validate peptides from 6 out of 12 EDGE-significant proteins for further perturbation experiments (Fig. 2.6). Despite the high specificity of MRM, some transitions exhibited multiple peaks. In these cases, MRM-triggered MS/MS spectra were acquired in order to unambiguously assign retention times to true peptide peaks [227]. Peptides unique to specific protein isoforms (signature peptides) were demonstrated to be very important in the selection of peptides to monitor by MRM. This was evident by the inconsistent peptide ratios in cases where peptides used were shared among homologous proteins. To illustrate this, BLAST searches of the peptides we measured for HSPA1L and PKM2 revealed these peptides are shared among members of

their respective protein families. The peptide DAGVIAGLNVLR is shared between HSPA1 and A1L, TTPSYVAFTDTER is shared among HSPA1, A2, and A6-8, and VEIIANDQGNR is shared among HSPA1, HSPA1L, HSPA2, HSPA5, and HSPA8. Since we were unable to quantify unique peptides from these proteins, validation of relative expression changes specific to members of the HSPA group was not possible. BLAST searches of the peptides from the HSPA8, LDHA, NACA, and CTSD revealed that the measured peptides were unique to those proteins, perhaps explaining the more consistent measurements for their peptides. HSPA8, HSPA1L, and PKM2 showed differences between the mean of the peptide ratios from the iTRAQ discovery phase analysis, and that of the verification experiments, as shown adjacent to the peptides in Fig. 2.6. This discrepancy occurred because some of the peptides were not detected using only one dimension of separation. Since peptide uniqueness is an issue for these proteins, differences in the peptides measured by the two approaches are reflected in the mean ratios.

In the case of PKM2, the peptide CCSGAIIVLTK is specific to the M2 isoform, GDYPLEAVR and GIFPVLCK are shared between M1 and M2, and GDLGIEIPAEK is shared among PKM1,M2,R, and L. The relative expression change after 24 h - 1.8 - of the unique PKM2 peptide, CCSGAIIVLTK (Fig. 2.6), showed that relative expression changes appeared to be specific to the M2 isoform of pyruvate kinase. Recent work has shown the M2 isoform of pyruvate kinase to be very important in tumour metabolism and growth [19]. Using an MRM approach to target the signature peptide may be useful to monitor the M2 pyruvate kinase isoform during perturbation experiments directly related to cancer cell metabolism. This type of targeted analysis of signature peptides is an excellent method for measuring relative expression of protein isoforms, and has been used to date in successful quantification of alcohol dehydrogenase isoenzymes [228] as well as P450 isoforms [229].

2.5 Conclusion

Our comprehensive 2D-LC-MS/MS analysis of the temporal changes in relative protein expression is part of our broader strategy to understand the proteomic changes

downstream of IGF-1R signalling. Through this quantitative proteomics approach, using iTRAQ followed by two statistical analyses, we have observed major increases in vesicle trafficking activity as well as specific proteins involved in altered metabolism and cell stress in response to IGF-1R stimulation of MCF-7 breast adenocarcinoma cells. Using targeted MRM, we have validated the changes of several of these proteins and, for other proteins, we have observed differences in relative expression among peptides. We believe these differences to be biologically relevant as they pertain to measurable abundance changes in M2 pyruvate kinase isoform in MCF-7 cells. For future work, monitoring glycolysis by assaying PKM2, LDHA and other glycolytic proteins, is necessary to explore the changes in glycolysis as a whole in response to IGF-1 stimulation. Functional trends changing over time and proteins with differential relative expression have provided insight into mechanistic actions relating IGF-1R to cancer. Upon further verification, the proteins in this work may also be useful as therapeutic targets for, or biomarkers indicative of, pathogenesis where dysregulated IGF-1R is involved.

Chapter 3: Targeted Proteomic Analysis of Glycolysis in Cancer Cells[3]

Abstract

Altered expression of glycolysis proteins is an important yet poorly understood characteristic of cancer. To better understand the glycolytic changes during tumourigenesis, we designed a liquid chromatography multiple reaction monitoring (LC-MRM) assay targeting the "glycolysis proteome" in MCF-7 breast cancer cells, using isotope-coded dimethylation of peptides for relative quantification. *In silico,* dimethyl labelled tryptic peptides $[M+2H]^{2+}$ (of length n) and their y_{n-1} fragment ions were determined based on UniprotKB database sequence entries for glycolysis proteins, related branching pathways, and reference proteins. Using predicted transitions ($[M+2H]^{2+} \rightarrow y_{n-1}$), MRM-initiated detection and sequencing (MIDAS) was performed on a dimethyl-labelled, tryptic digest from MCF-7 cells, using two-dimensional liquid chromatography mass spectrometry analysis. Three transitions for each peptide were selected from identified spectra, and assessed using 1D-LC-MRM-MS. Collision energy (CE) and dwell times were optimized and matching transitions for "heavy" isotope-coded dimethylated peptides were calculated. Resulting LC-MRM transitions were then used to measure changes in the glycolytic proteome in insulin-like growth factor-1 (IGF-1)-stimulated MCF-7 cells and other breast cell lines. Increases in the expression of glycolysis proteins leading to lactic acid production were observed common to IGF-1-stimulated MCF-7 cells and the invasive MDA-MB-231 cell line. Preliminary analysis of lung tumours with varied states of differentiation demonstrated the clinical applicability of LC-MRM and showed increased levels of PGK1 in well differentiated tumours.

[3] Published; J. Patrick Murphy and Devanand M. Pinto. 2010. *J. Proteome Res.*; 10(2) 604-613. JPM and DPM are affiliated with Dalhousie Biology, Halifax, NS and the National Research Council Institute for Marine Biosciences, Halifax, NS.

3.1 Introduction

Glycolysis is highly conserved in nature and is a source of ATP and intermediates for amino acids, lipids, and nucleotides in proliferating cells [11]. Proliferative advantages conferred by increased use of the glycolysis pathway are closely tied to cancer as first proposed by Otto Warburg in the 1920's [230] and referred to as "the Warburg effect". The increased glucose consumption in tumours is now commonly used for tumour imaging by [^{18}F] fluoro-2-deoxyglucose positron emission tomography (^{18}FDG-PET) technology [128]. Several growth factor-related oncogenes and tumour suppressors such as *Ras* and *c*-Myc can alter the expression levels of glycolysis proteins [81, 126]. The pathway is also regulated through expression of alternate isoforms with different activities, such as isoform 2 of hexokinase (HK2) [13], and the M2 splice variant of pyruvate kinase [19, 198]. System-wide investigations into altered glycolysis protein expression in cancer cells have the potential to reveal novel therapeutic targets and serve as prognostic indicators.

To quantify the changes in pre-determined sets of proteins, like those of glycolysis, liquid chromatography multiple reaction monitoring (LC-MRM) is increasingly being used. Optional, affinity-based, approaches such as Western blots or enzyme-linked immunosorbent assays can be used but are time consuming and sensitive to non-specific binding effects[231]. Targeted proteomics, however, with LC-MRM enables quantification of 10's to 100's of peptides from sets of proteins in a single chromatographic period [120]. High specificity is achieved by monitoring multiple parent to product ion transitions for each peptide. The glycolysis proteome is particularly amenable to LC-MRM since the proteins are above the limit of detection by 1D-LC-MRM (~10 ng/mL complex digest) [125]. Proteomic subsets that have been targeted thus far include abundant proteins from human plasma [232], known virulence factors [233], and lists of proteins from discovery-based proteomics studies [234]. Targeted analysis by LC-MRM of a predetermined set of metabolic proteins has been conducted in yeast [119], but an analogous approach in cultured human cells has not been done.

Targeting predetermined proteins requires choosing optimal peptides and transitions to monitor for each peptide, chosen either computationally or empirically. Transition selection based on empirical data is considered the most reliable and can be

guided by techniques such as MRM-initiated detection and sequencing (MIDAS) [123]. Here, with the premise that y_{n-1} ions are consistently enhanced in dimethyl-labelled peptides [183, 184], we have predicted dimethyl labelled peptide transitions ($[M+2H]^{2+} \rightarrow y_{n-1}$) to sequence tryptic peptides of the glycolysis proteome by the MIDAS approach. We then selected and optimized transitions for an LC-MRM assay representing the stable isotope-labelled glycolysis proteome. To investigate some key features of glycolysis in cancer, we employed the assay to compare glycolysis proteomes of MCF-7 cells exposed to insulin-like growth factor -1 (IGF-1) to those left untreated for 24 h. We further surveyed the glycolysis proteomes of several cell lines, and the observed altered expression patterns suggest that glycolysis plays a role in invasion.

3.2 Experimental Procedures

3.2.1 Cell Culture and Protein Extraction

MCF-7, T47-D, MDA-MB-231, HeLa, and MCF10A cells were from the American Type Culture Collection and HMEC cells were from Lonza (Basel, Switzerland). MCF-7, T47-D, MDA-MB-231, and HeLa cells were cultured in DMEM (Invitrogen) 10% fetal bovine serum (FBS), at 5% CO_2. MCF10A cells were cultured in 1:1 DMEM:F12 media (Invitrogen) with 5% horse serum (Invitrogen), 20 mM HEPES, 10 ng/mL EGF (Invitrogen), 29.2 mg/mL L-glutamine, 10 µg/mL insulin (Invitrogen), 0.1 µg/mL Cholera toxin (Sigma-Aldrich) and 500 ng/mL hydrocortisone (Sigma-Aldrich). HMEC cells were grown using MEGM Bullet Kit (Lonza) without the SingleQuot vial containing antibiotics.

Cells were grown to ~70% confluency, washed with PBS, detached with 0.25% Trypsin/EDTA (Invitrogen), and pelleted by centrifugation at 2,000 x g for 5 min. Supernatants were discarded, cell pellets were washed twice with PBS, and collected by centrifugation at 2,000 x g for 2 min. Cells were lysed in 500 mM tri-ethyl ammonium bicarbonate (TEAB) buffer (pH 8.5) (Sigma-Aldrich) (1 mL per ~3.0×10^6 cells) by passing through a 21 G 1.5 needle 20 times. The cytosolic fraction was clarified by centrifugation at 110,000 x g for 1 h, and total protein concentration in this fraction was estimated using a Bradford assay [169] with BSA as a standard.

3.2.2 Digestion and Dimethyl Labelling

All protein samples were reduced with 5 mM DTT, alkylated with 12 mM iodoacetamide, and digested overnight by reacting 50 µg protein/µg trypsin (Promega) at 37°C. Derivatization was carried out as described previously[18]. Briefly, peptide primary amine groups were converted to their dimethyl derivatives using either 100 µM CH_2O or 100 µM CD_2O per 100 µg of total protein for 5 min followed by reaction with an equimolar amount of 6M $NaCNBH_3$ for 2 h. The reaction adds 28 Da (M+28) or 32 Da (M+32) respectively to each amino group. Labelled samples were acidified by adding TFA to a final concentration of 0.1%, then desalted using C18 SepPak Light cartridges (Waters), dried in a vacuum centrifuge, and stored in 5% acetonitrile (ACN) (0.1% formic acid) at -40°C.
Safety considerations: formaldehyde is toxic and should be handled in a fume hood.

3.2.3 Target Peptide Set Selection

The target set of proteins included the core enzymes of glycolysis and related proteins of branching metabolic pathways taken from pertinent literature [30, 235, 236]. Accession numbers for all isoforms and splice variants for the chosen protein set as well as, the common reference proteins, β-actin (ACTAB), Ribosomal protein S6 (RLPL0), Peptidyl-prolyl cis-trans isomerase A (PPIA), β-tubulin, (TUBB) and TATA binding protein (TBP) were retrieved from the UniprotKB human database (http://www.uniprot.org/) (Table 3.1). Selection of proteins was restricted to the cytosolic form, if so stated by the Uniprot entry, and only "reviewed" entries were selected. The protein IPI number for each Uniprot entry was submitted to a searchable database containing the m/z for parent ($[M+2H]^{2+}$) and y_{n-1} ions for dimethylated tryptic peptides (http://rita.imb.nrc.ca/~spenny/mrm/mrm_predict.php). The resulting peptide list was filtered to exclude peptides with a high propensity for missed cleavages or with an m/z that did not fall between 450 and 1000.

3.2.4 MIDAS Product Ion Generation

An aliquot from MCF-7 cells (~1.5 x 10^6), containing 600 ug of cytosolic protein, was digested, desalted, labelled M+28 (described above), dried in a vacuum centrifuge and re-suspended in 100 µL of 10 mM ammonium formate (25% ACN, pH 2.8). Peptides were

separated by strong cation exchange (SCX) separation as described previously [234]. Fractions (600 µL) were collected every 3 min from 12 to 48 min, dried, and re-suspended in 75 µL of 5% ACN, 0.1% formic acid. Using the predicted target transition list (described above), MIDAS of each SCX fraction was conducted using an Agilent 1100 capillary RP-HPLC coupled to a 4000 QTrap mass spectrometer (AB Sciex) equipped with a nano-electrospray source as described previously[234]. Each SCX fraction was injected 8 times with a unique batch of predicted MRM transitions in each injection (~100 transitions/acquisition), where acquisition parameters were as follows; 100 ms dwell time, collision energy (CE) = parent m/z ÷ 20, MRM intensity threshold of 1000 cps, 2 enhanced product ion scans using a rolling CE, and Q1/Q3 set to unit resolution.

3.2.5 Transition Selection for Target Proteins

MS/MS from MIDAS were searched against the IPI Human database (v3.59) using Protein Pilot (v3.0) (AB Sciex) with the following parameters: iodoacetamide cysteine alkylation, dimethyl labelling of lysine and N-termini as fixed modifications, Rapid ID, and a detected protein threshold of 0.05. Peptides identified from the target set were exported to MRM Pilot (v2.0) (AB Sciex). Additional, isoform-unique, peptides matching the target protein list, were retrieved from previously acquired two-dimensional liquid chromatography mass spectrometry datasets from complex digests of IGF-1 stimulated, iTRAQ labelled, MCF-7 cells [234] and manually added (in their dimethylated form) to the MRM Pilot transition list. The 3 most intense fragment ions from MIDAS-confirmed or additional peptides were used to represent the peptide.

Table 3.1. Target Set of Metabolic and Reference Proteins. Members of the target set include only the accession numbers for reviewed versions (as stated in Uniprot).

Protein Group	Isoform	Uniprot Accession Number
Core Glycolysis		
Hexokinase	HK1(1-4), HK2, HK3, GCK, HKDC1	P19367(1-4), P52789, P52790, P35557-1, Q2TB90-1
Glucose-6-phosphate isomerase	GPI	P06744
Phosphofructokinase	PFKL(1&2), PFKM(1&2), PFKP	P17858(1&2), P08237(1&2), Q01813
Aldolase	ALDOA, ALDOB, ALDOC	P04075, P05062, P09972
Triosephosphate isomerase	TPI1(1&2)	P60174(1&2)
Glyceraldehyde-3-phosphate dehydrogenase	GAPDH, GAPDHS	P04406, O14556
Phosphoglycerate kinase	PGK1, PGK2	P00558, P07205
Phosphoglycerate mutase	PGAM1, PGAM2, PGAM4, PGAM5(1&2)	P18669, P15259, Q8N0Y7, Q96HS1(1&2)
Enolase	ENO1, ENO2, ENO3	P06733(1&2), P09104, P13929
Pyruvate kinase	PKM1/M2, PKLR	P14618(1&2), P30613(1&2)
Glycolysis Regulation		
Fructose-1,6-bisphosphatase	FBP1, FBP2	P09467, O00757
6-phosphofructo-2-kinase/fructose-2,6-bisphosphatase	PFKFB1, PFKFB2, PFKFB3, PFKFB4	P16118, O60825(1&2), Q16875(1&2), Q16877
TP53-induced glycolysis and apoptosis regulator	TIGAR	Q9NQ88
Pentose Phosphate Pathways and Other Metabolism		
Glucose-6-phosphate 1-dehydrogenase	G6PD(1-3)	P11413(1-3)
Lactate dehydrogenase	LDHA, LDHB, LDHC, LDHD, LDHAL6A, LDHAL6B	P00338(1&2), P07195, P07864, Q86WU2(1&2), Q6ZMR3, Q9BYZ2
ATP-citrate lyase	ACL	P53396
Fatty acid synthase	FASN	P49327
Isocitrate dehydrogenase, cytosolic	IDH1	O75874
Malate dehydrogenase	MDH1	P40925
Malic enzyme, cytosolic	ME1	P14863
Carbamoyl phosphate synthase aspartate-carbamoyltransferase dihydroorotase	CAD	P27708
Reference Proteins		
Beta Actin	ACTAB	P60709
60S Ribosomal Protein	RLPL0	P05388
Peptidyl-prolyl cis-trans isomerase A	PPIA	P62937
Tubulin beta chain	TUBB	P07437
14-3-3 protein zeta/delta	YWHAZ	P63104

3.2.6 LC-MRM Evaluation and Optimization

An aliquot of protein (~200 μg) was digested, labelled, desalted, dried (as above) and resuspended in 5% ACN (0.1% formic acid). Reversed phase chromatography was performed as previously described [234] except a monolithic 200 μm x 150 mm column (EMD4 Biosciences) was used at a flow rate of 5 μL/min, injection volumes were 6 μL and a shallower gradient (5-30% mobile phase B in 50 min) was employed to maximize chromatographic resolution. The MRM Pilot transitions were divided into 5 lists and each was used for a separate injection. Initial MRM transitions were assessed using 50 ms dwell time, 0 ms settling time, CE = parent m/z ÷ 20, declustering potential = 70, and Q1/Q3 set to unit resolution. Integration of MRM chromatograms and S:N calculations were conducted using Multiquant (v.1.2) (AB Sciex) using the following parameters; smoothing width = 1 point, retention time half window = 30 s, min peak width = 3 points, min peak height = 0, noise percentage = 40%, baseline subtract window = 2 min, and peak splitting factor = 1 point. Peptides were selected for further optimization if their selected transitions co-eluted at a single retention time with an S:N > 10:1. Peptides with an S:N < 10:1 for the selected transitions were re-acquired using 250 ms dwell time, and re-assessed for co-elution and an S:N > 10:1. For peptides with transitions of suitable S:N using either 50 ms or 250 ms, dwell times were normalized to an S:N of 50:1. The minimum and maximum dwell times were 5 ms and 100 ms respectively. Using normalized dwell times, MRM transitions were re-acquired with CE's over a range of +/- 10 eV from their original value in 2 eV increments in order to establish the optimal CE for each transition. An overview of the MIDAS workflow for MRM generation is shown in Fig. 3.1. M+32 transitions were calculated to match the optimized M+28 transitions and 5 LC-MRM acquisition methods of approximately equal cycle times (~3.5 s) were formed (Appendix A) for quantitative analysis of each peptide. Identical CE and dwell times (as optimized) were used for M+32-M+28 transition pairs.

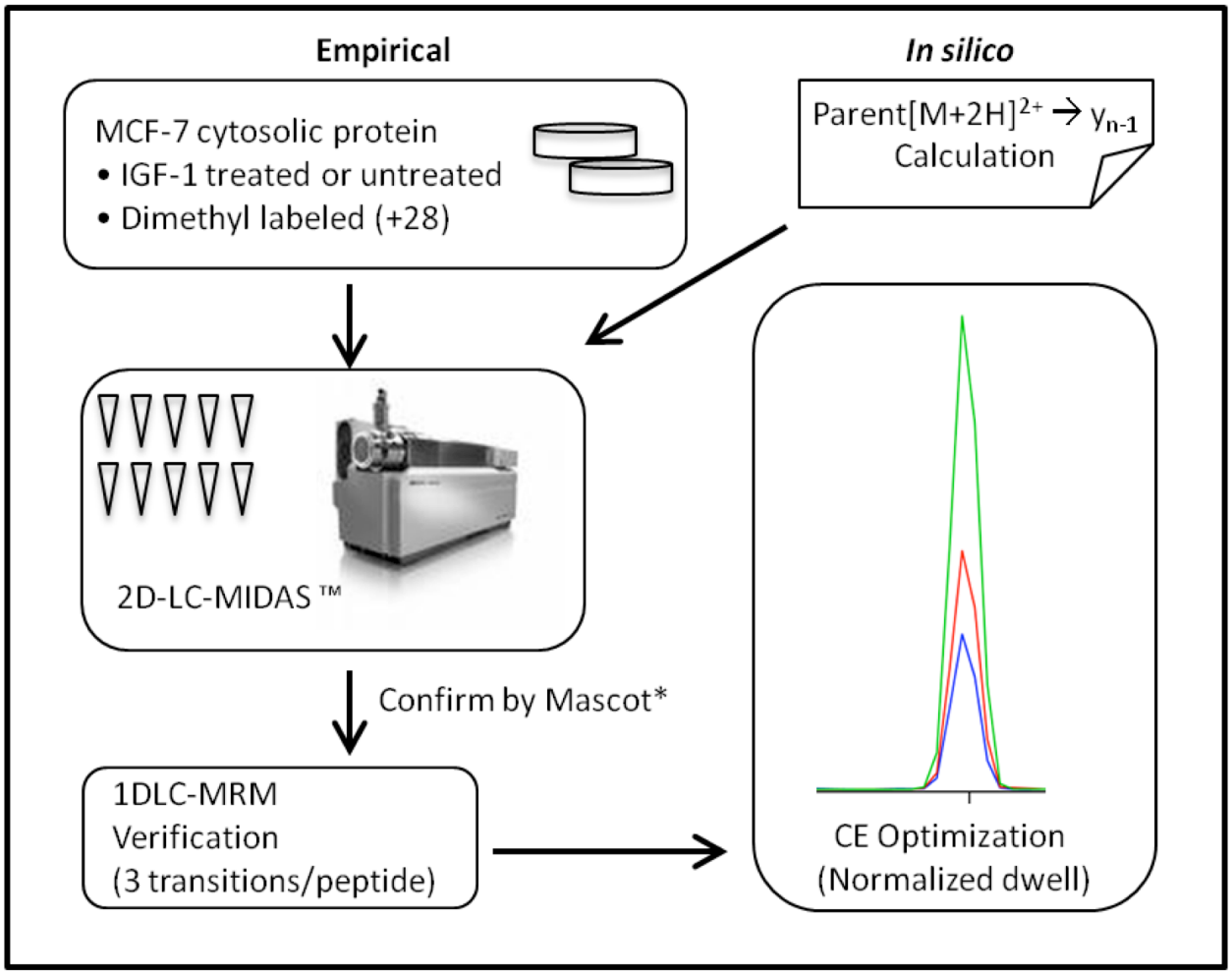

Figure 3.1. Overview of MRM Assay Design by MIDAS. For proteins in Table I, parent → y_{n-1} transitions were predicted for $[M + 2H]^{2+}$ dimethyl labelled tryptic peptides ($450 < m/z < 1000$). Using these transitions, MIDAS was conducted on 10 SCX fractions from a complex digest of dimethyl-labelled peptides from MCF-7 cells. Peptide identifications were confirmed by searching MS/MS from each fraction against the IPI Human database (v3.59) using Protein Pilot. For each confirmed peptide, 3 transitions were selected for validation by MRM analysis, as in Fig. 3.2. Dwell times were adjusted by normalizing each transition to a target S:N of 50:1, then CE was optimized for each transition.

3.2.7 Relative Quantitative LC-MRM of IGF-1 Exposure

In triplicate, MCF-7 cells were serum starved for 48 h, then treated with 100 ng/mL IGF-1 or left untreated for 24 h. Aliquots of IGF-1-treated and untreated samples (100 µg) were digested, labelled M+32 (described above), and combined equally with a reference sample (100 µg) composed of a pool of the untreated, M+28 labelled samples. The mixture

was desalted (as above), and suspended in 100 µL of 5% ACN (0.1% formic acid). Each sample was injected three times with each of the 5 optimized LC-MRM acquisition methods, using LC conditions and peak area integration parameters stated in the previous section. For statistical treatment, M+32:M+28 (Ctrl or IGF-1:Reference) peak area ratios were $\log_2$ transformed and a two-tailed, paired t-test ($\alpha = 0.5$) (paired between matching M+32:M+28 transitions) was conducted for each protein. Peptides shared between isoforms were excluded from the analysis. T-tests were implemented through the R statistical package (http://www.R-project.org).

3.2.8 Relative Quantitative LC-MRM of Various Cell Lines

Aliquots of cytosolic protein (60 µg) from MCF-7, MDA-MB-231, T-47D, MCF10A, HeLa, and HMEC cells were digested, labelled M+32, and desalted (as described above). Samples from all cell lines were combined with 60 µg of a complex digest from T-47D cells (labelled M+28). Mixtures were desalted, dried, and suspended in 5% ACN (0.1 % formic acid). Each cell line sample was injected with the 5 optimized LC-MRM acquisition methods (except transitions for FASN and MDH1), using LC conditions and peak area integration parameters stated previously for LC-MRM. Mean M+32:M+28 ratios for each protein were $\log_2$-transformed, normalized to the ratios for the reference proteins (excluding ß-actin) then expressed in relation to the HMEC cell line.

3.2.9 Clinical Analysis of Lung Cancer Biopsies

Lung tumour biopsies of various degrees of differentiation (5 poor, 3 medium, and 2 well) were snap frozen in liquid nitrogen and stored at -80°C until analysis. Sections of biopsies (~20 mg per patient sample) were weighed accurately then RNA, DNA, and protein were extracted with Trizol reagent (Invitrogen) according to the manufacturer's instructions. The resulting protein pellet was solubilized in 300 µL of 0.1% Rapigest by using a probe sonicator (Fisher Scientific, Fair Lawn, NJ) using 3, 10 s pulses. Samples were digested, labelled M+32, and desalted (as described above). An aliquot containing 50 µg of protein was taken from each patient sample and mixed with 20 µg of a complex digest from MCF-7 cells labelled M+28. The mixture was desalted, dried and resuspended in 50 µL of

5% ACN (0.1% formic acid) then analyzed using the optimized LC-MRM assay (as described above).

3.3 Results

3.3.1 Metabolic Proteome LC-MRM Assay Design

Targeted proteomics towards a set of pre-determined glycolysis proteins was performed. Use of *in silico*-predicted transitions to collect product ion spectra by a MIDAS workflow (Fig. 3.1), confirmed the identification of 109 peptides (MASCOT ion-score > 15) from our target protein set; ~12% of those predicted. An example of product ion acquisition (showing the intense y_{n-1} fragment ion, m/z = 1290.7) and subsequent verification of peptide transitions is illustrated by our analysis of the ENO1 peptide, YISPDQLADLYK, in Fig. 3.2. MIDAS-identified spectra have been converted using the PRoteomics IDEentifications database (PRIDE) converter [176] (http://code.google.com/p/pride-converter) and are available in the PRIDE database [177] (www.ebi.ac.uk/pride) under the accession number 12915. For additional coverage, a further 9 isoform-unique peptides from the targeted protein set, not identified by the MIDAS approach, were added from previously acquired shotgun datasets [234] totalling 118 peptides (Table 3.2). Evaluating the peptide transitions using 1D-LC-MRM resulted in the verification of 80 peptides (Table 3.2). This corresponds to a success rate of 68% of those peptides identified using 2D-LC-MS/MS (Table 3.2).

By normalizing dwell times to an S:N of 50:1, they were tailored to the transition intensity. This step was necessary since initial attempts to perform scheduled MRM acquisition based on calibrated retention times failed to provide sufficient dwell time for many low-intensity transitions co-eluting with more intense ones. Overall, from the entire set of 27 targeted proteins, successful peptide transitions were generated for 15 of the 22 proteins of glycolysis and related pathways, and 4 of the 5 reference proteins, as summarized in Table 3.2. The MIDAS approach was effective for targeting glycolysis proteins since successful transitions were generated for at least one isoform of the main glycolysis pathway except for hexokinases. For the proteins of glycolysis pathway alone, 43

of 64 peptides identified by MIDAS were detectable by LC-MRM (67%) compared to 39 of 107 peptides (36%) identified from a previous shotgun 2D-LC-MS/MS dataset (Fig. 3.3).

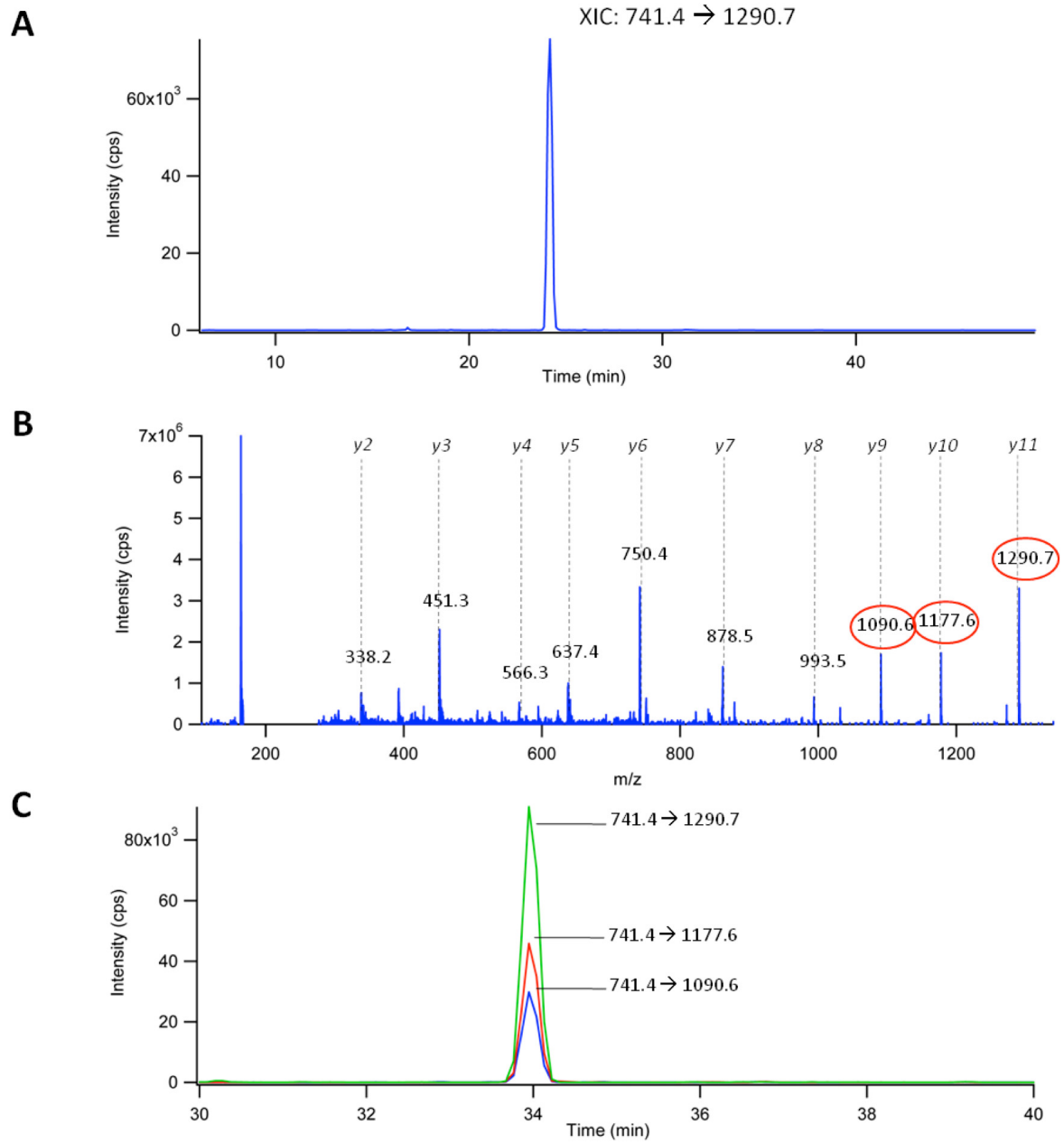

Figure 3.2. Selection of MRM Transitions for the ENO1 Peptide, YISPDQLADLYK ([M+2H]$^{2+}$=741.4). A) XIC of MRM chromatogram of the transition (741.4→1290.7) used to trigger MS/MS. B) MS/MS confirming the identification of YISPDQLADLYK and used to select 3 fragment ions for multiple transitions (*circled*). C) MRM chromatograms of the 3 transitions selected in B with optimized CE and normalized dwell times. MRM transitions for successfully confirmed peptides from the glycolysis proteome were all designed in the illustrated manner. Note: Different retention times between A and C are the result of a shallower gradient in C.

Table 3.2. Summary of Targeted Peptides for Each Protein Group at Various Stages of MRM Generation.

Protein Group	Predicted Peptides (m/z 450-1000, 2+)	Protein Mascot Score (2D-LC-MIDAS*)	ID'd Peptides (2D-LC-MIDAS*)	Verified (1D-LC-MRM)
Metabolic Proteins				
TPI	12	530	9	9
ENO	36	440	8	6
GPI	13	358	8	3
PGK	32	349	8	6
PKM	44	346	9	9
G6PD	25	291	7	5
FASN	72	258	13	5
GAPDH	15	163	4	2
ALDOA	30	132	5	5
PFK	55	128	5	4
FBP	19	109	3	3
LDH	67	106	6	6
PGAM	26	103	3	3
IDH1	17	87	3	0
HK	149	66	4	0
TKT	40	56	2	2
PFKBP	73	0	0	0
TIGAR	8	0	0	0
ACL	37	0	0	0
ME1	14	0	0	0
CAD	57	0	0	0
MDH1	9	70	2	2
Reference Proteins				
ACTAB	10	769	6	5
TUBB	11	305	2	0
PPIA	6	176	6	3
RPLP0	9	116	3	1
YWHAZ	5	79	2	1
Total	891	NA	117	80

*9 additional peptides were added from previous datasets

Besides the main glycolysis pathway, additional transitions were successfully generated for important proteins involved in diverting glycolytic flux to biosynthetic intermediates (G6PD, TKT, and LDHA) and 2 proteins involved in fatty acid synthesis and cycling of acetyl CoA (FASN and MDH1). The 7 proteins from the entire target list (Table 3.1) that were not detected by our analysis are perhaps expressed below our limits of detection or localized in sub-cellular compartments. Also, while peptides for all isoforms of each glycolysis protein were targeted, in most cases the identified peptides belonged to a specific isoform of the protein. Exceptions were the phosphofructokinases and enolases, of which peptides unique to PFKL, PFKP, ENO1, and ENO3 were identified.

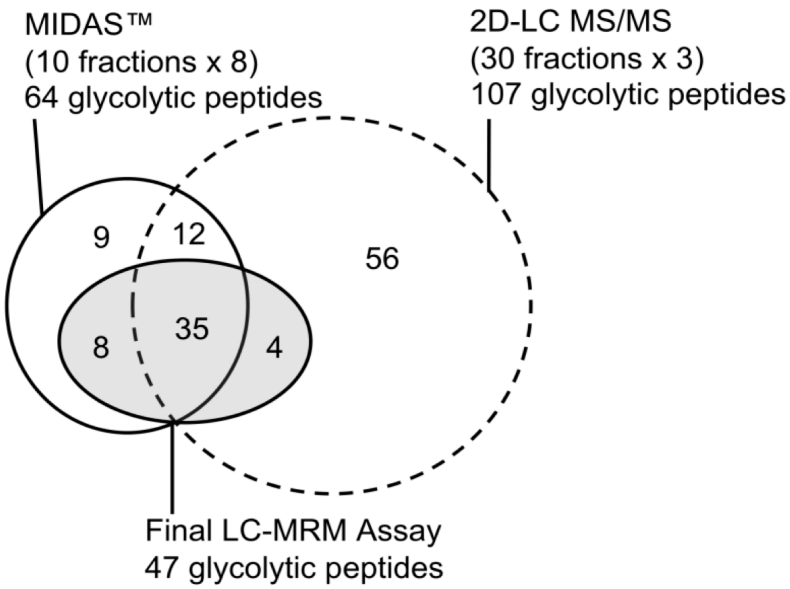

Figure 3.3. Comparison of the MIDAS Approach Versus non-targeted Shotgun Proteomics to Select MRM Transitions for Glycolysis Proteins. Previously acquired data from 2D-LC-MS/MS analysis (using 3 biological replicates) (*inside dotted circle*) generated many peptide identifications from the glycolysis pathway (107) of which 39 were detectable by 1D-LC-MRM (*shaded circle*). Data from the targeted, MIDAS approach (using 8 different injections) (*solid, un-shaded circle*) generated fewer peptide identifications from the glycolysis pathway (64) but 43 were detectable by LC-MRM.

3.3.2 Glycolytic Proteome Changes in Response to Growth Factor Exposure

Optimized LC-MRM transitions were employed to measure changes in glycolysis proteins in response to growth factor stimulation by exposing MCF-7 cells to IGF-1. After calculating the M+32 transitions (matching the M+28 transitions) for each peptide, the complete MRM analysis consisted of 480 transitions. These were split into 5 LC-MRM acquisition methods, which are downloadable (Appendix A) for direct import into Analyst (v1.4+) software (AB Sciex). MRM transitions for 20 of the peptides from the optimization experiment did not give sufficiently consistent S:N between the MRM optimization and experimental samples and were discarded from peak area comparisons. Use of LC-MRM for relative quantification of peptides is illustrated through the PKM1/M2 peptide, GIFPYLK, in Fig. 3.4A. Comparing both 24 h IGF-1 treated and un-treated MCF-7 samples to an equal amount of reference sample allowed for the assessment of significance using a paired t-test, where pairs were the M+28 and M+32 versions of each transition. Of note, the reference protein, β-Actin, was significantly up-regulated by IGF-1 exposure with a difference in $\log_2$ ratios between stimulated and un-stimulated cells - expressed as a "mean $\Delta\log_2$(ratio)" - of 0.92 ± 0.07. The mean $\Delta\log_2$(ratio) for all other reference proteins was much lower (0.61 ± 0.09), which better reflected overall protein content indicative of cell growth (data not shown). Due to observed differences between treated and untreated samples, β-Actin was discarded as reference protein. This observation is consistent with numerous studies that show that β-Actin levels increase in proliferating cells [237]. Overall, nearly all of the glycolytic proteome and closely associated proteins showed significant increases ($\alpha = 0.05$) in response to growth factor exposure, except for PFKL and PGAM1 (Fig. 3.4B). The greatest increases in proteins levels were observed for proteins near the final stages of glycolysis and lactate production – ENO1, PKM2, and LDHA (Fig. 3.4B). Using the mean $\Delta\log_2$(ratio) of the reference proteins (PPIA, RLPL0, and YWHAZ) as an indicator of overall cell growth and protein content (Fig. 3.4B), suggests ENO1, PKM2, and LDHA levels increased greater than overall growth of cells. Alternatively, the lowest mean $\Delta\log_2$(ratio) values were observed for PFKL and proteins directing carbon flux towards pentose phosphate pathways and gluconeogenesis (G6PD, TKT, and FBP1). Mean $\Delta\log_2$(ratio)

values were not significantly different (α = 0.05) for PFKL, FBP1, and TKT and therefore did not change in response to growth factor exposure.

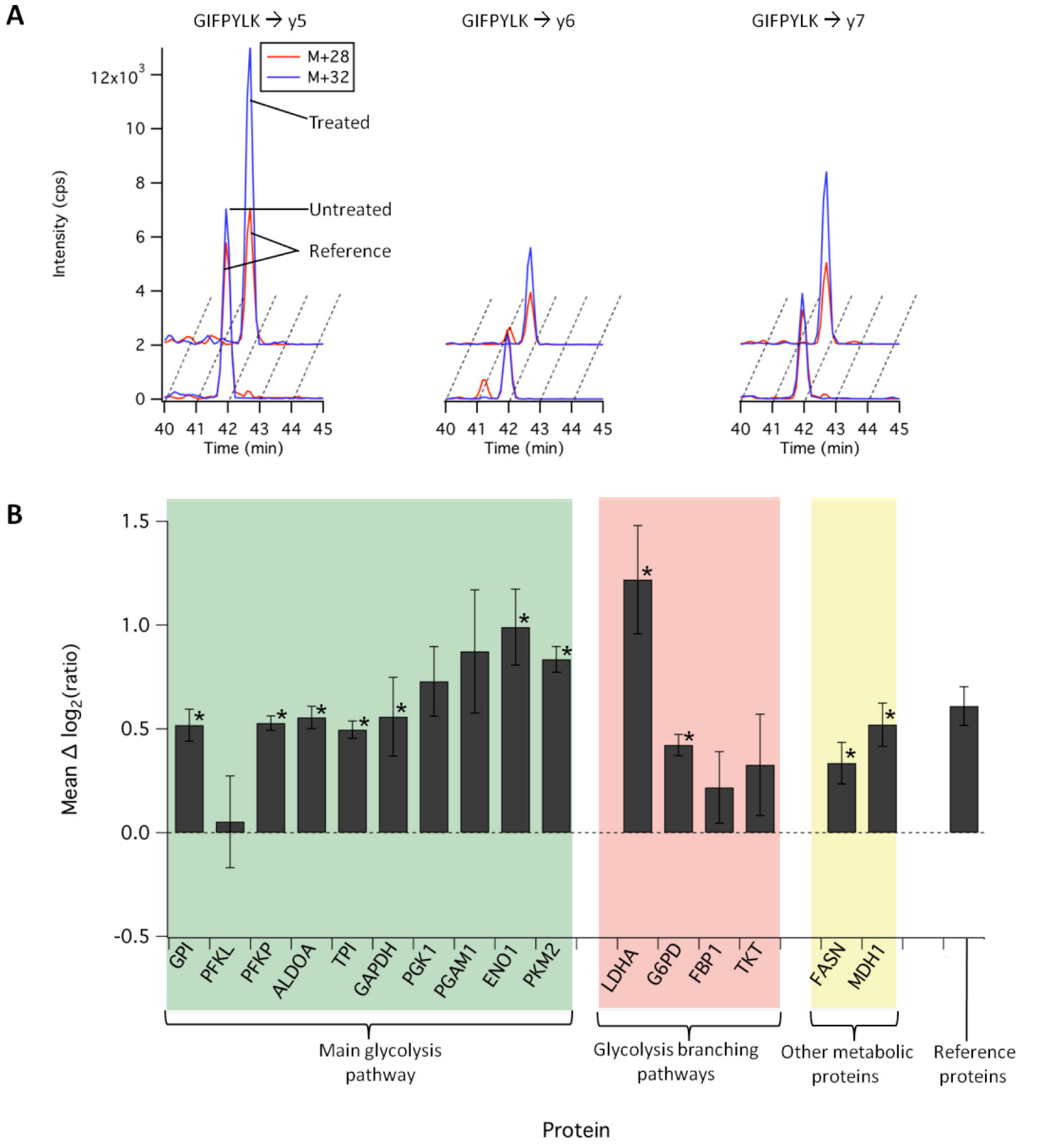

Figure 3.4. Relative Quantification of the Glycolysis Proteome in Response to Treatment of MCF-7 Cells with IGF-1. A) MRM chromatograms of the PKM2 peptide, GIFPYLK, and either the untreated or IGF-1-treated chromatograms, for the three

transitions representing the peptide. For each transition, $\Delta\log_2$(ratio) were calculated as the difference between the $\log_2$ peak area ratios for IGF-1-treated/reference (M+32:M+28) and untreated/reference (M+32:M+28). B) Mean $\Delta\log_2$(ratio) (+/- SE) for detected glycolysis proteins, associated branching proteins, and other metabolic proteins as indicated. *IGF-1 treated and untreated samples are significantly different in a paired t-test ($\alpha = 0.05$).

3.3.3 Glycolytic Proteome Differences Between Various Cell Lines

The quantitative LC-MRM assay was used to compare glycolysis among two normal mammary epithelial cell lines (HMEC and MCF10A) and four tumour-derived cell lines; MCF-7 (non-invasive breast), T-47D (non-invasive breast), MDA-MB-231 (invasive breast)[238], and HeLa (cervical). Protein ratios were generated by LC-MRM, comparing each cell line to a separately prepared T-47D complex digest. Log_2 ratios were adjusted to the reference proteins (without β-actin) then expressed in comparison to the HMEC cell line (Fig. 3.5). All cell types had higher ENO1 levels than HMEC. The three tumour-derived breast cells, MCF-7, T-47D, and MDA-MB-231, had the highest ENO1 levels with HMEC-adjusted $\log_2$ ratios of 1.4, 1.9, and 2.0, respectively (Fig. 3.5). MCF-10A cells displayed fewer positive HMEC-adjusted $\log_2$ ratios (5 of 14 proteins) than other cell type (Fig. 3.5). In the invasive, MDA-MB-231, cells the highest levels of glycolysis protein expression occurred towards the latter stages of glycolysis with PGAM1, ENO1, PKM2, and LDHA displaying HMEC-adjusted $\log_2$ ratios of 0.7, 0.8, 2.0, 0.8, and 1.1, respectively (Fig. 3.5). A similar trend was observed in HeLa cells, in which ENO1, PKM2, and LDHA, showed HMEC-adjusted $\log_2$ ratios of 0.4, 0.8, and 0.4, respectively. Alternatively, the non-invasive MCF-7 and T-47D breast cancer cells did not show this trend and expression of glycolysis proteins was biased towards early stages of glycolysis and branching pathways (PFKP, TPI1, G6PD, and FBP1).

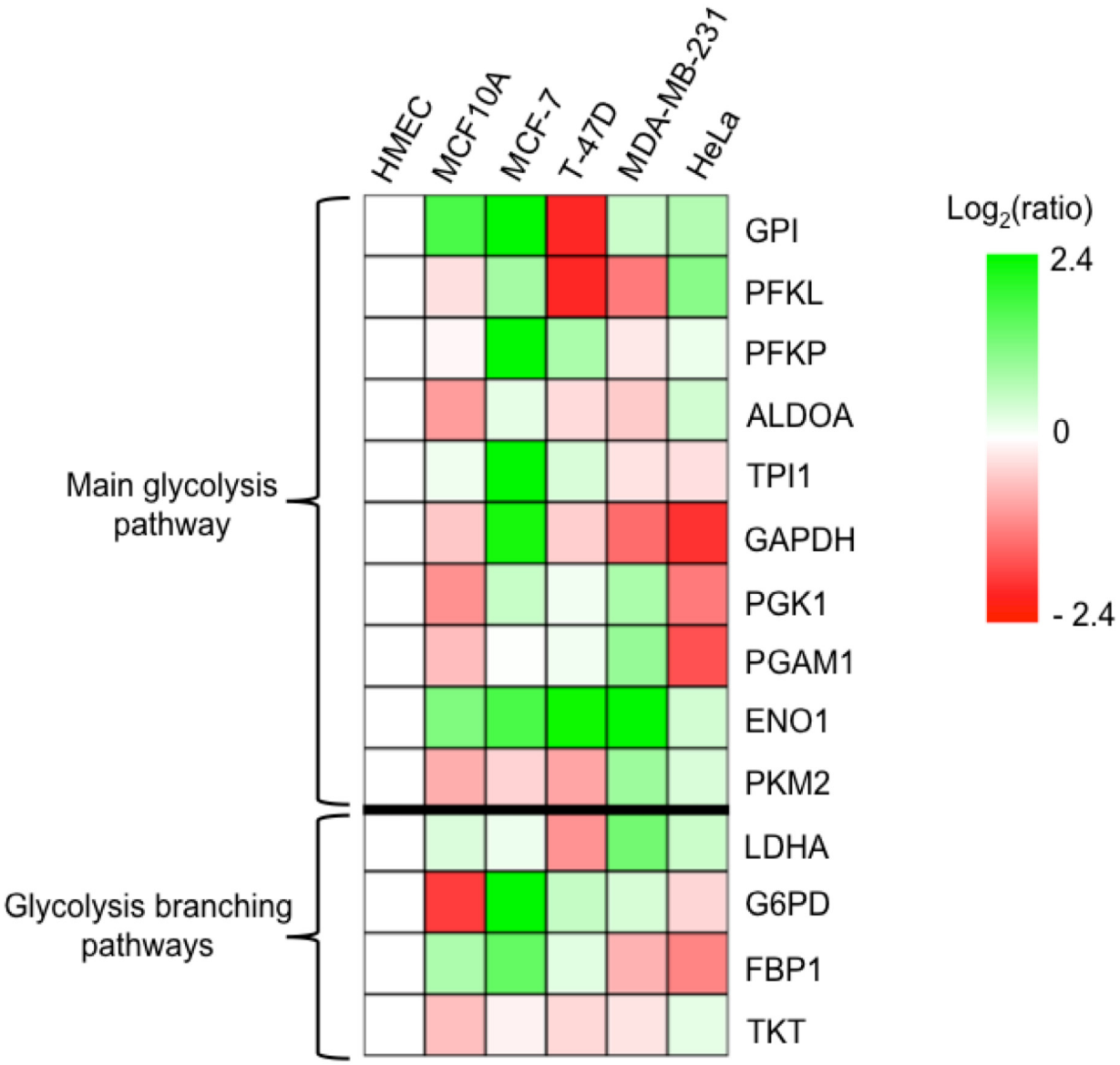

Figure 3.5. Expression of Glycolysis Proteins in Various Cell Lines. Shown from left to right are two normal epithelial cell lines (HMEC and MCF-10A), three breast cancer cell lines ordered by increasing invasiveness (MCF-7, T-47D, and MDA-MB-231)[238], and a cervical cancer cell line (HeLa). Reference protein-normalized $\log_2$ ratios for each protein are expressed in relation to the HMEC cells.

3.3.4 Preliminary Glycolytic Proteome Analysis of Lung Cancer Biopsies

To assess the clinical applicability of targeting glycolysis we obtained a set of 10 lung cancer biopsies (poor, medium, or well differentiated). Using our quantitative LC-MRM assay, each patient sample was compared to an equal amount of complex digest from MCF-7 cells used as a common reference. Several proteins in our LC-MRM assay did not give sufficient S/N in all patient samples (GPI, PFK, PGAM, G6PD, FBP1 and TKT). Log_2 ratios (Lung Tissue/MCF-7 cell reference) for proteins which sufficient S/N was achieved are shown in Fig. 3.6. Variance in the protein levels between patient samples was high (Fig. 3.6) and the levels of the important cancer metabolism proteins (PKM2, ENO1, and LDHA) showed no correlation with the degree of cell differentiation. However, poorly differentiated tumours had significantly lower PGK1 levels than medium and well differentiated tumour samples and well differentiated tumours had slightly lower levels of GAPDH (Fig. 3.6).

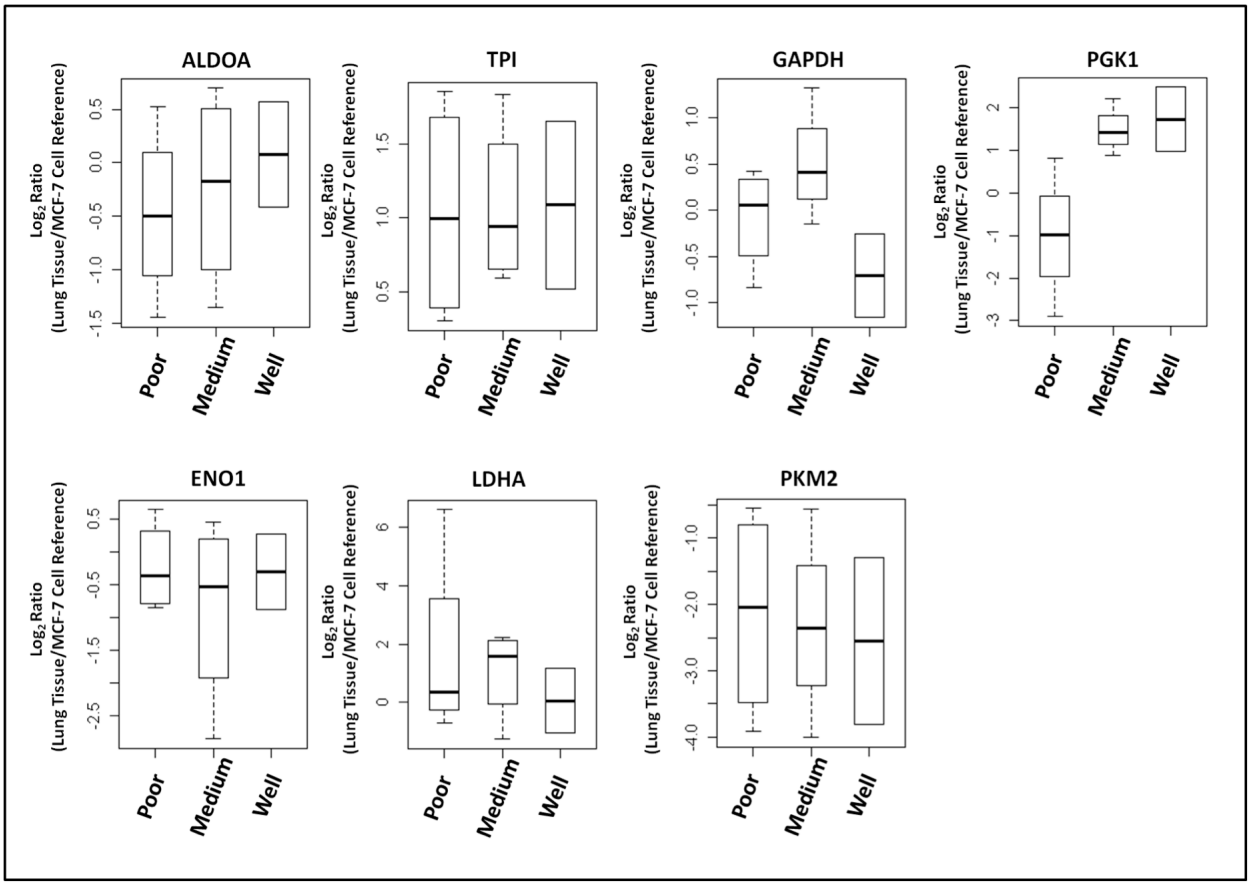

Figure 3.6. Glycolysis Proteins in Lung Cancer Biopsies. Samples were divided into groups according to their level of differentiation; poor (n=5), medium (n=3), and well (n=2). Shown are the mean $\log_2$ protein ratios for measured glycolysis proteins from lung tumour biopsies compared to a common reference sample (MCF-7 cell complex digest).

3.4 Discussion

3.4.1 Targeting the Glycolytic Proteome Using MIDAS of Dimethylated Peptides

Targeted, hypothesis-driven proteomics using LC-MRM, allows for accurate quantitative analysis of subsets of proteins [123]. For targeting metabolic pathways LC-MRM was recently conducted on central carbon metabolism in yeast (*S. cerevisiae*), where a switch to glycoxylate metabolism was quantitatively monitored in a time course experiment [119]. This previous work achieved absolute quantification by the use of internal peptide standards. Our analysis extends the use of targeted proteomics to study glycolysis in human carcinoma cells. Here, using LC-MRM-based targeted proteomics, we quantified at least one isoform of all of the major proteins of glycolysis, except for hexokinases. The association of hexokinases with the outer membrane of the mitochondria [15] likely prevented their detection by LC-MRM since our analysis was based on a cytosolic sample preparation. Indeed since most of the glycolytic proteins reside in the cytosol, they were detectable by LC-MRM using detergent-free sample preparation, thus alleviating ion suppression issues encountered when using detergents [239]. Although higher sensitivity is achieved by LC-MRM than other MS scanning methods, a number of enrichment steps are often still employed to detect sets of proteins. For example, peptide detection by LC-MRM usually involves affinity removal of high abundant proteins [120] or capture with anti-peptide antibodies [139]. Detection of glycolysis proteins was possible using only one dimension of separation because of their high abundance [4, 240]. This makes the glycolytic proteome particularly amenable to 1D-LC-MRM analysis.

Normally, in targeted proteomics approaches, proteotypic peptides (frequently observed peptides in MS experiments) are selected to generate the LC-MRM transitions using databases and software tools such as Peptide Atlas (http://www.peptideatlas.org), the Global Proteome Machine (the GPM) (http://www.thegpm.org), and the PRoteomics IDEtifications (PRIDE) database (http://www.ebi.ac.uk/pride). It is preferred, however, to derive LC-MRM transitions based on empirical product ion spectra because databases contain spectra detected by specific instrument or sample preparation types, perhaps not employed by the user [122]. Here, targeting y_{n-1} ions allowed highly specific targeting of

dimethyl labelled peptides from MCF-7 cells using MIDAS. Indeed, this specificity is supported by the general observation that the extracted ion chromatograms of the sequenced peak for most $[M+2H]^{2+} \rightarrow y_{n-1}$ transitions was usually the most intense. In addition, the high mass of this fragment ion results in MRM transitions with very low chemical noise. Therefore, by targeting the parent $[M+2H]^{2+} \rightarrow y_{n-1}$ transitions, we were able to efficiently determine proteotypic peptides, and generate high scoring spectra for further transition selection. The technique was also efficient since most of the confirmed peptide spectra (109) were collected using 2D-LC-MIDAS where only 9 peptide spectra were successfully added from previously collected shotgun analyses (4 from glycolysis proteins, (Fig. 3.3). This comparison may not be entirely representative, however, since the previously data set was collected using a QTOF mass spectrometer. Still, the predictable fragment ion enhancement by dimethylation in combination with the MIDAS workflow was effective for targeting peptide product ion spectra collection to generate LC-MRM transitions for the set of proteins we targeted in MCF-7 cells.

3.4.2 Growth Factor-induced Changes in Glycolysis Protein Levels

Measurement of changes in glycolysis protein levels in MCF-7 cells exposed to IGF-1 demonstrated the effect of growth factors in altering glycolysis. The influences of growth factors over glycolysis has become apparent where, for example, in mouse FL5.12 cells, increased GLUT1, HK2, PFK1 and glycolysis rates were observed followed by stimulation with the growth factor, interleukin-3. [160]. Shifts in protein expression for the entire glycolysis pathway in response to growth factor exposure have not been explored. Our observation of significant up-regulation of ENO1, PKM2, and LDHA is consistent with previous observations using non-targeted, shotgun proteomics [234]. This view was expanded here, where proteins regulating carbon fluxes to pentose phosphate metabolism and gluconeogenesis (G6PD, FBP1, and TKT) showed only minor changes in response to IGF-1 exposure. Taken together, these observations suggest that cellular response to IGF-1 alters protein expression to bias glycolytic flux towards lactic acid production instead of alternative branching pathways.

Several studies have indicated a similar shift in growth-factor-induced glycolytic flux in a piece-wise manner. For instance, increased lactic acid flux in response to IGF-1

exposure has been shown in RPMI 8226 myeloma cells [241]. ENO1 has also previously shown induction by IGF-1 stimulation in mouse C2C12 cells [242]. Moreover, the reaction catalyzed by PKM2 in glycolysis, is a major regulatory step for glycolytic flux and is important in tumourigenesis [198], where dysregulated growth factor signalling is also a hallmark. However, the glycolytic shift towards lactic acid flux is complicated by increased levels of the M2 splice variant of PKM2 - predominant in our analysis. The M2 variant results in the build-up of intermediates used for high rates of fatty acid and nucleotide synthesis needed for proliferating cells [198], potentially off-setting lactic acid flux. However, the observed growth factor-induced increase in LDHA may facilitate the lactic acid formation - a key feature of the Warburg effect in cancer [243]. Other pathways such as glutamine metabolism also play a role in lactate flux[21], therefore, the putative shift we describe is complex and demands further attention at the metabolite level.

3.4.3 Cell line-specific Expression of Glycolysis Proteins

A survey of glycolysis protein levels in several cell lines by LC-MRM indicates cell-type biases towards protein expression in specific stages of glycolysis (Fig. 3.5). The characteristic of a general increase in glycolytic protein levels in tumour-derived cell lines (Fig. 3.5) is consistent with the increase in glycolysis proteins commonly observed in cancer [6]. Data showing increased ENO1 levels in breast tumour-derived cell lines agrees with observations that ENO1 is commonly elevated in breast cancer [244, 245]. The bias towards increased levels of proteins in the latter stages of glycolysis and lactate formation in invasive MDA-MB-231 cells indicates that direction of carbon flow towards lactic acid is an invasive characteristic. Although no direct measurements of invasion or pH were taken in this study, the shift towards lactic acid formation has previously shown importance in the acid-mediated tumour invasion model [246]. The pattern in MDA-MB-231 cells is identical to that which we observed in growth-factor-induced MCF-7 cells, where increased expression of ENO1, PKM2, and LDHA was common to both. This data is also consistent with studies demonstrating that IGF-1 induces invasiveness in tumours [247, 248]. The notion of growth factor involvement in invasiveness is further promoted by constitutive activation of the downstream effector of IGF-1 signalling, *Ras*, in MDA-MB-231 cells [249]. Mechanisms

of invasiveness are, however, poorly understood and complex, therefore the involvement of glycolysis with invasion should be further explored.

3.4.4 Glycolytic Proteome Targeting in Lung Cancer Biopsies

Targeted proteomics analysis of glycolysis in lung cancer biopsies using LC-MRM was successfully used for relative quantification of the proteins of glycolysis which were shown to have importance in growth-factor driven cell proliferation in cell line experiments (ENO1, PKM2, and LDHA). Insufficient MRM signal from several other proteins in the patient biopsy samples, as compared to the cell line experiments, likely resulted from both the increased complexity of the tissue homogenate and a more complicated extraction procedure involving removal of RNA for a separate study in our laboratory. A more direct sample preparation might also have enhanced the overall completeness of the glycolytic proteome as is currently being undertaken in our laboratory. Since the poorly differentiated tumours are likely to be more proliferative, the lack of difference in ENO1, PKM2, and LDHA was unexpected since our cell line experiments showed increased levels of these proteins in growth factor stimulated cells. We suspect other tumour characteristics besides differentiation status might correlate to ENO1, PKM2, and LDHA but more elaborate studies are needed to explore these relationships. Also unexpected, based on our cell line experiments, was the lower level of PGK1 in the poorly differentiated tumours. Increased levels of PGK1 however, have been associated with poor survival in Stage I lung cancer[133].

3.5 Conclusion

Despite the proposed importance of glycolysis in cancer, and the relatively high abundance of glycolysis proteins, this work represents the first, targeted proteomic analysis of glycolysis. By using a targeted proteomics approach employing MIDAS, an LC-MRM assay was successfully designed based on a limited set of, *in silico* predicted, $[M+2H]^{2+} \rightarrow y_{n-1}$ transitions. Applying the assay *in vitro* revealed a similar glycolytic protein expression profile in MCF-7 cells exposed to IGF-1 as that observed in invasive MDA-MB-

231 cells. This finding demonstrates that increased expression of specific glycolysis proteins may funnel carbon flux towards lactic acid production in invasive cancers, supporting the acid-mediated invasion model. Finally, the robust LC-MRM assay for glycolysis proteins is directly applicable across multiple laboratories and has potential for analysis of patient biopsies.

Chapter 4: Targeted Proteomics Reveals Changes in hnRNP A/B Levels Associated with Cell Proliferation

Abstract

Heterogeneous nuclear ribonucleoproteins (hnRNPs) play important roles in many cellular processes such as transcription, translation, chromatin remodelling, and signalling. Although several hnRNPs are elevated in various cancers, the association of many family members with cell proliferation is not well known. Here, we sought to investigate the altered expression of hnRNP family members during cell proliferation by examining the changes in expression of hnRNP proteins under IGF-1 stimulation, c-Myc knockdown, and in the differentiation of C2C12 cells. Our approach employed multiple reaction monitoring (MRM)-based mass spectrometry by which successful relative quantification was achieved for peptides representing most of the hnRNP family. Our results showed interesting differences in hnRNP K specific to the peptide GSDFDCELR, which was increased by IGF-1-stimulation in Hek 293 and HeLa cells and decreased by c-Myc knockdown in Hek 293 cells. Our more significant finding was the decreased levels of a lesser-known hnRNP (A/B) under c-Myc knockdown in Hek 293, HeLa, and MCF-7 cells as well as in differentiated C2C12 cells. Since other hnRNPs have been shown to influence mRNA splicing, we assessed whether decreased hnRNP A/B levels accompany increased levels of pyruvate kinase M1 and M2 splice variant peptides using synthetic pyruvate kinase peptides as internal standards. Increased levels of the M1 splice variant accompanied decreased levels of hnRNP A/B in C2C12 cells but no differences in alternatively spliced peptides were observed under c-Myc knockdown in Hek 293, HeLa, and MCF-7 cells. These findings indicate that the lesser known hnRNP protein (A/B) may be involved in c-Myc-directed cell proliferation and warrants further study.

4.1 Introduction

The interface between RNA transcription and eventual protein translation in cells is highly regulated by RNA/protein complexes. Comprising a major portion of these complexes are heterogeneous nuclear ribonucleoproteins (hnRNPs). As a result of their essential role in the proper expression of transcripts, alterations in hnRNP expression could have dramatic effects on cell processes. The hnRNP family of proteins consists of about 20 major members (A1-U), most are highly abundant in both the nucleus and the cytosol[250] and they influence mRNA splice site selection, translation, and transport but some also play a role in signalling[251]. Many hnRNPs have been shown to be elevated in different cancers. For example, hnRNP A1 is increased in chronic myelogenous leukemia and in myeloid progenitor cells expressing the $p210^{BCR/ABL}$ oncoprotein[252]. hnRNP A2 has been shown to be highly expressed in lung, [253, 254] breast, [255] and pancreatic[256] cancers. Additionally, hnRNPs A1, A0, and A3 in the nuclear matrix have also been associated with colon cancer[257].

The hnRNP proteins are thought to be crucial in bridging growth-related signals to the regulation of mRNA transcription, transport, and degradation. Growth factor signalling pathways and oncogenic transcription factors such as c-Myc are altered in many cancers and, among other roles, facilitate metabolic changes necessary for cancer cell growth[258]. In growth factor stimulated Rat-1 cells, hnRNP A1 levels increase[259] which correlates with induction of several glycolysis proteins[260] and the c-Myc transcription factor[261]. Increases in hnRNP K levels have been shown to occur in growth factor-stimulated breast cancer cells[262] and among the many roles proposed for hnRNP K, it may act as a key co-factor for activation of the tumour suppressor protein p53[263]. Recently, hnRNP A1, hnRNP A2, and hnRNP I (also called polypyrimidine tract binding protein 1; PTB1), under control of *c*-Myc, have been shown to alter metabolism in proliferating cells by altering splice site selection towards the M2 splice variant of pyruvate kinase[60, 61].

Since it is evident that growth signalling through c-Myc appears to affect several hnRNPs we sought to fully characterize the expression changes in the hnRNP family under stimulation by IGF-1 and c-Myc knockdown. The current method of choice for targeted analysis of proteomic subsets is multiple reaction monitoring (MRM) analysis of

representative tryptic peptides. Peptide analysis by MRM is efficiently multiplexed to quantify pre-determined set of proteins and the advantages are outlined in Chapter 1. Here, we used peptide MRM analysis to determine the expression of the entire hnRNP family in both IGF-1 stimulated and c-Myc siRNA-transfected cells. We also use MRM to quantify hnRNP expression changes accompanying levels of M1 and M2-unique peptides between differentiated and proliferating C2C12 cells. While interesting peptide-specific changes were observed for hnRNP K, our major finding indicates altered expression of hnRNP A/B occurs under c-Myc knockdown and in C2C12 cells. hnRNP A/B does not appear to be involved in pyruvate kinase splice site selection, is not well characterized, and as a result of our findings, warrants further study.

4.2 Experimental Procedures

4.2.1 Cell Culture, IGF-1 Treatment, and C2C12 Cell Differentiation

MCF-7, HeLa, Hek 293, C2C12, and MDA-MB-231 cells were from the American Type Culture Collection and cultured in DMEM (Invitrogen) with 10% fetal bovine serum (FBS) at 5% CO_2. Several 75 cm^2 flasks of MCF-7, HeLa, and MDA-MB-231 were cultured for use as a stock for MRM transition selection and optimization. For IGF-1 stimulation experiments, MCF-7, HeLa, and Hek 293 cells were seeded at 100 000 cells per well in 6-well (9.8 cm^2) culture plates, serum starved for 48 h (in triplicate), and were either left untreated for 24 h (non-treated control), or treated for 6, 12, or 24 h with 100 ng/mL IGF-1. C2C12 cells were harvested at 60% confluence (proliferating) or grown to confluence then switched to media containing 2% horse serum (differentiated). Both IGF-1 and differentiation experiments were conducted in triplicate.

4.2.2 siRNA Transfection and Western Blotting.

Cells were seeded at 100,000 cells per well, in 6-well (9.8 cm^2) culture plates, grown for 24 h, then serum starved for 24 h. Media was then replaced with 10% FBS (non-treated; NT), 10% FBS with 0.1% Lipofectamine 2000 (Invitrogen) and 50 nM positive control siRNA (Ambion, Austin, TX) (mock-treated), or 10% FBS with 0.1% Lipofectamine 2000 (Invitrogen) and 50 nM c-Myc siRNA (Cell Signalling Technologies, Danver, MA) (c-Myc

knockdown). Transfection proceeded for 48 h. Cells were harvested as below and split prior to pelleting to reserve a sample for confirmation of c-Myc knockdown by Western blot. The c-Myc antibody was from Cell Signalling Technologies and Actin and GAPDH antibodies were from Santa Cruz (Santa Cruz, CA). Western blotting was performed as per the manufacturer's instructions.

4.2.3 Protein Extraction and Labelling of Peptides

Cells were washed with PBS, detached with 0.25% Trypsin/EDTA (Invitrogen), immersed in 1 mL PBS and pelleted by centrifugation at 5000 x g. Lysis for hnRNP analysis was conducted in 500 mM tri-ethyl ammonium bicarbonate (TEAB) (Sigma-Aldrich), pH 8.5, with 0.1% Rapigest (Waters) (1 mL per 75 cm^2 surface area of cells) using 3, 5 s, pulses with a probe sonicator (Fisher Scientific). Lysis for analysis of PKM1/M2 peptides was conducted in 500 mM TEAB by 20 passes through a 21 G 1 ½ needle and was followed by centrifugation at 110 000 x g for 1 h. Total protein concentration was estimated using a Bradford assay [169] with BSA as a standard. Digestion and stable isotope labelling by reductive methylation of peptides (M+28 or M+32) was performed as described previously [264].

4.2.4 hnRNP Peptide Product Ion Generation

Product ions for tryptic peptides from hnRNP proteins (accession numbers listed in Fig. 4.1A) were acquired by a MIDAS approach towards MCF-7, MDA-MB-231 and HeLa cells as described previously[264] and from an MS/MS dataset from MDA-MB-231 cells acquired using a TripleTOF 5600 mass spectrometer (AB Sciex). MDA-MB-231 cell preparation was as above except 4 mM methylmethane thiosulfanate (MMTS) and 2 mM tris(2-carboxyethyl)phosphine (TCEP) were used as reducing and alkylating reagents respectively. Online chromatography for TripleTOF MS/MS acquisition was performed using an Eksigent nanoLC Ultra using a 200 µm x 0.5 mm trap column, a 75 µm x 15 cm ChromXP C18-CL analytical column and a flow rate of 300 nL/min using a 60 minute gradient of 10-30% mobile phase B (mobile phase A = 2% acetonitrile, 0.1% formic acid, mobile phase B = 98% acetonitrile, 0.1% formic acid). TripleTOF acquisition setup was as follows: >30000 resolution TOF MS survey scan, MS accumulation time of 250 ms, 20 IDA

precursors selected at unit resolution, MS/MS accumulation time of 50 ms at > 15000 resolution, and a 1.3 s fixed cycle time.

4.2.5 hnRNP MRM Transition Selection

Spectra collected by MIDAS were searched against the IPI human database (v3.65) using ProteinPilot (v3.0, AB Sciex) with iodoacetamide cysteine alkylation and dimethyl labelling of lysine and N-termini as fixed modifications, rapid ID, and a protein detection threshold of 0.05. Spectra collected by TripleTOF were searched against the IPI human database (v3.65) using ProteinPilot (v.4.0, AB Sciex) with MMTS set as a fixed modification and thorough ID. Positively identified spectra by MIDAS or TripleTOF analysis were exported to MRM Pilot (v2.0, AB Sciex) and the four most intense fragment ions were chosen for parent to fragment ion pairs (MRM transitions) for peptides. MRM transitions were tested and optimized for 1D-LC-MRM (as described previously[264]) using complex digests of MCF-7, HeLa, and MDA MB-231 cells labeled M+28. Matching heavy isotope-labeled (M+32) pairs were calculated for relative quantification.

4.2.6 Relative Quantification of hnRNPs

Aliquots (200 µL/40 µg) of complex digests from IGF-1 treatment (0 IGF, 6 IGF, 12 IGF, and 24 IGF) were labeled M+32, mixed with 50 µL (10 µg) of peptides from a stock digest of the same cell line (labeled M+28) and desalted, all as described previously[264]. Aliquots (200 µL/40 µg) from siRNA-treated digests (mock and c-Myc) were labeled M+32 and mixed with 100 µL (20 µg) of, M+28-labeled, non-treated digest (NT). Aliquots (200 uL/40 µg) from differentiated and proliferating C2C12 cell complex digests were labelled M+32 and M+28 respectively. Transitions selected and optimized for MRM were divided into 3 acquisition methods (Appendix B) and hnRNP peptides were analyzed using 3 separate injections. For normalizing relative quantification, a fourth injection was made using transitions for relative quantification of reference proteins (ACTAB, PPIA, RLPL0, and YWHAZ) described previously[264], except peptides shared with actin isoforms other than ACTAB were excluded. MRM analysis and generation of $\log_2$ ratios was conducted using Multiquant (v2.0) with acquisition and peak area calculation parameters described

previously[264]. Log_2 ratios were normalized so the mean log_2 ratio of the reference proteins was 0.

4.2.7 Absolute Quantification of Pyruvate Kinase Splice Variants

Peptides unique to the M1 (EAEAAMFHR) and M2 (CCSGAIIVLTK) isoforms and a shared peptide (GDYPLEAVR) were synthesized and purified to >95% (Bio Basic Inc., Markam, ON, Canada). Peptides were dissolved in 50% acetonitrile, then diluted in 500 mM TEAB (pH 8.5) to a final concentration of 10 pmol/µL, labeled M+36, and desalted and dried as above. Labelled and desalted peptides were resuspended in 5% acetonitrile (0.1% formic acid) and 10 pmol was injected onto a 300 µm x 10 cm C18 column (Waters) and eluted into a Waters Quattro mass spectrometer using a gradient of 5 to 65% acetonitrile (0.1% formic acid) over 10 minutes. Daughter scans were collected for each peptide parent ($[M+2H]^{2+}$) using source voltage=3.4 eV, cone voltage=20 V, and collision energy (V)=parent m/z ÷ 25. Four transitions for each peptide were formed using the most intense fragment ions (Appendix C). Further quantitative analysis was performed by MRM on a 4000 Qtrap mass spectrometer using parameters described previously[264]. Endogenous levels of PKM2 peptides in MCF-7 and HeLa cells were determined by using a peak area calibration curve of a dilution series of M+36-labeled peptides (5000 fmol to 0.01 fmol per µg of complex digest). For absolute quantification of PKM1 and M2 and shared peptides, peak areas in M+28 labelled digests were calculated by reference to an internal standard of 100 fmol M+36 labeled peptide/µg protein (the approximate concentration of the endogenous PKM2 peptides). Since the M1-unique peptide contains a potentially oxidized methionine, additional transitions were included in each acquisition method to detect possible oxidized peptides and prevent their interference with quantification. The calculated levels of the M1-unique and M2-unique peptides were adjusted by setting the the shared (total PKM) peptide equal to the mean of the shared peptide amount for each cell line.

4.3 Results

4.3.1 Targeting hnRNP Peptides Using MRM

To design an MRM assay for proteins belonging to the hnRNP family of proteins, accession numbers for 23 hnRNP proteins selected from the UniprotKB database (www.uniprot.org) (Fig. 4.1A) were used for peptide product ion generation by MIDAS, based on predicted $[M+2H]^{2+} \rightarrow y_{n-1}$ dimethyl labeled peptide transitions. A total of 389 hnRNP tryptic peptides, 7-20 amino acids long, were predicted. Product ions for peptides from hnRNP proteins were also selected from a dataset of MS/MS acquired using a 5600 TripleTOF mass spectrometer (AB Sciex) at a high sampling rate (20 MS/MS per s). The number of hnRNP peptides identified from TripleTOF and MIDAS approaches was 159 and 49 respectively, with 29 identified by both approaches (Fig. 4.1B & 4.1C). The initial success rate of these transitions by MRM was 26% and 55% for TripleTOF and MIDAS respectively, to a total of 46 detectable hnRNP peptides by MRM (Fig. 4.1B). More peptides (39) were identified for the hnRNPA group (hnRNPA0, hnRNPA1, hnRNPA2, and hnRNPA3) and hnRNPM (24) than in other subgroups (Fig. 4.1C) suggesting that the A subgroup and hnRNPM could be more abundant than other subgroups (D,C,H,U/R) in the cell lines used for product ion generation (HeLa, MCF-7, and MDA MB-231).

A

hnRNP	Alternate Name	UniprotKB Accession
R		O43390
Q	SYNCRIP, NSAP1	O60506
UL	SAFA	Q00839
UL2	SAFA2	Q1KMD3
A1		P09651
A3		P51911
A2		P22626
A0		Q13151
D	AUF1	Q14103
A/B	ABBP-1	Q99729
DL	JKTBP1	O14979
CL2	RALY	Q9UKM9
C		P07910
CL		O60812
G	RBMXP1	P38159
H1		P13493
H2		P55795
F		P52597
H3		P31942
K	TUNP	P61978
L		P14866
I	PTB1	P26599
M	NAGR	P52272

B

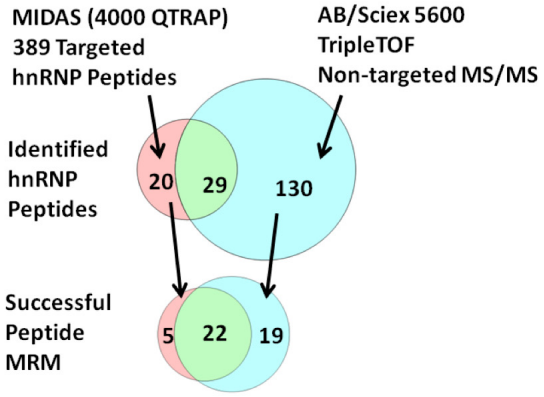

C

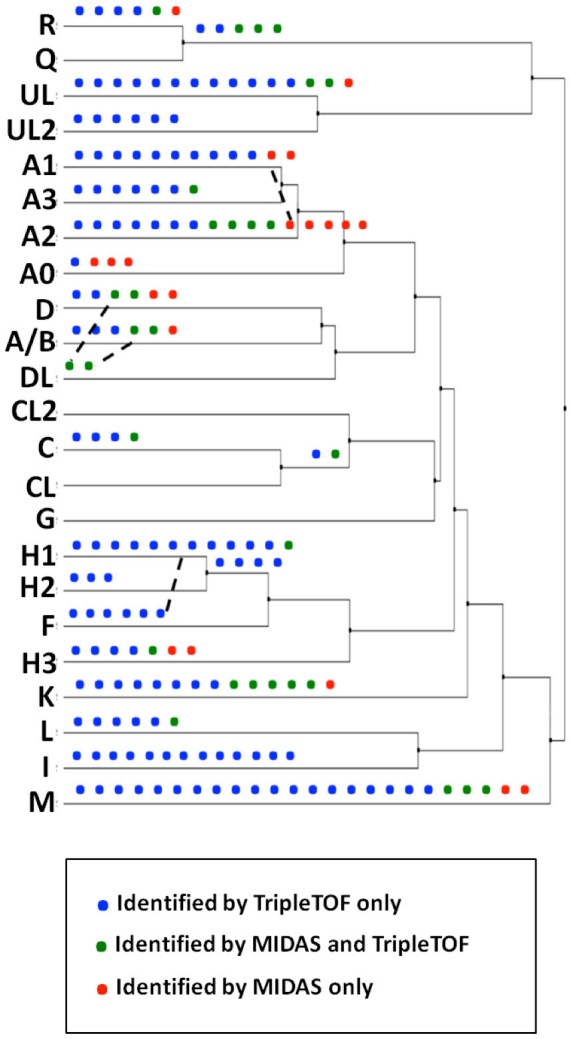

Figure 4.1. Summary of Peptide Identifications from the hnRNP Protein Family. A) Targeted hnRNP proteins and their accession numbers. B) Venn diagrams illustrating the number of peptides identified using targeted (MIDAS) and non-targeted (TripleTOF) datasets and, of the identified peptides, those which gave successful MRM transitions for each approach. C) Peptide identifications for each hnRNP protein from either dataset (colored dots) depicted by their protein location in an average distance tree using BLOSOM62 from a ClustalW multiple sequence alignment. Shared peptides are indicated by "----".

4.3.2 Relative hnRNP Quantification in Growth Factor-treated Cells

Using our optimized MRM assay we measured the effects of IGF-1 stimulation on the levels of hnRNPs. Relative quantitative MRM was used to compare protein expressed by IGF-1 stimulated MCF-7, HeLa, and Hek 293 cells, to a control digest for each cell line. Several peptides previously detected at the validation and optimization stages were not successfully detected at an acceptable S/N for relative quantification under IGF-1 stimulation. Nevertheless, 26 hnRNP peptides, representing most of the family, were measured by MRM for MCF-7, HeLa and Hek 293 cells (Fig. 4.2A). Normalized mean relative expression (log_2 ratio) differences for peptides at each time point compared to the un-stimulated digest are shown in Fig 4.2A. Differences in the levels of hnRNP peptides in response to IGF-1 stimulation were mild and varied among cell lines. There was also considerable variation for peptides of the same hnRNP, most likely attributable to complexities in abundance from post-translational modifications. For example, in IGF-1 stimulated MCF-7 cells, the 24 h log_2 ratio differences from the un-stimulated digest for IFVGGLSPDTPEEK and FGEVVDCTIK of hnRNP D were 0.79 and -0.42 respectively (Fig. 4.2A). The most notable differences were observed for hnRNP K, of which most of the peptides were slightly elevated temporally in IGF-1 stimulated Hek 293 and Hela cells. However, peptide-specific differences were observed for hnRNP K. Although measurements were variable between biological replicates, the hnRNP K peptide, GSDFDCELR, appeared to preferentially elevated over other peptides in Hek 293 (mean log_2 ratio difference of 0.75 over 24h) and HeLa cells (mean log_2ratio difference of 0.56 over 12h) (Fig. 4B). The specific effect on GSDFDCELR was not observed in MCF-7 cells, however (Fig. 4B).

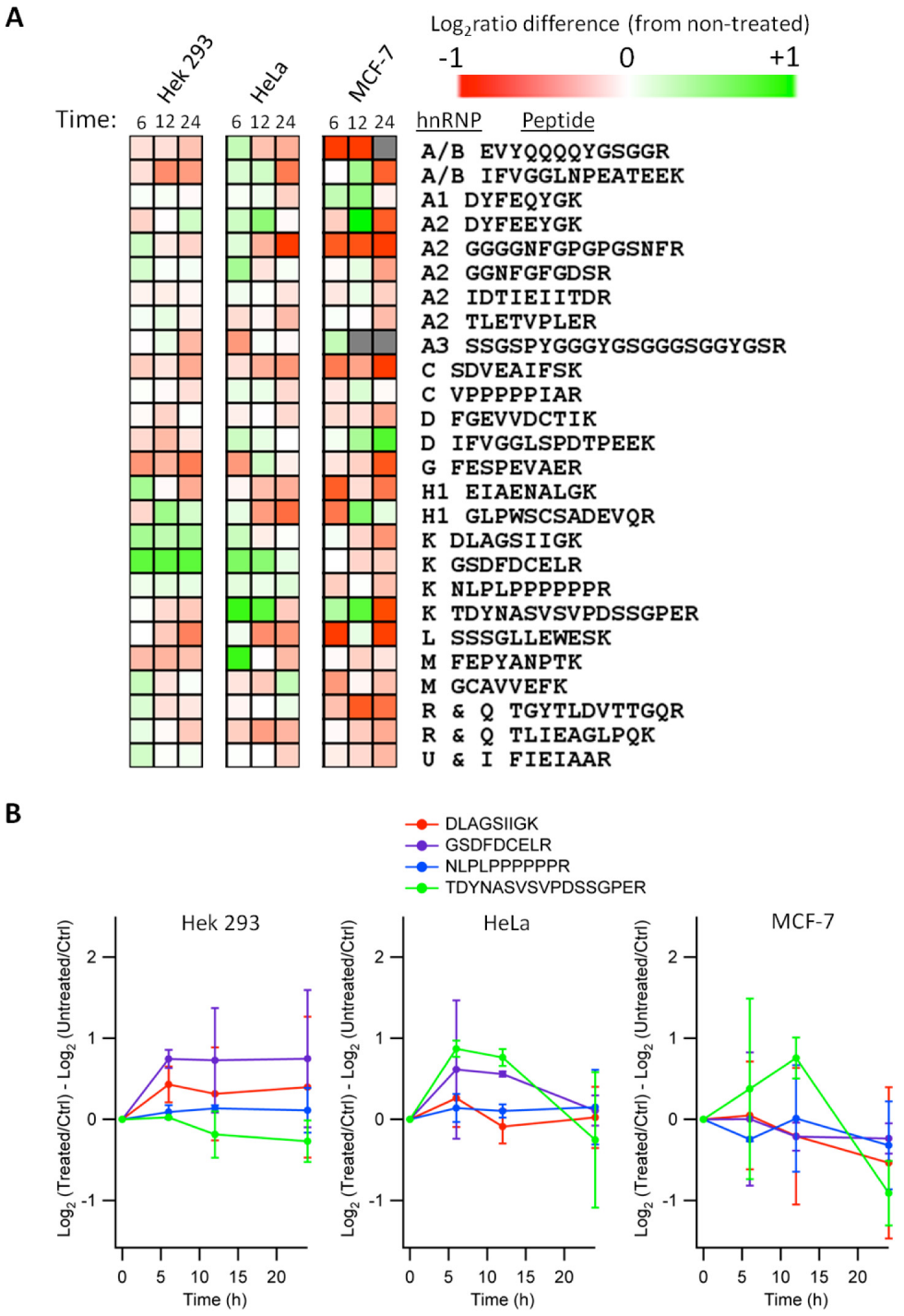

Figure 4.2. Changes in hnRNP Expression in IGF-1-stimulated Cells. A) Relative quantification for hnRNP peptides in IGF-1-stimulated Hek 293, HeLa, and MCF-7 cells as determined by LC-MRM. Changes are expressed as a mean of the differences between each time point [$\log_2$ ratio (treated/control)] and non-treated cells [$\log_2$ ratio (non-treated/control)]. B) The hnRNP K peptide GSDFDCELR appears to be preferentially up-regulated in growth factor stimulated Hek 293 and HeLa cells but not in MCF-7 cells. Error bars are the standard error of the mean.

4.3.3 Relative hnRNP Quantification Under c-Myc Knockdown

As a result of evidence that c-Myc influences the levels of several hnRNPs (A1 and A2) and that c-Myc is influenced by growth signals, we measured changes in the expression of hnRNPs under c-Myc knockdown in Hek 293, HeLa, and MCF-7 cells using relative quantitative MRM. Mock siRNA and c-Myc siRNA transfected cell digests were both compared to untreated cell digests (Fig. 4.3A). Similarly to the IGF-1 experiment, 28 hnRNP peptides were detected at an acceptable S/N for relative quantification by MRM (Fig. 4.3B). Also similar to the IGF-1 experiment, c-Myc siRNA knockdown affected hnRNP levels differently among cell lines and peptides of the same hnRNP (Fig. 4.3B). For example, the hnRNP H1 peptide GLPWSCSADEVQR showed mean $\log_2$ ratio differences between c-Myc siRNA and mock siRNA treated digests in Hek 293 and HeLa cells of -1.47 and 0.69 respectively. Interestingly, c-Myc knockdown resulted in specifically decreased levels of the hnRNP K peptide GSDFDCELR in Hek 293 cells (Fig 4.3C) - also increased by IGF-1 stimulation. In all 3 cell lines, c-Myc knockdown resulted in decreased levels of hnRNP A/B peptides (Fig. 4.3D). Unfortunately, the hnRNP A/B peptide, EVTQQQQYGSGGR gave a poor signal in HeLa cells. These results were again mild and differences in hnRNP A/B peptides between c-Myc siRNA and mock treated digests were not statistically significant in a two-tailed t-test (α=0.05). Nevertheless, results were consistent between cell lines. In Hek 293 and HeLa cells, c-Myc knockdown decreased the levels of peptides shared between hnRNP R and hnRNP Q (Fig 4.3D), although again, results were not statistically significant (α=0.05).

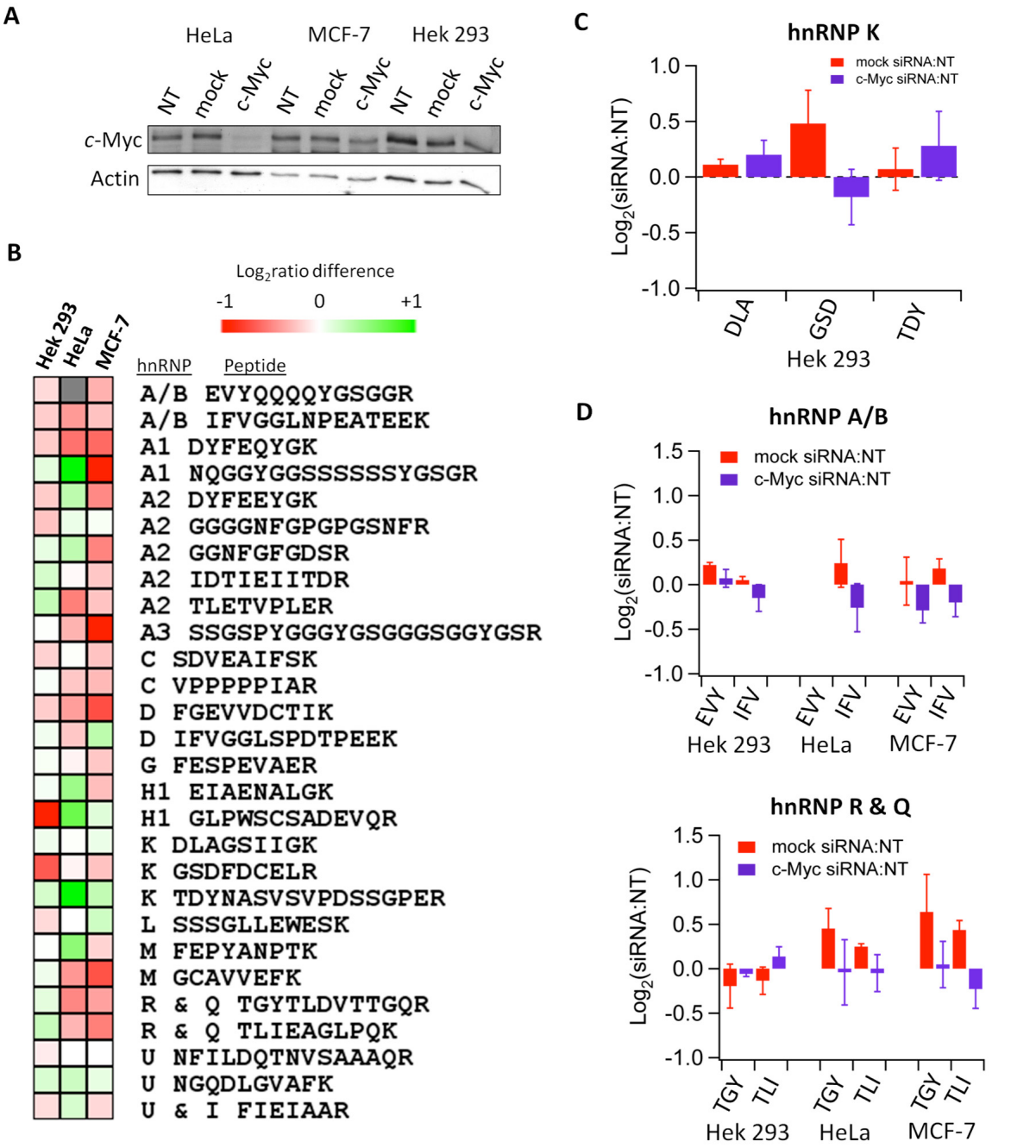

Figure 4.3. Changes in hnRNP Expression by c-Myc Knockdown. A) Western blot confirmation of c-Myc knockdown in HeLa, MCF-7, and Hek 293 cells. B) Changes in hnRNP peptides under c-Myc knockdown as determined by MRM expressed as a mean $\log_2$ ratio difference [mean $\log_2$ ratio (c-Myc siRNA/NT) – mean $\log_2$ ratio (mock siRNA/NT)]. C) Relative quantification showing specifically decreased levels of the hnRNP K peptide, GSDFDCELR, in Hek 293 cells. D) Relative quantification showing decreased levels of hnRNP A/B in Hek 293, HeLa, and MCF-7 cells and decreased levels of shared peptides of hnRNP R and Q. Peptides are designated by the first 3 amino acids in the sequence. Error bars are the standard error of the mean.

4.3.4 Relative hnRNP Quantification and Absolute PKM1/M2 Quantification in Differentiated C2C12 Cells

To further examine whether expression changes in proteins such as hnRNP K or hnRNP A/B during cell proliferation and relate them to pyruvate kinase splice variant expression, we conducted relative quantitative MRM of hnRNPs in mouse C2C12 cells. These cells switch from proliferating cells to differentiated muscle-type cells upon exposure to 2% horse serum (Fig. 4.4A), which is accompanied by increase levels of PKM1[61]. Western blots performed for c-Myc expression confirmed previous reports of increased c-Myc expression in proliferating C2C12 cells (Fig. 4.4B). Relative quantification of hnRNP peptides was performed using MRM, comparing differentiated and proliferating C2C12 cells. Since hnRNPs from human and mouse are similar, many of the peptides (18) could be detected in C2C12 cells as were in the IGF-1 and c-Myc experiments. Interestingly, the greatest differences between differentiating and proliferating cells were observed for hnRNP A/B, of which EVYQQQQYGSGGR and IFVGGLNPEATEEK show $\log_2$ ratios (Differentiated:Proliferating) of -1.88 and -1.31 respectively (Fig 4.4C). Thus, the level of hnRNP A/B expression is much higher in proliferating C2C12 cells and accompanies increased c-Myc levels. Although hnRNP K showed no apparent differences, peptides of hnRNP A1, A3, C, and D also showed decreased levels in differentiated C2C12 cells.

In addition to relative quantification of hnRNPs, we also assessed whether changes in pyruvate kinase splicing accompanied the decreased levels of hnRNP A/B observed in both differentiated C2C12 cells and cells under c-Myc knockdown. M1-unique (EAEAAMFHR), M2-unique (CCSGAIIVLTK), and M1/M2-shared (GDYPLEAVR) (Fig 4.5A) synthetic M+36-labeled peptides were used for absolute quantification by spiking approximately endogenous levels (100 fmol/ug protein) into digests as internal standards. Increased levels of the M1-unique peptide were observed in differentiated C2C12 cells but surprisingly, increased levels of the M2-unique peptide were also observed. In Hek 293, HeLa, and MCF-7 cells, we could not detect the M1-unique peptide thus levels of M1 expression in these cells were below the detection limit of EAEAAMFHR (~0.1 fmol/ug protein). Further, we did not detect any differences in the M2-unique peptide between non-

treated, mock siRNA-treated, or c-Myc siRNA-treated digests for any of the cell lines (Fig. 4.5C).

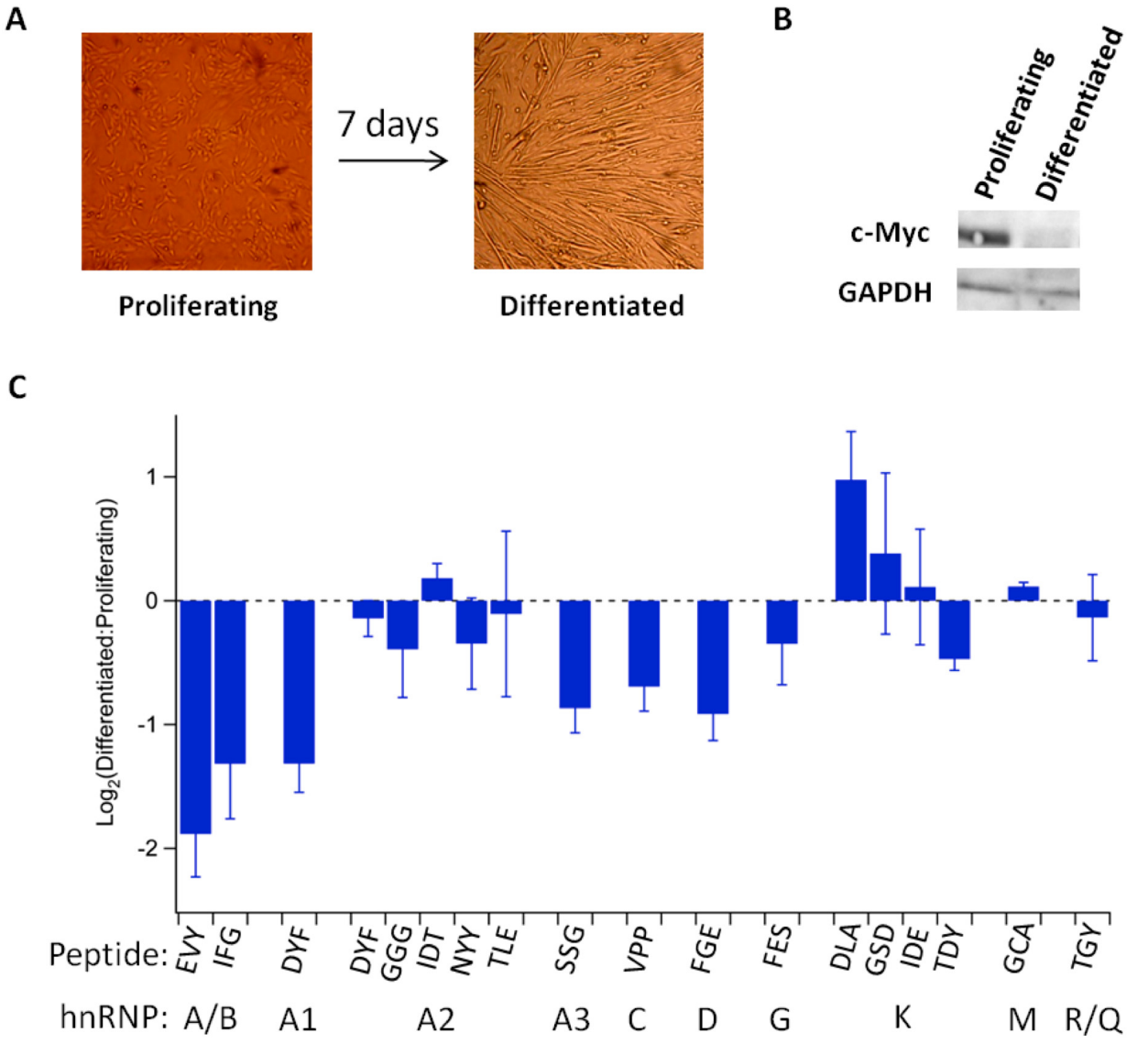

Figure 4.4. Changes in hnRNP Expression in Differentiated C2C12 Cells. A) C2C12 cells differentiated by switching to 2% horse serum for 7 days. B) Western blot showing c-Myc expression in proliferating and differentiated C2C12 cells. C) Relative expression by LC-MRM of hnRNP peptides showing decreased levels of hnRNP A/B, A1, A3, C, and D in differentiated C2C12 cells. Peptides are designated by the first 3 amino acids in the sequence. Error bars are the standard error of the mean.

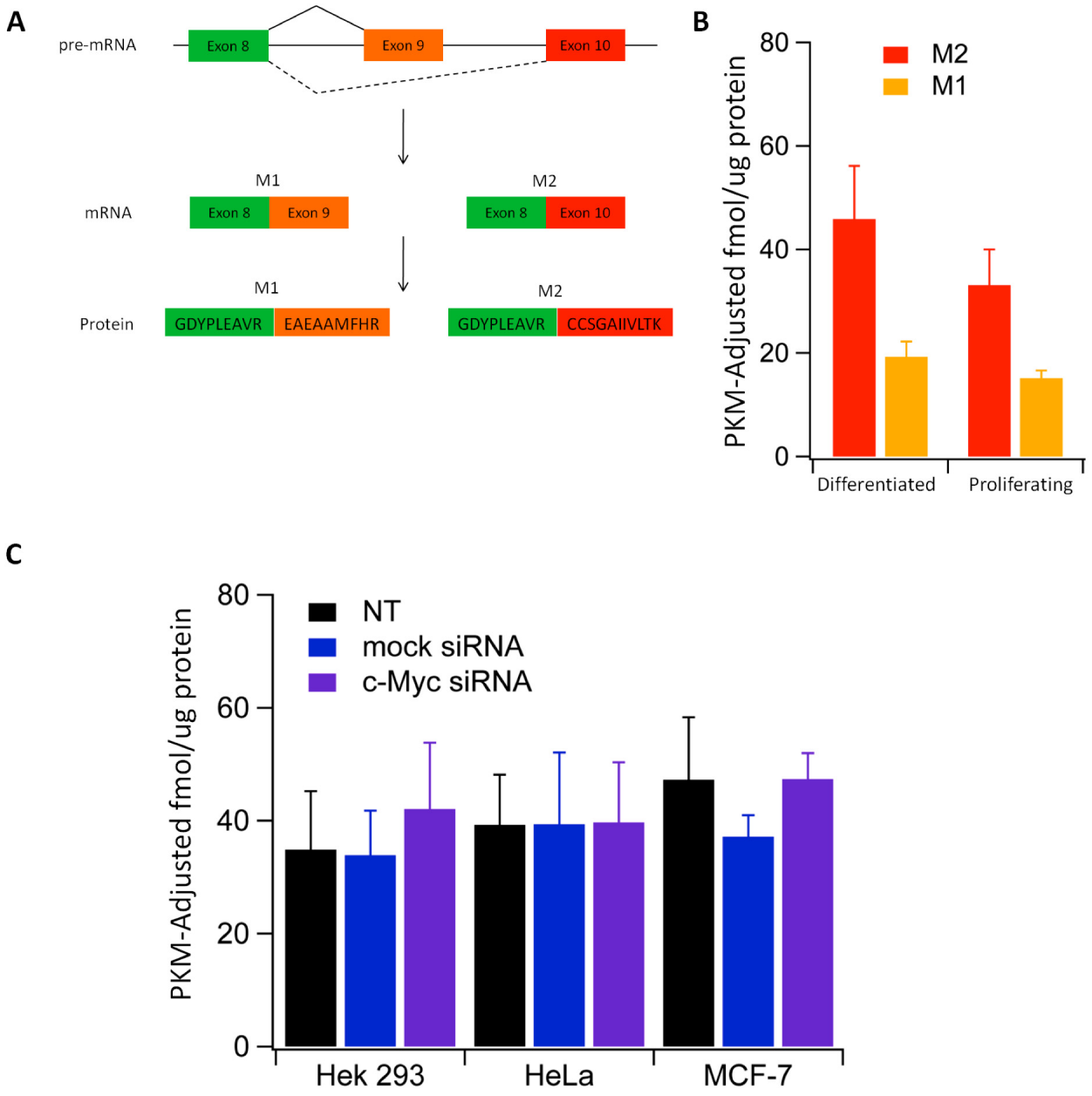

Figure 4.5. Absolute Quantification of the M2 Pyruvate Kinase Splice Variant in C2C12 Cells and *c*-Myc siRNA Transfected Hek 293, HeLa and MCF-7 Cells. A) The peptides GDYPLEAVR, EAEAAMFHR, and CCSGAIIVLTK were chosen to represent the protein sequence encoded by exon 8 (shared by both variants), exon 9 (unique to the M1 variant), and exon 10 (unique to the M2 variant). Absolute quantification of each peptide was achieved using M+36-labeled synthetic peptides as spiked internal standards. B) Levels of the M2-unique and M1-unique peptides, normalized to the shared peptide (total PKM) in proliferating and differentiated C2C12 cells. C) Levels of the M2-unique peptides, normalized to the total PKM under c-Myc knockdown in Hek 293, HeLa, and MCF-7 cells.

4.4 Discussion

Here, a novel targeted proteomics approach was taken to study the hnRNP family of proteins and to determine changes in the levels of family members in response to growth factor stimulation and c-Myc knockdown. We also determined hnRNPs accompanying pyruvate kinase splice variants in C2C12 cells. As hnRNP proteins are involved in mRNA splicing, transport, and translation, they are relatively abundant [250]. As such, we were able to identify many peptides from this family of proteins using both targeted and non-targeted product ion generation approaches (Fig. 4.1C). The success rate for choosing suitable MRM transitions from peptides from targeted (55%) and non-targeted (26%) approach was slightly lower than our previous use of the same approaches (67% and 36% respectively) to target glycolysis proteins[264]. Incomplete overlap between the optimization and experimental stages, where only the most robust peptide transitions were observed in all experiments, is also consistent with our previous analysis[264]. The low overlap is likely due to variations in sample preparation including cell growth, digestion, labelling, and desalting.

Using relative quantitative MRM to characterize hnRNP expression changes showed mildy increased levels of a specific peptide (GSDFDCELR) of hnRNP K in IGF-1-stimulated Hek 293 and HeLa cells. Interestingly, this peptide decreased under c-Myc knockdown in Hek 293 cells (Fig. 4.2B & 4.3C). hnRNP K is a multifunctional protein that consists of several splice variants each existing in many post-translationally modified forms[265] and has been shown to interact with c-Src[266], perhaps mediating growth factor activated kinases and regulation of mRNA[265] processing. Although our results of growth factor stimulation on increasing hnRNPK expression levels were mild and peptide specific, increases in hnRNPK have been previously observed in EGF-stimulated cells[262]. Also of note, hnRNP K is a cofactor for p53 in response to DNA damage. The existence of known hnRNP K isoforms might explain the peptide-specific differences we observed. However, GSDFDCELR does not contain any recently reported hnRNP K splice variant or post-translational modifications in serum stimulated cells[267]. The specific differences we observed in GSDFDCELR could also be related to RNA binding[268] since this peptide is part of the KH2 (RNA interaction) domain of hnRNP K, but it is unclear how this could have affected our results mechanistically.

Further study is needed to explain whether peptide-specific differences in hnRNP K are because of new variants, RNA-binding effects, or anomalies resulting from sample preparation.

Our most intriguing finding from the relative quantitative MRM results showed evidence for the control of hnRNP A/B (also call APOBEC1-binding protein 1) levels by c-Myc in Hek 293, HeLa, and MCF-7 cells (Fig 4.3D). Although changes were small and biological variation precluded statistical significance, this is further supported by decreased hnRNP A/B in differentiated C2C12 cells, in which c-Myc also decreased (Fig 4.4B). In comparison to the hnRNP A, D, and K-type proteins, hnRNP A/B is poorly characterized. hnRNP A/B, although its naming would suggest otherwise, has a greater sequence similarity with the hnRNP D group than the hnRNP A group (Fig 4.1). It has been proposed that hnRNP A/B, by interacting with APOBEC1, could be involved in RNA editing of apolipoprotein B[269]. If shown to influence RNA editing for other proteins, hnRNP A/B could have a profound effect on proper protein expression involved in many cellular processes. Although the changes were again small, we also observed evidence for the control of hnRNP R or Q expression by c-Myc in HeLa and MCF-7 cells (Fig. 4.3D). The measurement of hnRNP R or Q could not be discerned because only peptides shared between both isoforms were detected in this experiment. However, the lack of hnRNP Q-unique peptides detected at the MRM-development stage (Fig. 4.1C) suggests hnRNP R was predominant in the cells we used. The functions of hnRNP R are not well characterized but it has recently been shown that it rapidly and strongly enhances transcription of the proto-oncogene *c-fos*, which is a key response to external growth signals in cells[270]. Additionally, hnRNP R has been shown to play a role in axonal growth by interacting with β-actin in motor neurons[271]. If further shown that our data resulted from differences in hnRNP Q levels, it is noteworthy that hnRNP Q (like hnRNP A/B) has also been implicated in RNA editing by association with APOBEC1[272].

MRM investigation of changes in PKM1/M2 splicing under c-Myc knockdown or in C2C12 cells showed that hnRNP A/B was not correlated with PKM1/M2 splicing (Fig 4.4B & 4.5C). Although it has previously been shown that c-Myc has been shown to influence PKM1/M2 splicing through hnRNP A1, A2, and I (PTB) in mouse NIH 3T3 cells, our results agree with previous work showing that the c-Myc knockdown effect on PKM1/M2 is not

evident in HeLa cells[61]. Also of interest, our observed decreases in hnRNP A1 levels in differentiated C2C12 cells were not accompanied by decreases in hnRNP A2, previously reported by others in the same scenario[60, 61]. Higher levels of PKM1 and persistent but slightly decreased PKM2 levels were previously observed when comparing differentiated and proliferating C2C12 cells[60, 61] but our MRM results show increased levels of peptides representing both splice variants (Fig. 4.5B). These discrepancies are not entirely surprising since the influence of hnRNPs over PKM1/M2 splicing is a delicate balance likely requiring recruitment of multiple hnRNP proteins into an mRNA-processing complex[60, 61]. In fact, hnRNPs are typically found together in large nuclear complexes with other mRNA-binding proteins and such interactions are required for hnRNPs to influence the processing of pre-mRNA [273, 274]. The levels of PKM2 we measured in Hek 293, HeLa, and MCF-7 cells (Fig. 4.5), are close to those reported by LC-MRM analysis in cancerous endometrial tissues of 85 fmol/μg protein[275]. Finally, although we show that hnRNP A/B appears to be influenced by c-Myc knockdown, no known c-Myc transcriptional promoter binding sites are documented, evident by manual inspection of the genomic sequence, or predicted using a promoter search tool (http://www-bimas.cit.nih.gov/molbio/proscan/) for hnRNP A/B. Influences on hnRNP levels by c-Myc may then be indirect. Further, since differences under c-Myc knockdown were small it is possible that hnRNP A/B changes in C2C12 and other cell lines are regulated by proteins other than c-Myc. Nevertheless, our results show evidence that hnRNP A/B could be influenced by proliferative growth signals and if validated, hnRNP A/B and other hnRNPs such as hnRNP K may prove to be valuable targets for novel cancer therapeutics.

4.5 Conclusion

The hnRNP proteins may serve as a key bridge between growth signalling pathways and regulation of mRNA transcription and translation. Here, by targeted proteomics of the hnRNP family using LC-MRM we revealed interesting peptide-specific differences in hnRNP K and evidence that hnRNP A/B levels are influenced by c-Myc. We also show that hnRNP A/B and c-Myc do not appear to be correlated with PKM1/M2 splicing in the human cell

lines tested. Since the expression of hnRNPs has been associated with various cancers, the roles of hnRNP A/B and perhaps hnRNP K should be addressed. If further shown to be required for cancer cell proliferation, hnRNPs such as A/B could serve as novel therapeutic targets for cancer.

Chapter 5: Conclusion

Signal transduction pathways have been well studied in cancer since they harbour many of the oncogenes and tumour suppressors that are mutated resulting in dysregulated cell growth. As opposed to the study of immediately activated signal transduction effectors, this study examines the changes that occur in protein expression far downstream of growth factor signalling. Since constitutively active growth factor signalling pathways play a significant role in cancer[157], this work enhances our understanding of the protein-expression phenotype or "proteotype" that might be observed in cancers. Such proteotypes might be associated with known cancer genotypes (mutated oncogenes and tumour suppressors) and phenotypes and ultimately used to design novel therapeutics and biomarker signatures for cancer and other growth signalling-related diseases[276]. To study these far downstream protein expression changes, we employed both non-targeted shotgun proteomics using 2D-LC-MS/MS as well as targeted proteomics using MRM.

Through our proteomics experiments, we show evidence that up regulation of the final stages of glycolysis (ENO1, PKM2, and LDHA) could be a proteotype for aberrant growth signals. These results were initially indicated in discovery phase work and then confirmed by more targeted approaches with MRM. Of benefit to targeted analysis of patterns of glycolysis proteins, is their high abundance level in cells, leading to their successful detection by LC-MRM from both cultured cells and cancerous lung tissue. Targeted proteomics with LC-MRM has advantages over non-targeted shotgun proteomics techniques such as increased throughput and better overlap in terms of peptides measured between biological replicates, albeit at the expense of a global view of protein expression[120]. There are also inherent LC-MRM advantages over traditional affinity-based detection such as Western blot or ELISA such as increased selectivity and the efficiency at which quantification can be multiplexed[231]. As a result of this success, LC-MRM of glycolysis has immediate potential to contribute to a better understanding of the metabolism of cancer cells, as well as its use in assessing the metabolic potential of tumours from patient biopsies.

The biological consequences of our LC-MRM-based results, which showed increased ENO1, PKM2, and LDHA in growth-factor driven cells, likely center around a key regulator of glycolysis in cancer - PKM2. The M2 pyruvate kinase variant is important for cell proliferation which occurs as a result of its lower activity than the M1 variant[277,278] and consequent funnelling of glycolytic intermediates to biosynthetic pathways[258]. High levels of ENO1, PKM2, and LDHA in response to growth signals might, at first glance, serve to alleviate the assimilation of upstream metabolites and direct the glycolytic flux to pyruvate thus explaining how high levels of pyruvate (the immediate pyruvate kinase product) and lactate are observed in cancer cells with a low activity pyruvate kinase variant. However, it has recently been demonstrated that a phosphate from the substrate for pyruvate kinase, phosphoenolpyruvate (PEP), can be transferred to PGAM1. Thus, our observed increases in ENO1 and LDHA could be part of a continual cycle sustaining high PEP rates for PGAM1 phosphorylation and removal of pyruvate in the form of lactate. It is therefore fitting, and perhaps necessary for cancer cell proliferation that growth factor signalling upregulates this important metabolic control point. Key questions still remain in this system however since the stoichiometries of the reactions are not known and pyruvate can also accumulate through glutamine metabolism pathways[279].

Much of the redirection of glycolysis intermediates to biosynthesis is through the oxidative and non-oxidative pentose phosphate pathways which are respectively catalyzed by G6PD and TKT[26]. It was therefore unexpected that we did not observe equally elevated levels of G6PD and TKT as we did ENO1, PKM2, and LDHA in growth-factor-driven cells. It is conceivable however, that reaction rates for biosynthesis might proceed in a concentration-dependent manner, not requiring high increases in G6PD and TKT. Our results, taken together with recent studies, suggest that the glycolytic proteins from PGAM1 to LDHA represent an important axis in cell proliferation, yet needs further study into its regulation by downstream effectors of growth factors. Our findings will also need to be correlated with metabolomic data to trace the destination of glycolysis intermediates in proliferating cells.

Besides glycolytic proteins, our initial discovery-phase growth factor experiments using MCF-7 cells showed evidence that IGF-1 stimulation appears to either up-regulate the expression of Rab protein-regulated vesicle trafficking or results in their accumulation in

the cytosol after 24 h of stimulation. Targeted proteomic analysis could not be successfully conducted for the Rab family of proteins because most of the peptides measurable by LC-MRM in preliminary analyses were shared between members of the family. However, previous reports that Rab proteins are involved in endocytosis of receptors, suggest that IGF-1 could stimulate Rab-mediated endocytosis of IGF-1R. Recent work shows that upon activation by the IGF-1 ligand, IGF-1R translocates to the nucleus by endocytosis and interacts with chromatin, putatively directly regulating transcription[280]. Nuclear-localized IGF-1R was subsequently detected in renal cancer, pre-invasive breast, and non-malignant proliferating cells[280]. Since we observed IGF-1 stimulation to accompany increased levels of several Rab proteins, we question whether Rab proteins facilitate IGF-1R endocytosis. Moreover, perhaps endocytosis of IGF-1R directly regulates gene expression changes in ENO1, PKM2, and LDHA – mechanisms which are currently poorly established and should be addressed.

To attempt to explain the mechanism for consistent splice site regulation towards the M2 variant of pyruvate kinase we based further targeted proteomic experiments on two recent studies demonstrating that the constitutive expression of the M2 pyruvate kinase variant is influenced by hnRNP proteins. Since hnRNP proteins are highly abundant, we were able to successfully employ our previous techniques using MRM to study the hnRNP family of proteins and to determine those that are increased in growth-factor stimulated cells. Again, we propose that the MRM assay we have designed has the potential to contribute to a better understanding of mRNA processing events in cells. Regulated by c-Myc, the constitutive splice site selection towards the M2 splice variant of pyruvate kinase in proliferating cells has recently been shown to be partly facilitated by hnRNPA1, hnRNPA2, and hnRNPI (also called PTB) in NIH 3T3 cells [61]. In the same study though, c-Myc knockdown in HeLa cells showed no difference in hnRNPA1, hnRNPA2, hnRNPI, or PKM2 splice site selection [61]. Our LC-MRM analysis of hnRNP family peptides implicates another lesser-known hnRNP (A/B) associated with cell proliferation. Our results show hnRNP A/B appears to be increased in a c-Myc dependent manner. Regulation of PKM2 splice site selection by hnRNP A/B under the control of c-Myc was not evident here however. It is possible that PKM2 splicing is influenced by other factors such as E2F and AP1 or other means such as direct interaction of nuclear localized IGF-1R with chromatin.

These are interesting hypotheses for tumour metabolism and should be evaluated. Evidence we observed for peptide-specific differences in hnRNPK under c-Myc is novel and possibly related to expression of new isoforms or post-translational modifications for hnRNP K. Indeed, more isoforms of hnRNP K are thought to exist than those currently known[267]. Increased levels of hnRNPK are consistently shown in proliferating cells, to which numerous functions have been attributed (as has been reviewed [265]). Finally, hnRNP proteins likely function in large complexes with considerable functional redundancy among closely related members of the family[250]. The necessity of formation of complexes is evidenced by previous work showing that the M2 splice variant in cells is not completely switched to M1 upon depletion of hnRNPA1, hnRNPA2, and hnRNPI[61].

The work described in this study has increased our understanding of some of the fundamental far-downstream changes in the proteome of human cells in response to growth signals. We propose that this knowledge can be used in guiding rational drug design towards targets that might be more direct catalysts of cell proliferation than switch-like oncogenes and tumour suppressors. It appears that metabolism proteins will play key roles in this new direction for cancer therapeutics. Still, there are many unanswered questions in this area of cancer. For example, how do the influences of growth signals effect metabolic fluxes from glucose as opposed to other sources of carbon such as glutamine? How do oncogene and tumour suppressor mutations directly result in altered metabolism? As the population of cancer cells in a tumor evolves, do micro-environmental changes (hypoxia, pH, etc.) select for metabolically-fit cells? If so, do proteins like ENO1, PKM2, and LDHA provide selective advantages and can they be targeted to successfully kill cancer cells? Finally, are poorly characterized, yet highly abundant proteins such as hnRNP A/B required for cell proliferation? Continual efforts in this intriguing area of cell biology will hopefully provide bring about answers to these questions.

References

1. Kim, J.; Dang, C. V., Cancer's molecular sweet tooth and the Warburg effect. *Cancer Res.* **2006,** 66, 8927-8930.
2. Lu, Y.; Yi, Y.; Liu, P.; Wen, W.; James, M.; Wang, D.; You, M., Common human cancer genes discovered by integrated gene-expression analysis. *PLoS ONE* **2007,** 2, (11), e1149.
3. Altenberg, B.; Greulich, K., Genes of glycolysis are ubiquitously overexpressed in 24 cancer classes. *Genomics* **2004,** 84, (6), 1014-1020.
4. Bi, X.; Lin, Q.; Foo, T. W.; Joshi, S.; You, T.; Shen, H. M.; Ong, C. N.; Cheah, P. Y.; Eu, K. W.; Hew, C. L., Proteomic analysis of colorectal cancer reveals alterations in metabolic pathways: mechanism of tumorigenesis. *Mol. Cell. Proteomics* **2006,** 5, (6), 1119-1130.
5. Totty, N.; Knowles, M.; Eardley, I.; Selby, P.; Banks, R., Proteomic changes in renal cancer and co-ordinate demonstration of both the glycolytic and mitochondrial aspects of the Warburg effect. *Proteomics* **2003,** 3, 1620-1632.
6. Gillies, R. J.; Gatenby, R. A., Adaptive landscapes and emergent phenotypes: why do cancers have high glycolysis? *J. Bioenerget. Biomembr.* **2007,** 39, (3), 251-257.
7. Lu, H.; Forbes, R.; Verma, A., Hypoxia-inducible factor 1 activation by aerobic glycolysis implicates the Warburg effect in carcinogenesis. *J. Biol. Chem.* **2002,** 277, (26), 23111-23115.
8. Foldi, M.; Stickeler, E.; Bau, L.; Kretz, O.; Watermann, D.; Gitsch, G.; Kayser, G.; Zur Hausen, A.; Coy, J., Transketolase protein TKTL 1 overexpression: A potential biomarker and therapeutic target in breast cancer. *Oncol. Rep.* **2007,** 17, (4), 841-845.
9. Rijken, P.; Bernsen, H.; Peters, J. P. W.; Hodgkiss, R. J.; Raleigh, J. A.; van der Kogel, A. J., Spatial relationship between hypoxia and the (perfused) vascular network in a human glioma xenograft: a quantitative multi-parameter analysis. *Int. J. Radiat. Oncol. Biol. Phys.* **2000,** 48, (2), 571-582.
10. Venables, J., Unbalanced alternative splicing and its significance in cancer. *Bioessays* **2006,** 28, (4), 378-386.
11. Fothergill-Gilmore, L. A., The evolution of the glycolytic pathway. *Trend Biochem. Sci.* **1986,** 11, (1), 47-51.
12. House, A. E.; Lynch, K. W., Regulation of alternative splicing: more than just the ABCs. *J. Biol. Chem.* **2008,** 283, (3), 1217-1221.
13. Mathupala, S. P.; Ko, Y. H.; Pedersen, P. L., Hexokinase II: cancer's double-edged sword acting as both facilitator and gatekeeper of malignancy when bound to mitochondria. *Oncogene* **2006,** 25, (34), 4777-4786.
14. Bustamante, E.; Morris, H.; Pedersen, P., Energy metabolism of tumor cells. Requirement for a form of hexokinase with a propensity for mitochondrial binding. *J. Biol. Chem.* **1981,** 256, (16), 8699-8704.
15. Nakashima, R. A.; Mangan, P. S.; Colombini, M.; Pedersen, P. L., Hexokinase receptor complex in hepatoma mitochondria: evidence from N, N'-dicyclohexlycarbodiimide-labelling studies for the involvement of the pore-forming protein VDAC. *Biochemistry (Mosc.)* **1986,** 25, (5), 1015-1021.
16. Pastorino, J.; Shulga, N.; Hoek, J., Mitochondrial binding of hexokinase II inhibits Bax-induced cytochrome c release and apoptosis. *J. Biol. Chem.* **2002,** 277, (9), 7610-7618.

17. Jurica, M.; Mesecar, A.; Heath, P.; Shi, W.; Nowak, T.; Stoddard, B., The allosteric regulation of pyruvate kinase by fructose-1, 6-bisphosphate. *Structure* **1998,** 6, (2), 195-210.
18. Eigenbrodt, E.; Mazurek, S.; Friis, R. R., Double role of pyruvate kinase type M2 in the regulation of phosphometabolite pools. *Cell Growth Oncogen.* **1998**, 15–30.
19. Christofk, H. R.; Vander Heiden, M. G.; Harris, M. H.; Ramanathan, A.; Gerszten, R. E.; Wei, R.; Fleming, M. D.; Schreiber, S. L.; Cantley, L. C., The M2 splice isoform of pyruvate kinase is important for cancer metabolism and tumour growth. *Nature* **2008,** 452, (7184), 230-233.
20. Vander Heiden, M. G.; Locasale, J. W.; Swanson, K. D.; Sharfi, H.; Heffron, G. J.; Amador-Noguez, D.; Christofk, H. R.; Wagner, G.; Rabinowitz, J. D.; Asara, J. M., Evidence for an alternative glycolytic pathway in rapidly proliferating cells. *Science* **2010,** 329, (5998), 1492-1499.
21. DeBerardinis, R. J.; Mancuso, A.; Daikhin, E.; Nissim, I.; Yudkoff, M.; Wehrli, S.; Thompson, C. B., Beyond aerobic glycolysis: transformed cells can engage in glutamine metabolism that exceeds the requirement for protein and nucleotide synthesis. *Proc. Natl. Acad. Sci. U. S. A.* **2007,** 104, (49), 19345-19350.
22. Christofk, H.; Vander Heiden, M.; Wu, N.; Asara, J.; Cantley, L., Pyruvate kinase M2 is a phosphotyrosine-binding protein. *Nature* **2008,** 452, (7184), 181-186.
23. Mazurek, S.; Grimm, H.; Boschek, C. B.; Vaupel, P.; Eigenbrodt, E., Pyruvate kinase type M2: a crossroad in the tumor metabolome. *Br. J. Nutrit.* **2002,** 87, (S1), 23-29.
24. Acebo, P.; Giner, D.; Calvo, P.; Blanco-Rivero, A.; Ortega, Á.; Fernández, P. L.; Roncador, G.; Fernández-Malavé, E.; Chamorro, M.; Cuezva, J. M., Cancer abolishes the tissue type-specific differences in the phenotype of energetic metabolism. *Translat. Oncol.* **2009,** 2, (3), 138-145.
25. Steták, A.; Veress, R.; Ovádi, J.; Csermely, P.; Kéri, G.; Ullrich, A., Nuclear translocation of the tumor marker pyruvate kinase M2 induces programmed cell death. *Cancer Res.* **2007,** 67, (4), 1602-1608.
26. Tong, X.; Zhao, F.; Thompson, C. B., The molecular determinants of de novo nucleotide biosynthesis in cancer cells. *Curr. Opin. Genet. Dev.* **2009,** 19, (1), 32-37.
27. Schafer, Z.; Grassian, A.; Song, L.; Jiang, Z.; Gerhart-Hines, Z.; Irie, H.; Gao, S.; Puigserver, P.; Brugge, J., Antioxidant and oncogene rescue of metabolic defects caused by loss of matrix attachment. *Nature* **2009,** 461, 109-113.
28. Boada, J.; Roig, T.; Perez, X.; Gamez, A.; Bartrons, R.; Cascante, M.; Bermudez, J., Cells overexpressing fructose-2, 6-bisphosphatase showed enhanced pentose phosphate pathway flux and resistance to oxidative stress. *FEBS Lett.* **2000,** 480, (2-3), 261-264.
29. Okar, D.; Lange, A.; Manzano; Navarro-Sabat , A.; Riera, L.; Bartrons, R., PFK-2/FBPase-2: maker and breaker of the essential biofactor fructose-2, 6-bisphosphate. *Trends Biochem. Sci.* **2001,** 26, (1), 30-35.
30. Minchenko, O. H.; Ochiai, A.; Opentanova, I. L.; Ogura, T.; Minchenko, D. O.; Caro, J.; Komisarenko, S. V.; Esumi, H., Overexpression of 6-phosphofructo-2-kinase/fructose-2, 6-bisphosphatase-4 in the human breast and colon malignant tumors. *Biochimie* **2005,** 87, (11), 1005-1010.
31. Gatenby, R. A.; Gawlinski, E. T.; Gmitro, A. F.; Kaylor, B.; Gillies, R. J., Acid-mediated tumor invasion: a multidisciplinary study. *Cancer Res.* **2006,** 66, (10), 5216-5223.

32. Fantin, V. R.; St-Pierre, J.; Leder, P., Attenuation of LDH-A expression uncovers a link between glycolysis, mitochondrial physiology, and tumor maintenance. *Cancer Cell* **2006**, 425-434.
33. Ullah, M. S.; Davies, A. J.; Halestrap, A. P., The plasma membrane lactate transporter MCT4, but not MCT1, is up-regulated by hypoxia through a HIF-1 -dependent mechanism. *J. Biol. Chem.* **2006,** 281, (14), 9030-9037.
34. Kim, J.; Tchernyshyov, I.; Semenza, G.; Dang, C., HIF-1-mediated expression of pyruvate dehydrogenase kinase: a metabolic switch required for cellular adaptation to hypoxia. *Cell Metabol.* **2006,** 3, (3), 177-185.
35. Semenza, G., Hypoxia, clonal selection, and the role of HIF-1 in tumor progression. *Crit. Rev. Biochem. Mol. Biol.* **2000,** 35, (2), 71-103.
36. Vogelstein, B.; Kinzler, K., Cancer genes and the pathways they control. *Nature Med.* **2004,** 10, (8), 789-799.
37. Ak, P.; Levine, A. J., p53 and NFκB: different strategies for responding to stress lead to a functional antagonism. *FASEB J.* **2010,** 24, (10), 3643-3652.
38. Feng, Z.; Hu, W.; de Stanchina, E.; Teresky, A. K.; Jin, S.; Lowe, S.; Levine, A. J., The regulation of AMPKβ1, TSC2, and PTEN expression by p53: stress, cell and tissue specificity, and the role of these gene products in modulating the IGF-1-AKT-mTOR pathways. *Cancer Res.* **2007,** 67, (7), 3043-3053.
39. Huang, L., Carrot and stick: HIF- engages c-Myc in hypoxic adaptation. *Cell Death Differ.* **2008,** 15, (4), 672-677.
40. Semenza, G., Targeting HIF-1 for cancer therapy. *Nature Rev. Cancer* **2003,** 3, (10), 721-732.
41. Papandreou, I.; Cairns, R. A.; Fontana, L.; Lim, A. L.; Denko, N. C., HIF-1 mediates adaptation to hypoxia by actively downregulating mitochondrial oxygen consumption. *Cell Metab.* **2006,** 3, (3), 187-197.
42. An, W.; Kanekal, M.; Simon, M.; Maltepe, E.; Blagosklonny, M.; Neckers, L., Stabilization of wild-type p53 by hypoxia-inducible factor 1. *Nature* **1998,** 392, (6674), 405-408.
43. Wojtczak, L., The Crabtree effect: a new look at the old problem. *Acta Biochim. Pol.* **1996,** 43, 361-368.
44. Gogvadze, V.; Orrenius, S.; Zhivotovsky, B., Mitochondria in cancer cells: what is so special about them? *Trends Cell Biol.* **2008,** 18, (4), 165-173.
45. Laderoute, K. R.; Amin, K.; Calaoagan, J. M.; Knapp, M.; Le, T.; Orduna, J.; Foretz, M.; Viollet, B., 5'-AMP-activated protein kinase (AMPK) is induced by low-oxygen and glucose deprivation conditions found in solid-tumor microenvironments. *Mol. Cell. Biol.* **2006,** 26, (14), 5336-5347.
46. Budanov, A. V.; Karin, M., p53 target genes sestrin1 and sestrin2 connect genotoxic stress and mTOR signalling. *Cell* **2008,** 134, (3), 451-460.
47. Almeida, A.; Moncada, S.; Bolaños, J. P., Nitric oxide switches on glycolysis through the AMP protein kinase and 6-phosphofructo-2-kinase pathway. *Nat. Cell Biol.* **2003,** 6, (1), 45-51.
48. Ho, H.; Cheng, M.; Chiu, D. T., Glucose-6-phosphate dehydrogenase from oxidative stress to cellular functions and degenerative diseases. *Redox Report* **2007,** 12, (3), 109-118.

49. Greer, E. L.; Oskoui, P. R.; Banko, M. R.; Maniar, J. M.; Gygi, M. P.; Gygi, S. P.; Brunet, A., The energy sensor AMP-activated protein kinase directly regulates the mammalian FOXO3 transcription factor. *J. Biol. Chem.* **2007,** 282, (41), 30107-30119.
50. Van Der Horst, A.; Burgering, B., Stressing the role of FoxO proteins in lifespan and disease. *Nat. Rev. Mol. Cell Biol.* **2007,** 8, (6), 440-450.
51. Jones, R.; Plas, D.; Kubek, S.; Buzzai, M.; Mu, J.; Xu, Y.; Birnbaum, M.; Thompson, C., AMP-activated protein kinase induces a p53-dependent metabolic checkpoint. *Mol. Cell* **2005,** 18, (3), 283-293.
52. Salminen, A.; Kaarniranta, K., Glycolysis links p53 function with NFκB signalling: Impact on cancer and aging process. *J. Cell. Physiol.* 224, (1), 1-6.
53. Towler, M. C.; Hardie, D. G., AMP-activated protein kinase in metabolic control and insulin signalling. *Circ. Res.* **2007,** 100, (3), 328-341.
54. Osthus, R. C.; Shim, H.; Kim, S.; Li, Q.; Reddy, R.; Mukherjee, M.; Xu, Y.; Wonsey, D.; Lee, L. A.; Dang, C. V., Deregulation of glucose transporter 1 and glycolytic gene expression by c-Myc. *J. Biol. Chem.* **2000,** 275, (29), 21797-21800.
55. Neiman, P.; Ruddell, A.; Jasoni, C.; Loring, G.; Thomas, S.; Brandvold, K.; Lee, R.; Burnside, J.; Delrow, J., Analysis of gene expression during myc oncogene-induced lymphomagenesis in the bursa of Fabricius. *Proc. Natl. Acad. Sci. U.S.A.* **2001,** 98, (11), 6378-6383.
56. O'Connell, B.; Cheung, A.; Simkevich, C.; Tam, W.; Ren, X.; Mateyak, M.; Sedivy, J., A large scale genetic analysis of c-Myc-regulated gene expression patterns. *J. Biol. Chem.* **2003,** 278, (14), 12563-12573.
57. Menssen, A.; Hermeking, H., Characterization of the c-MYC-regulated transcriptome by SAGE: identification and analysis of c-MYC target genes. *Proc. Natl. Acad. Sci. U.S.A.* **2002,** 99, (9), 6274-6279.
58. Bonafe, M.; Barbieri, M.; Marchegiani, F.; Olivieri, F.; Ragno, E.; Giampieri, C.; Mugianesi, E.; Centurelli, M.; Franceschi, C.; Paolisso, G., Polymorphic variants of insulin-like growth factor I (IGF-I) receptor and phosphoinositide 3-kinase genes affect IGF-I plasma levels and human longevity: cues for an evolutionarily conserved mechanism of life span control. *J. Clin. Endocrinol. Metabol.* **2003,** 88, (7), 3299-3304.
59. Kaidi, A.; Williams, A.; Paraskeva, C., Interaction between B-catenin and HIF-1 promotes cellular adaptation to hypoxia. *Nat. Cell Biol.* **2007,** 9, (2), 210-217.
60. Clower, C.; Chatterjee, D.; Wang, Z.; Cantley, L.; Vander Heiden, M.; Krainer, A., The alternative splicing repressors hnRNP A1/A2 and PTB influence pyruvate kinase isoform expression and cell metabolism. *Proc. Natl. Acad. Sci. U. S. A.* **2009,** 107, (5), 1894-1899.
61. David, C.; Chen, M.; Assanah, M.; Canoll, P.; Manley, J., HnRNP proteins controlled by c-Myc deregulate pyruvate kinase mRNA splicing in cancer. *Nature* **2009,** 463, (7279), 364-368.
62. Xia, Y.; Padre, R. C.; De Mendoza, T. H.; Bottero, V.; Tergaonkar, V. B.; Verma, I. M., Phosphorylation of p53 by IκB kinase 2 promotes its degradation by β-TrCP. *Proc. Natl. Acad. Sci. U.S.A.* **2009,** 106, (8), 2629-2634.
63. Chiao, P.; Miyamoto, S.; Verma, I. M., Autoregulation of I kappa B alpha activity. *Proc. Natl. Acad. Sci. U.S.A.* **1994,** 91, (1), 28-32.
64. Pahl, H., Activators and target genes of Rel/NF-kappaB transcription factors. *Oncogene* **1999,** 18, (49), 6853-6866.

65. Buckbinder, L.; Talbott, R.; Velasco-Miguel, S.; Takenaka, I.; Faha, B.; Seizinger, B. R.; Kley, N., Induction of the growth inhibitor IGF-binding protein 3 by p53. *Nature* **1995,** 377, 646-649.
66. Bensaad, K.; Tsuruta, A.; Selak, M.; Vidal, M.; Nakano, K.; Bartrons, R.; Gottlieb, E.; Vousden, K., TIGAR, a p53-inducible regulator of glycolysis and apoptosis. *Cell* **2006,** 126, (1), 107-120.
67. Kondoh, H.; Lleonart, M.; Gil, J.; Wang, J.; Degan, P.; Peters, G.; Martinez, D.; Carnero, A.; Beach, D., Glycolytic enzymes can modulate cellular life span. *Cancer Res.* **2005,** 65, (1), 177-185.
68. Matoba, S.; Kang, J.; Patino, W.; Wragg, A.; Boehm, M.; Gavrilova, O.; Hurley, P.; Bunz, F.; Hwang, P., p53 regulates mitochondrial respiration. *Science* **2006,** 312, (5780), 1650-1653.
69. Schwartzenberg-Bar-Yoseph, F.; Armoni, M.; Karnieli, E., The tumor suppressor p53 down-regulates glucose transporters GLUT1 and GLUT4 gene expression. *Cancer Res.* **2004,** 64, (7), 2627-2633.
70. DiDonato, J.; Mercurio, F.; Rosette, C.; Wu-Li, J.; Suyang, H.; Ghosh, S.; Karin, M., Mapping of the inducible IkappaB phosphorylation sites that signal its ubiquitination and degradation. *Mol. Cell. Biol.* **1996,** 16, (4), 1295-1304.
71. Haltiwanger, R. S.; Holt, G. D.; Hart, G. W., Enzymatic addition of O-GlcNAc to nuclear and cytoplasmic proteins. Identification of a uridine diphospho-N-acetylglucosamine: peptide beta-N-acetylglucosaminyltransferase. *J. Biol. Chem.* **1990,** 265, (5), 2563-2568.
72. Secomb, T. W.; Hsu, R.; Dewhirst, M. W.; Klitzman, B.; Gross, J. F., Analysis of oxygen transport to tumor tissue by microvascular networks. *Int. J. Radiat. Oncol. Biol. Phys.* **1993,** 25, 481-481.
73. Heldin, C. H.; Rubin, K.; Pietras, K.; Ostman, A., High interstitial fluid pressure - an obstacle in cancer therapy. *Nat. Rev. Cancer* **2004,** 4, (10), 806-813.
74. Semenza, G.; Nejfelt, M.; Chi, S., Hypoxia-inducible nuclear factors bind to an enhancer element located 3' to the human erythropoietin gene. *Proc. Natl. Acad. Sci. U.S.A.* **1991,** 88, (13), 5680-5684.
75. Ryan, H. E.; Lo, J.; Johnson, R. S., HIF-1 alpha is required for solid tumor formation and embryonic vascularization. *EMBO J.* **1998,** 17, (11), 3005-3015.
76. Semenza, G.; Roth, P.; Fang, H.; Wang, G., Transcriptional regulation of genes encoding glycolytic enzymes by hypoxia-inducible factor 1. *J. Biol. Chem.* **1994,** 269, (38), 23757-23763.
77. Greijer, A.; Van der Groep, P.; Kemming, D.; Shvarts, A.; Semenza, G.; Meijer, G.; Van de Wiel, M.; Belien, J.; Van Diest, P.; van Der Wall, E., Up-regulation of gene expression by hypoxia is mediated predominantly by hypoxia-inducible factor 1 (HIF-1). *J. Pathol.* **2005,** (3), 291-304.
78. Bergeron, M.; Yu, A.; Solway, K.; Semenza, G.; Sharp, F., Induction of hypoxia-inducible factor-1 (HIF-1) and its target genes following focal ischaemia in rat brain. *Eur. J. Neurosci.* **1999,** 11, (12), 4159-4170.
79. Brunelle, J. K.; Bell, E. L.; Quesada, N. M.; Vercauteren, K.; Tiranti, V.; Zeviani, M.; Scarpulla, R. C.; Chandel, N. S., Oxygen sensing requires mitochondrial ROS but not oxidative phosphorylation. *Cell Metab.* **2005,** 1, (6), 409-414.

80. Guzy, R.; Hoyos, B.; Robin, E.; Chen, H.; Liu, L.; Mansfield, K.; Simon, M.; Hammerling, U.; Schumacker, P., Mitochondrial complex III is required for hypoxia-induced ROS production and cellular oxygen sensing. *Cell Metab.* **2005,** 1, (6), 401-408.
81. Dang, C. V.; Semenza, G. L., Oncogenic alterations of metabolism. *Trend Biochem. Sci.* **1999,** 24, (2), 68-72.
82. King, A.; Selak, M.; Gottlieb, E., Succinate dehydrogenase and fumarate hydratase: linking mitochondrial dysfunction and cancer. *Oncogene* **2006,** 25, (34), 4675-4682.
83. Semenza, G. L., Hypoxia-inducible factor 1 (HIF-1) pathway. *Sci. STKE* **2007,** 2007, (407), cm8.
84. Laderoute, K.; Amin, K.; Calaoagan, J.; Knapp, M.; Le, T.; Orduna, J.; Foretz, M.; Viollet, B., 5'-AMP-activated protein kinase (AMPK) is induced by low-oxygen and glucose deprivation conditions found in solid-tumor microenvironments. *Mol. Cell. Biol.* **2006,** 26, (14), 5336-5347.
85. Kwon, S.; Lee, Y., Effect of low glutamine/glucose on hypoxia-induced elevation of hypoxia-inducible factor-1 in human pancreatic cancer MiaPaCa-2 and human prostatic cancer DU-145 cells. *Clin. Cancer. Res.* **2005,** 11, (13), 4694-4700.
86. Dang, C.; Lewis, B.; Dolde, C.; Dang, G.; Shim, H., Oncogenes in tumor metabolism, tumorigenesis, and apoptosis. *J. Bioenerg. Biomembr.* **1997,** 29, (4), 345-354.
87. Dang, C.; Kim, J.; Gao, P.; Yustein, J., The interplay between MYC and HIF in cancer. *Nat. Rev. Cancer* **2008,** 8, (1), 51-56.
88. Gordan, J. D.; Thompson, C. B.; Simon, M. C., HIF and c-Myc: sibling rivals for control of cancer cell metabolism and proliferation. *Cancer Cell* **2007,** 12, (2), 108-113.
89. Levine, A., p53, the cellular gatekeeper for growth and division. *Cell* **1997,** 88, (3), 323-332.
90. Vogelstein, B.; Lane, D.; Levine, A., Surfing the p53 network. *Nature* **2000,** 408, (6810), 307-310.
91. Nieminen, A. L.; Qanungo, S.; Schneider, E. A.; Jiang, B. H.; Agani, F. H., Mdm2 and HIF 1 interaction in tumor cells during hypoxia. *J. Cell. Physiol.* **2005,** 204, (2), 364-369.
92. Chen, D.; Li, M.; Luo, J.; Gu, W., Direct interactions between HIF-1 and Mdm2 modulate p53 function. *J. Biol. Chem.* **2003,** 278, (16), 13595-13598.
93. Ogawara, Y.; Kishishita, S.; Obata, T.; Isazawa, Y.; Suzuki, T.; Tanaka, K.; Masuyama, N.; Gotoh, Y., Akt enhances Mdm2-mediated ubiquitination and degradation of p53. *J. Biol. Chem.* **2002,** 277, (24), 21843-21850.
94. Bai, D.; Ueno, L.; Vogt, P. K., Akt-mediated regulation of NFκB and the essentialness of NFκB for the oncogenicity of PI3K and Akt. *Int. J. Cancer* **2009,** 125, 2863-2870.
95. Kawauchi, K.; Araki, K.; Tobiume, K.; Tanaka, N., p53 regulates glucose metabolism through an IKK-NF- B pathway and inhibits cell transformation. *Nat. Cell Biol.* **2008,** 10, (5), 611-618.
96. Zelzer, E.; Levy, Y.; Kahana, C.; Shilo, B. Z.; Rubinstein, M.; Cohen, B., Insulin induces transcription of target genes through the hypoxia-inducible factor HIF-1 alpha/ARNT. *EMBO J.* **1998,** 17, (17), 5085-5094.
97. Treins, C.; Giorgetti-Peraldi, S.; Murdaca, J.; Semenza, G.; Van Obberghen, E., Insulin stimulates hypoxia-inducible factor 1 through a phosphatidylinositol 3-kinase/target of rapamycin-dependent signalling pathway. *J. Biol. Chem.* **2002,** 277, (31), 27975-27981.
98. Luo, J.; Manning, B.; Cantley, L., Targeting the PI3K-Akt pathway in human cancer: rationale and promise. *Cancer Cell* **2003,** 4, (4), 257-262.

99. Elstrom, R.; Bauer, D.; Buzzai, M.; Karnauskas, R.; Harris, M.; Plas, D.; Zhuang, H.; Cinalli, R.; Alavi, A.; Rudin, C., Akt stimulates aerobic glycolysis in cancer cells. *Cancer Res.* **2004,** 64, (11), 3892-3899.
100. Roos, S.; Jansson, N.; Palmberg, I.; Saljo, K.; Powell, T.; Jansson, T., Mammalian target of rapamycin in the human placenta regulates leucine transport and is down-regulated in restricted fetal growth. *J. Physiol.* **2007,** 582, (1), 449-459.
101. Barata, J.; Silva, A.; Brandao, J.; Nadler, L.; Cardoso, A.; Boussiotis, V., Activation of PI3K is indispensable for interleukin 7-mediated viability, proliferation, glucose use, and growth of T cell acute lymphoblastic leukemia cells. *J. Exp. Med.* **2004,** 200, (5), 659-669.
102. Wieman, H.; Wofford, J.; Rathmell, J., Cytokine stimulation promotes glucose uptake via phosphatidylinositol-3 kinase/Akt regulation of Glut1 activity and trafficking. *Mol. Biol. Cell* **2007,** 18, (4), 1437-1446.
103. Barthel, A.; Okino, S.; Liao, J.; Nakatani, K.; Li, J.; Whitlock, J.; Roth, R., Regulation of GLUT1 gene transcription by the serine/threonine kinase Akt1. *J. Biol. Chem.* **1999,** 274, (29), 20281-20286.
104. Taha, C.; Liu, Z.; Jin, J.; Al-Hasani, H.; Sonenberg, N.; Klip, A., Opposite translational control of GLUT1 and GLUT4 glucose transporter mRNAs in response to insulin: Role of mammalian target of rapamycin, protein kinase B, and phosphatidylinositol 3-kinase in GLUT1 mRNA translation. *J. Biol. Chem.* **1999,** 274, (46), 33085-33091.
105. Majewski, N.; Nogueira, V.; Bhaskar, P.; Coy, P. E.; Skeen, J. E.; Gottlob, K.; Chandel, N. S.; Thompson, C. B.; Robey, R. B.; Hay, N., Hexokinase-mitochondria interaction mediated by Akt is required to inhibit apoptosis in the presence or absence of Bax and Bak. *Mol. Cell* **2004,** 16, (5), 819-830.
106. Majewski, N.; Nogueira, V.; Robey, R.; Hay, N., Akt inhibits apoptosis downstream of BID cleavage via a glucose-dependent mechanism involving mitochondrial hexokinases. *Mol. Cell. Biol.* **2004,** 24, (2), 730-740.
107. Chiang, G. G.; Abraham, R. T., Targeting the mTOR signalling network in cancer. *Trends Mol. Med.* **2007,** 13, (10), 433-442.
108. Albanell, J.; Dalmases, A.; Rovira, A.; Rojo, F., mTOR signalling in human cancer. *Clin. Translat. Oncol.* **2007,** 9, (8), 484-493.
109. Martin, D. E.; Hall, M. N., The expanding TOR signalling network. *Curr. Opin. Cell Biol.* **2005,** 17, (2), 158-166.
110. Hudson, C. C.; Liu, M.; Chiang, G. G.; Otterness, D. M.; Loomis, D. C.; Kaper, F.; Giaccia, A. J.; Abraham, R. T., Regulation of hypoxia-inducible factor 1α expression and function by the mammalian target of rapamycin. *Mol. Cell. Biol.* **2002,** 22, (20), 7004-7014.
111. Majumder, P. K.; Febbo, P. G.; Bikoff, R.; Berger, R.; Xue, Q.; McMahon, L. M.; Manola, J.; Brugarolas, J.; McDonnell, T. J.; Golub, T. R., mTOR inhibition reverses Akt-dependent prostate intraepithelial neoplasia through regulation of apoptotic and HIF-1-dependent pathways. *Nat. Med.* **2004,** 10, (6), 594-601.
112. Gera, J.; Mellinghoff, I.; Shi, Y.; Rettig, M.; Tran, C.; Hsu, J.; Sawyers, C.; Lichtenstein, A., AKT activity determines sensitivity to mTOR inhibitors by regulating cyclin D1 and c-myc expression. *J Biol Chem* **2004,** 279, (4), 2737-2746.
113. Uhlén, M.; Hober, S., Generation and validation of affinity reagents on a proteome-wide level. *J. Mol. Recognit.* **2008,** 22, (2), 57-64.
114. Ong, S. E.; Mann, M., Mass spectrometry–based proteomics turns quantitative. *Nature Chem. Biol.* **2005,** 1, (5), 252-262.

115. Domon, B.; Broder, S., Implications of new proteomics strategies for biology and medicine. *J. Proteome Res.* **2004,** 3, (2), 253-260.
116. Wolf-Yadlin, A.; Hautaniemi, S.; Lauffenburger, D. A.; White, F. M., Multiple reaction monitoring for robust quantitative proteomic analysis of cellular signalling networks. *Proc. Natl. Acad. Sci. U.S.A.* **2007,** 104, (14), 5860-5865.
117. Whiteaker, J. R.; Zhao, L.; Zhang, H. Y.; Feng, L. C.; Piening, B. D.; Anderson, L.; Paulovich, A. G., Antibody-based enrichment of peptides on magnetic beads for mass-spectrometry-based quantification of serum biomarkers. *Anal. Biochem.* **2007,** 362, (1), 44-54.
118. Anderson, N. L., The roles of multiple proteomic platforms in a pipeline for new diagnostics. *Mol. Cell. Proteomics* **2005,** 4, (10), 1441-1444.
119. Picotti, P.; Bodenmiller, B.; Mueller, L. N.; Domon, B.; Aebersold, R., Full dynamic range proteome analysis of S. cerevisiae by targeted proteomics. *Cell* **2009,** 138, (4), 795-806.
120. Anderson, L.; Hunter, C. L., Quantitative mass spectrometric multiple reaction monitoring assays for major plasma proteins. *Mol. Cell. Proteomics* **2006,** 5, (4), 573-588.
121. Sherman, J.; McKay, M. J.; Ashman, K.; Molloy, M. P., Unique ion signature mass spectrometry, a deterministic method to assign peptide identity. *Mol. Cell. Proteomics* **2009,** 8, (9), 2051-2062.
122. Sandhu, C.; Hewel, J. A.; Badis, G.; Talukder, S.; Liu, J.; Hughes, T. R.; Emili, A., Evaluation of data-dependent versus targeted shotgun proteomic approaches for monitoring transcription factor expression in breast cancer. *J. Proteome Res.* **2008,** 7, (4), 1529-1541.
123. Lange, V.; Picotti, P.; Domon, B.; Aebersold, R., Selected reaction monitoring for quantitative proteomics: a tutorial. *Mol. Sys. Biol.* **2008,** 4, (1), 222-235.
124. Blencowe, B. J., Alternative splicing: new insights from global analyses. *Cell* **2006**, 37-47.
125. Petrak, J.; Ivanek, R.; Toman, O.; Cmejla, R.; Cmejlova, J.; Vyoral, D.; Zivny, J.; Vulpe, C. D., Déjà vu in proteomics. A hit parade of repeatedly identified differentially expressed proteins. *Proteomics* **2008,** 8, (9), 1744-1749.
126. Ramanathan, A.; Wang, C.; Schreiber, S. L., Perturbational profiling of a cell-line model of tumorigenesis by using metabolic measurements. *Proc. Natl. Acad. Sci. U.S.A.* **2005,** 102, (17), 5992-5997.
127. Gatenby, R. A.; Gillies, R. J., Glycolysis in cancer: a potential target for therapy. *Int. J. Biochem. Cell Biol.* **2007,** 39, (7-8), 1358-1366.
128. Kelloff, G. J.; Hoffman, J. M.; Johnson, B.; Scher, H. I., Progress and promise of FDG-PET imaging for cancer patient management and oncologic drug development. *Clin. Cancer Res.* **2005**, 2785-2808.
129. Gambhir, S. S.; Czernin, J.; Schwimmer, J.; Silverman, D. H. S.; Coleman, R. E.; Phelps, M. E., A tabulated summary of the FDG PET literature. *J. Nucl. Med.* **2001,** 42, (5 suppl), 1S-93S.
130. Higashi, T.; Saga, T.; Nakamoto, Y.; Ishimori, T.; Mamede, M. H.; Wada, M.; Doi, R.; Hosotani, R.; Imamura, M.; Konishi, J., Relationship between retention index in dual-phase 18F-FDG PET, and hexokinase-II and glucose transporter-1 expression in pancreatic cancer. *J. Nucl. Med.* **2002,** 43, (2), 173-180.

131. Rho, M.; Kim, J.; Do Jee, C.; Lee, Y.; Lee, H.; Kim, M.; Lee, H.; Kim, W., Expression of type 2 hexokinase and mitochondria-related genes in gastric carcinoma tissues and cell lines. *Anticancer Res.* **2007,** 27, (1A), 251-258.
132. Bos, R.; van der Hoeven, J. J. M.; van Der Wall, E.; van Der Groep, P.; van Diest, P. J.; Comans, E. F. I.; Joshi, U.; Semenza, G. L.; Hoekstra, O. S.; Lammertsma, A. A., Biologic correlates of ^{18}fluorodeoxyglucose uptake in human breast cancer measured by positron emission tomography. *J. Clin. Oncol.* **2002,** 20, (2), 379-389.
133. Chen, G.; Gharib, T. G.; Wang, H.; Huang, C. C.; Kuick, R.; Thomas, D. G.; Shedden, K. A.; Misek, D. E.; Taylor, J. M. G.; Giordano, T. J., Protein profiles associated with survival in lung adenocarcinoma. *Proc. Natl. Acad. Sci. U. S. A.* **2003,** 100, (23), 13537-13542.
134. Cuezva, J. M.; Krajewska, M.; López de Heredia, M.; Krajewski, S.; Santamaría, G.; Kim, H.; Zapata, J. M.; Marusawa, C., The bioenergetic signature of cancer: a marker of tumor progression. *Cancer Res.***2010** 62, 6674–6681.
135. Etzioni, R.; Urban, N.; Ramsey, S.; McIntosh, M.; Schwartz, S.; Reid, B.; Radich, J.; Anderson, G.; Hartwell, L., The case for early detection. *Nat. Rev. Cancer* **2003,** 3, (4), 243-252.
136. Ye, X.; Blonder, J.; Veenstra, T., Targeted proteomics for validation of biomarkers in clinical samples. *Brief. Func. Genom.* **2009,** 8, (2), 126-135.
137. Rifai, N.; Gillette, M. A.; Carr, S. A., Protein biomarker discovery and validation: the long and uncertain path to clinical utility. *Nat. Biotechnol.* **2006,** 24, (8), 971-983.
138. Carr, S. A.; Anderson, L., Protein quantitation through targeted mass spectrometry: the way out of biomarker purgatory? *Clin. Chem.* **2008,** 54, (11), 1749-1752.
139. Anderson, N. L.; Anderson, N. G.; Haines, L. R.; Hardie, D. B.; Olafson, R. W.; Pearson, T. W., Mass spectrometric quantitation of peptides and proteins using Stable Isotope Standards and Capture by Anti-Peptide Antibodies (SISCAPA). *J. Proteome Res.* **2004,** 3, (2), 235-244.
140. Hoofnagle, A. N.; Becker, J. O.; Wener, M. H.; Heinecke, J. W., Quantification of thyroglobulin, a low-abundance serum protein, by immunoaffinity peptide enrichment and tandem mass spectrometry. *Clin. Chem.* **2008,** 54, (11), 1796-1804.
141. Issaq, H.; Veenstra, T., Would you prefer multiple reaction monitoring or antibodies with your biomarker validation? *Expert Rev. Proteomics* **2008,** 5, (6), 761-763.
142. Keshishian, H.; Addona, T.; Burgess, M.; Kuhn, E.; Carr, S. A., Quantitative, multiplexed assays for low abundance proteins in plasma by targeted mass spectrometry and stable isotope dilution. *Mol. Cell. Proteomics* **2007,** 6, (12), 2212-2229.
143. Zakikhani, M.; Dowling, R.; Fantus, I.; Sonenberg, N.; Pollak, M., Metformin is an AMP kinase-dependent growth inhibitor for breast cancer cells. *Cancer Res.* **2006,** 66, (21), 10269-10273.
144. Ko, Y. H.; Pedersen, P. L.; Geschwind, J. F., Glucose catabolism in the rabbit VX2 tumor model for liver cancer: characterization and targeting hexokinase. *Cancer Lett.* **2001,** 173, (1), 83-91.
145. Maher, J. C.; Krishan, A.; Lampidis, T. J., Greater cell cycle inhibition and cytotoxicity induced by 2-deoxy-D-glucose in tumor cells treated under hypoxic vs aerobic conditions. *Cancer Chemother. Pharmacol.* **2004,** 53, (2), 116-122.
146. Strumilo, S. A.; Senkevich, S. B.; Vinogradov, V. V., Effect of oxythiamine on adrenal thiamine pyrophosphate-dependent enzyme activities. *Biomed. Biochim. Acta* **1984,** 43, (2), 159-163.

147. Budihardjo, I.; Walker, D. L.; Svingen, P. A.; Buckwalter, C. A.; Desnoyers, S.; Eckdahl, S.; Shah, G. M.; Poirier, G. G.; Reid, J. M.; Ames, M. M., 6-Aminonicotinamide sensitizes human tumor cell lines to cisplatin. *Clin. Cancer Res.* **1998,** 4, (1), 117-130.
148. Elit, L., Drug evaluation: AP-23573--an mTOR inhibitor for the treatment of cancer. *IDrugs* **2006,** 9, (9), 636-644.
149. Yee, K. W. L.; Zeng, Z.; Konopleva, M.; Verstovsek, S.; Ravandi, F.; Ferrajoli, A.; Thomas, D.; Wierda, W.; Apostolidou, E.; Albitar, M., Phase I/II study of the mammalian target of rapamycin inhibitor everolimus (RAD001) in patients with relapsed or refractory hematologic malignancies. *Clin. Cancer Res.* **2006,** 12, (17), 5165-5173.
150. Chan, S.; Scheulen, M. E.; Johnston, S.; Mross, K.; Cardoso, F.; Dittrich, C.; Eiermann, W.; Hess, D.; Morant, R.; Semiglazov, V., Phase II study of temsirolimus (CCI-779), a novel inhibitor of mTOR, in heavily pretreated patients with locally advanced or metastatic breast cancer. *J. Clin. Oncol.* **2005,** 23, (23), 5314-5322.
151. Rapisarda, A.; Uranchimeg, B.; Sordet, O.; Pommier, Y.; Shoemaker, R. H.; Melillo, G., Topoisomerase I-mediated inhibition of hypoxia-inducible factor 1: mechanism and therapeutic implications. *Cancer Res.* **2004,** 64, (4), 1475-1482.
152. Hunter, T., Signalling--2000 and beyond. *Cell* **2000,** 100, (1), 113-127.
153. Sachdev, D.; Yee, D., Inhibitors of insulin-like growth factor signalling: A therapeutic approach for breast cancer. *J Mammary Gland Biol.* **2006,** 11, (1), 27-39.
154. Huang, P. H.; Mukasa, A.; Bonavia, R.; Flynn, R. A.; Brewer, Z. E.; Cavenee, W. K.; Furnari, F. B.; White, F. M., Quantitative analysis of EGFRvIII cellular signalling networks reveals a combinatorial therapeutic strategy for glioblastoma. *Proc. Natl. Acad. Sci. U.S.A.* **2007,** 104, (31), 12867-12872.
155. Gschwind, A.; Fischer, O.; Ullrich, A., The discovery of receptor tyrosine kinases: targets for cancer therapy. *Nat. Rev. Cancer* **2004,** 4, (5), 361-370.
156. Yee, D., Targeting insulin-like growth factor pathways. *Br. J. Cancer* **2006,** 94, (4), 465-468.
157. Baserga, R.; Peruzzi, F.; Reiss, K., The IGF-1 receptor in cancer biology. *Int. J. Cancer* **2003,** 107, (6), 873-877.
158. Dong, A.; Kong, M.; Ma, Z.; Qian, J.; Cheng, H.; Xu, X., Knockdown of insulin-like growth factor 1 receptor enhances chemosensitivity to cisplatin in human lung adenocarcinoma A549 cells. *Acta Biochim. Biophys. Sinica* **2008,** 40, (6), 497-504.
159. LeRoith, D.; Roberts, C. T., The insulin-like growth factor system and cancer. *Cancer Lett.* **2003,** 195, (2), 127-137.
160. Vander Heiden, M. G.; Plas, D. R.; Rathmell, J. C.; Fox, C. J.; Harris, M. H.; Thompson, C. B., Growth factors can influence cell growth and survival through effects on glucose metabolism. *Mol. Cell. Biol.* **2001,** 21, (17), 5899-5912.
161. Fukuda, R.; Hirota, K.; Fan, F.; Jung, Y. D.; Ellis, L. M.; Semenza, G. L., Insulin-like growth factor 1 induces hypoxia-inducible factor 1-mediated vascular endothelial growth factor expression, which is dependent on MAP kinase and phosphatidylinositol 3-kinase signalling in colon cancer cells. *J. Biol. Chem.* **2002,** 277, (41), 38205-38211.
162. Larsson, O.; Girnita, A.; Girnita, L., Role of insulin-like growth factor 1 receptor signalling in cancer. *Br. J. Cancer* **2005,** 92, 2097-2101.
163. Dupont, J.; Le Roith, D., Insulin-like growth factor 1 and oestradiol promote cell proliferation of MCF-7 breast cancer cells: new insights into their synergistic effects. *Mol. Pathol.* **2001,** 54, (3), 149-154.

164. Bartucci, M.; Morelli, C.; Mauro, L.; Ando, S.; Surmacz, E., Differential insulin-like growth factor I receptor signalling and function in estrogen receptor (ER)-positive MCF-7 and ER-negative MDA-MB-231 breast cancer cells. *Cancer Res.* **2001,** 61, (18), 6747-6754.
165. Yee, D.; Morales, F. R.; Hamilton, T. C.; Von Hoff, D. D., Expression of insulin-like growth factor I, its binding proteins, and its receptor in ovarian cancer. *Cancer Res.* **1991,** 51, (19), 5107-5112.
166. Planque, N., Nuclear trafficking of secreted factors and cell-surface receptors: New pathways to regulate cell proliferation and differentiation, and involvement in cancers. *J. Cell Comm. Sig.* **2003,** 1, 323-340.
167. Aggarwal, K.; Choe, L. H.; Lee, K. H., Shotgun proteomics using the iTRAQ isobaric tags. *Brief. Func. Genomics Proteomics* **2006,** 5, (2), 112-120.
168. Melanson, J. E.; Avery, S. L.; Pinto, D. M., High-coverage quantitative proteomics using amine-specific isotopic labelling. *Proteomics* **2006,** 6, (16), 4466-4474.
169. Bradford, M. M., A rapid and sensitive method for the quantitation of microgram quantities of protein utilizing the principle of protein-dye binding. *Anal. Biochem.* **1976,** 72, (1-2), 248-254.
170. Cottrell, J. S.; London, U. K., Probability-based protein identification by searching sequence databases using mass spectrometry data. *Electrophoresis* **1999,** 20, 3551-3567.
171. Troyanskaya, O.; Cantor, M.; Sherlock, G.; Brown, P.; Hastie, T.; Tibshirani, R.; Botstein, D.; Altman, R. B., Missing value estimation methods for DNA microarrays. *Bioinformatics* **2001,** 17, (6), 520-525.
172. Storey, J. D.; Xiao, W.; Leek, J. T.; Tompkins, R. G.; Davis, R. W., Significance analysis of time course microarray experiments. *Proc. Natl. Acad. Sci. U.S.A.* **2005,** 102, (36), 12837-12842.
173. Soukas, A.; Cohen, P.; Socci, N. D.; Friedman, J. M., Leptin-specific patterns of gene expression in white adipose tissue. *Gene Dev.* **2000,** 14, (8), 963-980.
174. Saeed, A. I.; Sharov, V.; White, J.; Li, J.; Liang, W.; Bhagabati, N.; Braisted, J.; Klapa, M.; Currier, T.; Thiagarajan, M.; Sturn, A.; Snuffin, M.; Rezantsev, A.; Popov, D.; Ryltsov, A.; Kostukovich, E.; Borisovsky, I.; Liu, Z.; Vinsavich, A.; Trush, V.; Quackenbush, J., TM4: a free, open-source system for microarray data management and analysis. *Biotechniques* **2003,** 34, (2), 374-378.
175. Berriz, G. F.; King, O. D.; Bryant, B.; Sander, C.; Roth, F. P., Characterizing gene sets with FuncAssociate. *Bioinformatics* **2003,** 19, (18), 2502-2504.
176. Martens, L.; Hermjakob, H.; Jones, P.; Adamski, M.; Taylor, C.; States, D.; Gevaert, K.; Vandekerckhove, J.; Apweiler, R., PRIDE: the proteomics identifications database. *Proteomics* **2005,** 5, (13), 3537-3545.
177. Barsnes, H.; Vizcaíno, J. A.; Eidhammer, I.; Martens, L., PRIDE Converter: making proteomics data-sharing easy. *Nat. Biotechnol.* **2009,** 27, (7), 598-599.
178. Eisen, M. B.; Spellman, P. T.; Brown, P. O.; Botstein, D., Cluster analysis and display of genome-wide expression patterns. *Proc. Natl. Acad. Sci. U.S.A.* **1998,** 95, (25), 14863-14868.
179. Törönen, P.; Kolehmainen, M.; Wong, G.; Castrén, E., Analysis of gene expression data using self-organizing maps. *FEBS Lett.* **1999,** 451, (2), 142-146.
180. Novick, P.; Zerial, M., The diversity of Rab proteins in vesicle transport. *Curr. Opin. Cell Biol.* **1997,** 9, (4), 496-504.
181. Leek, J.; Monsen, E.; Dabney, A.; Storey, J., EDGE: extraction and analysis of differential gene expression. *Bioinformatics* **2006,** 22, (4), 507-508.

182. Wang, Y., Mixed effects smoothing spline analysis of variance. *J. R. Stat. Soc. B* **1998,** 60, (1), 159-174.
183. Melanson, J. E.; Chisholm, K. A.; Pinto, D. M., Targeted comparative proteomics by liquid chromatography/matrix-assisted laser desorption/ionization triple quandrupole mass spectrometry. *Rapid Commun. Mass Spectrom.* **2006**, 904-910.
184. Locke, S. J.; Leslie, A. D.; Melanson, J. E.; Pinto, D. M., Deviation from the mobile proton model in amino-modified peptides: implications for multiple reaction monitoring analysis of peptides. *Rapid Commun. Mass Spectrom.* **2006,** 20, (10), 1525-1530.
185. Ciocca, D.; Calderwood, S., Heat shock proteins in cancer: diagnostic, prognostic, predictive, and treatment implications. *Cell Stress Chaperon.* **2005,** 10, (2), 86-103.
186. Xu, R.; Pelicano, H.; Zhou, Y.; Carew, J. S.; Feng, L., Inhibition of glycolysis in cancer cells: a novel strategy to overcome drug resistance associated with mitochondrial respiratory defect and hypoxia. *Cancer Res.* **2005,** 65, 613-621.
187. Stein, M.; Dong, J.; Wandinger-Ness, A., Rab proteins and endocytic trafficking: potential targets for therapeutic intervention. *Adv. Drug Deliver. Rev.* **2003,** 55, (11), 1421-1437.
188. Donaldson, J. G.; Lippincott-Schwartz, J., Sorting and signalling at the golgi complex. *Cell* **2000,** 101, (7), 693-696.
189. Kanekura, K.; Nishimoto, I.; Aiso, S.; Matsuoka, M., Characterization of Amyotrophic Lateral Sclerosis-linked P56S mutation of vesicle-associated membrane protein-associated protein B (VAPB/ALS8). *J. Biol. Chem.* **2006,** 281, (40), 30223-30233.
190. Grosshans, B.; Ortiz, D.; Novick, P., Rabs and their effectors: achieving specificity in membrane traffic. *Proc. Natl. Acad. Sci. U.S.A.* **2006,** 103, (32), 11821-11827.
191. Pereira-Leal, J. B.; Seabra, M. C., The mammalian Rab family of small GTPases: definition of family and subfamily sequence motifs suggests a mechanism for functional specificity in the Ras superfamily. *J. Mol. Biol.* **2000,** 301, (4), 1077-1087.
192. Lazar, T.; Gotte, M.; Gallwitz, D., Vesicular transport: how many Ypt/Rab-GTPases make a eukaryotic cell? *Trends Biochem. Sci.* **1997,** 22, (12), 468-472.
193. Hupfeld, C. J.; Olefsky, J. M., Regulation of receptor tyrosine kinase signalling by GRKs and beta-arrestins. *Ann. Rev. Physiol.* **2007,** 69, 561-577.
194. Girard, M.; McPherson, P. S., RME-8 regulates trafficking of the epidermal growth factor receptor. *FEBS Lett.* **2008,** 582, (6), 961-966.
195. Mukherjee, S.; Tessema, M.; Wandinger-Ness, A., Vesicular trafficking of tyrosine kinase receptors and associated proteins in the regulation of signalling and vascular function. *Circulation Res.* **2006,** 98, (6), 743-756.
196. Guha, M.; Srinivasan, S.; Biswas, G.; Avadhani, N. G., Activation of a novel calcineurin-mediated Insulin-like Growth Factor-1 Receptor pathway, altered metabolism, and tumor cell invasion in cells subjected to mitochondrial respiratory stress. *J. Biol. Chem.* **2007,** 282, (19), 14536-14546.
197. Ferguson, E.; Rathmell, J., New roles for pyruvate kinase M2: working out the Warburg effect. *Trends Biochem. Sci.* **2008,** 33, (8), 359-362.
198. Mazurek, S.; Boschek, C. B.; Hugo, F.; Eigenbrodt, E., Pyruvate kinase type M2 and its role in tumor growth and spreading. *Semin. Cancer Biol.* **2005,** 15, 300-308.
199. Hilf, R.; Rector, W. D.; Orlando, R. A., Multiple molecular forms of lactate dehydrogenase and glucose 6-phosphate dehydrogenase in normal and abnormal human breast tissues. *Cancer* **1976,** 37, (4), 1825-1830.

200. Thomas, M.; Monet, J. D.; Brami, M.; Dautigny, N.; Assailly, J.; Ulmann, A.; Bader, C. A., Comparative effects of 17 beta-estradiol, progestin R5020, tamoxifen and RU38486 on lactate dehydrogenase activity in MCF-7 human breast cancer cells. *J. Steroid Biochem.* **1989,** 32, (2), 271-277.
201. Jones, R.; Thompson, C., Tumor suppressors and cell metabolism: a recipe for cancer growth. *Gene Dev.* **2009,** 23, (5), 537-548.
202. Garrido, C.; Gurbuxani, S.; Ravagnan, L.; Kroemer, G., Heat shock proteins: Endogenous modulators of apoptotic cell death. *Biochem. Bioph. Res. Comm.* **2001,** 286, (3), 433-442.
203. Ahn, S. G.; Kim, S. A.; Yoon, J. H.; Vacratsis, P., Heat-shock cognate 70 is required for the activation of heat-shock factor 1 in mammalian cells. *Biochem. J.* **2005,** 392, (Pt 1), 145-152.
204. Wegele, H.; Muller, L.; Buchner, J., Hsp70 and Hsp90 - a relay team for protein folding. *Rev. Physiol. Bioch. P.* **2004,** 151, (1), 1-44.
205. Bakkenist, C. J.; Koreth, J.; Williams, C. S. M.; Hunt, N. C. A.; McGee, J. O., Heat shock cognate 70 mutations in sporadic breast carcinoma. *Cancer Res.* **1999,** 59, (17), 4219-4221.
206. Calderwood, S. K.; Khaleque, M. A.; Sawyer, D. B.; Ciocca, D. R., Heat shock proteins in cancer: chaperones of tumorigenesis. *Trends Biochem. Sci.* **2006,** 31, (3), 164-172.
207. Liaudet-Coopman, E.; Beaujouin, M.; Derocq, D.; Garcia, M.; Glondu-Lassis, M.; Laurent-Matha, V.; Prebois, C.; Rochefort, H.; Vignon, F., Cathepsin D: newly discovered functions of a long-standing aspartic protease in cancer and apoptosis. *Cancer Lett.* **2006,** 237, (2), 167-179.
208. Leto, G.; Tumminello, F. M.; Crescimanno, M.; Flandina, C.; Gebbia, N., Cathepsin D expression levels in nongynecological solid tumors: clinical and therapeutic implications. *Clin. Exp. Metastasis* **2004,** 21, (2), 91-106.
209. Moreau, A.; Yotov, W. V.; Glorieux, F. H.; St-Arnaud, R., Bone-specific expression of the alpha chain of the nascent polypeptide-associated complex, a coactivator potentiating c-Jun-mediated transcription. *Mol. Cell. Biol.* **1998,** 18, (3), 1312-1321.
210. Yotov, W. V.; Moreau, A.; St-Arnaud, R., The alpha chain of the nascent polypeptide-associated complex functions as a transcriptional coactivator. *Mol. Cell. Biol.* **1998,** 18, (3), 1303-1311.
211. Walter, P.; Funfschilling, U.; Rospert, S., Nascent polypeptide-associated complex stimulates protein import into yeast mitochondria. *Mol. Biol. Cell* **1999,** 10, (10), 3289-3299.
212. Lopez, S.; Stuhl, L.; Fichelson, S.; Dubart-Kupperschmitt, A.; StArnaud, R.; Galindo, J. R.; Murati, A.; Berda, N.; Dubreuil, P.; Gomez, S., NACA is a positive regulator of human erythroid-cell differentiation. *J. Cell Sci.* **2005,** 118, (8), 1595-1605.
213. Kisselev, L.; Ehrenberg, M.; Frolova, L., Termination of translation: interplay of mRNA, rRNAs and release factors? *EMBO J.* **2003,** 22, 175-182.
214. Shi, L.; Zhao, G.; Qiu, D.; Godfrey, W. R.; Vogel, H.; Rando, T. A.; Hu, H.; Kao, P. N., NF90 regulates cell cycle exit and terminal myogenic differentiation by direct binding to the 3'-Untranslated Region of MyoD and p21WAF1/CIP1 mRNAs. *J. Biol. Chem.* **2005,** 280, (19), 18981-18989.
215. Iritani, B. M.; Eisenman, R. N., c-Myc enhances protein synthesis and cell size during B lymphocyte development. *Proc. Natl. Acad. Sci. U.S.A.* **1999,** 96, (23), 13180-13185.

216. Wang, Y.; Ma, Y.; Lu, B.; Xu, E.; Huang, Q.; Lai, M., Differential expression of mimecan and thioredoxin domain containing protein 5 in colorectal adenoma and cancer: A proteomic study. *Exp.Biol. Med.* **2007,** 232, (9), 1152-1159.
217. Nissom, P. M.; Lo, S. L.; Lo, J. C. Y.; Ong, P. F.; Lim, J. W. E.; Ou, K.; Liang, R. C.; Seow, T. K.; Chung, M. C. M., Hcc-2, a novel mammalian ER thioredoxin that is differentially expressed in hepatocellular carcinoma. *FEBS Lett.* **2006,** 580, (9), 2216-2226.
218. Casella, J.; Craig, S.; Maack, D.; Brown, A., Cap Z (36/32), a barbed end actin-capping protein, is a component of the Z-line of skeletal muscle. *J. Cell Biol.* **1987,** 105, (1), 371-379.
219. Grunewald, T. G.; Kammerer, U.; Winkler, C.; Schindler, D.; Sickmann, A.; Honig, A.; Butt, E., Overexpression of LASP-1 mediates migration and proliferation of human ovarian cancer cells and influences zyxin localisation. *Br. J. Cancer* **2007,** 96, (2), 296-305.
220. Gruenbaum, Y.; Wilson, K. L.; Harel, A.; Goldberg, M.; Cohen, M., Review: nuclear lamins-structural proteins with fundamental functions. *J. Struct. Biol.* **2000,** 129, (2-3), 313-323.
221. Wendholt, D.; Spilker, C.; Schmitt, A.; Dolnik, A.; Smalla, K. H.; Proepper, C.; Bockmann, J.; Sobue, K.; Gundelfinger, E. D.; Kreutz, M. R., ProSAP-interacting protein 1 (ProSAPiP1), a novel protein of the postsynaptic density that links the spine-associated Rap-Gap (SPAR) to the scaffolding protein ProSAP2/Shank3. *J. Biol. Chem.* **2006,** 281, (19), 13805-13816.
222. Miyasaka, K. Y.; Kida, Y. S.; Sato, T.; Minami, M.; Ogura, T., Csrp1 regulates dynamic cell movements of the mesendoderm and cardiac mesoderm through interactions with Dishevelled and Diversin. *Proc. Natl. Acad. Sci. USA* **2007,** 104, (27), 11274-11279.
223. Michalak, M.; Milner, R.; Burns, K.; Opas, M., Calreticulin. *Biochem J* **1992,** 285, (Pt 3), 681-692.
224. Orrenius, S.; Zhivotovsky, B.; Nicotera, P., Regulation of cell death: the calcium-apoptosis link. *Nat. Rev. Mol. Cell Biol.* **2003,** 4, 552-565.
225. Grewal, T.; Tebar, F.; Pol, A.; Enrich, C., Annexin A6 and its role in Ras signalling. *Annexins* **2004,** 1, 62-67.
226. Pfeffer, S. R.; Dirac-Svejstrup, A. B.; Soldati, T., Rab GDP dissociation inhibitor: putting rab GTPases in the right place. *J. Biol. Chem.* **1995,** 270, (29), 17057-17059.
227. Unwin, R.; Griffiths, J.; Leverentz, M.; Grallert, A.; Hagan, I.; Whetton, A., Multiple Reaction Monitoring to Identify Sites of Protein Phosphorylation with High Sensitivity. *Mol. Cell. Proteomics* **2005,** 4, (8), 1134-1144.
228. Janecki, D.; Bemis, K.; Tegeler, T.; Sanghani, P.; Zhai, L.; Hurley, T.; Bosron, W.; Wang, M., A multiple reaction monitoring method for absolute quantification of the human liver alcohol dehydrogenase ADH1C1 isoenzyme. *Anal. Biochem.* **2007,** 369, (1), 18-26.
229. Jenkins, R.; Kitteringham, N.; Hunter, C.; Webb, S.; Hunt, T.; Elsby, R.; Watson, R.; Williams, D.; Penningtonand, S.; Park, B., Relative and absolute quantitative expression profiling of cytochromes P450 using isotope-coded affinity tags. *Proteomics* **2006,** 6, (6), 1934-1947.
230. Warburg, O., On the origin of cancer cells. *Science* **1956,** 123, (3191), 309-314.
231. Issaq, H. J.; Veenstra, T. D., Would you prefer multiple reaction monitoring or antibodies with your biomarker validation? *Expert Rev. Proteomics* **2008,** 5, (6), 761-763.
232. Kuzyk, M. A.; Smith, D.; Yang, J.; Cross, T. J.; Jackson, A. M.; Hardie, D. B.; Anderson, N. L.; Borchers, C. H., MRM-based, multiplexed, absolute quantitation of 45 proteins in human plasma. *Mol. Cell. Prot.* **2009**, 1860-1877.

233. Lange, V.; Malmström, J. A.; Didion, J.; King, N. L.; Johansson, B. P.; Schäfer, J.; Rameseder, J.; Wong, C. H.; Deutsch, E. W.; Brusniak, M. Y., Targeted quantitative analysis of Streptococcus pyogenes virulence factors by multiple reaction monitoring. *Mol. Cell. Prot.* **2008,** 7, (8), 1489-1500.
234. Murphy, J. P.; Pinto, D. M., Temporal proteomic analysis of IGF-1R signalling in MCF-7 breast adenocarcinoma cells. *Proteomics* **2010,** 10, (9), 1847-1860.
235. DeBerardinis, R. J.; Lum, J. J.; Hatzivassiliou, G.; Thompson, C. B., The biology of cancer: metabolic reprogramming fuels cell growth and proliferation. *Cell Metab.* **2008,** 7, (1), 11-20.
236. Gordan, J.; Thompson, C.; Simon, M., HIF and c-Myc: sibling rivals for control of cancer cell metabolism and proliferation. *Cancer Cell* **2007,** 12, (2), 108-113.
237. Glare, E. M.; Divjak, M.; Bailey, M. J.; Walters, E. H., Beta-Actin and GAPDH housekeeping gene expression in asthmatic airways is variable and not suitable for normalising mRNA levels. *Thorax* **2002,** 57, (9), 765-770.
238. Neve, R. M.; Chin, K.; Fridlyand, J.; Yeh, J.; Baehner, F. L.; Fevr, T.; Clark, L.; Bayani, N.; Coppe, J. P.; Tong, F., A collection of breast cancer cell lines for the study of functionally distinct cancer subtypes. *Cancer Cell* **2006,** 10, (6), 515-527.
239. Annesley, T. M., Ion suppression in mass spectrometry. *Clin. Chem.* **2003,** 49, (7), 1041-1044.
240. Totty, N.; Knowles, M.; Eardley, I.; Selby, P. J.; Banks, R. E., Proteomic changes in renal cancer and co-ordinate demonstration of both the glycolytic and mitochondrial aspects of the Warburg effect. *Proteomics* **2003,** 3, 1620-1632.
241. Freund, G.; Kulas, D.; Mooney, R., Insulin and IGF-1 increase mitogenesis and glucose metabolism in the multiple myeloma cell line, RPMI 8226. *J. Immunol.* **1993,** 151, (4), 1811-1820.
242. King, C. C.; Bouic, K.; Friedmann, T., A fractionation method to identify quantitative changes in protein expression mediated by IGF-1 on the proteome of murine C2C12 myoblasts. *Proteome Sci.* **2009,** 7, 28-46.
243. Walenta, S.; Mueller-Klieser, W. F., Lactate: mirror and motor of tumor malignancy. *Semin. Radiation Oncol.* **2004,** 14, 267-274.
244. Durany, N.; Joseph, J.; Jimenez, O. M.; Climent, F.; Fernandez, P. L.; Rivera, F.; Carreras, J., Phosphoglycerate mutase, 2, 3-bisphosphoglycerate phosphatase, creatine kinase and enolase activity and isoenzymes in breast carcinoma. *Br. J. Cancer* **2000,** 82, (1), 20-27.
245. Hennipman, A.; Smits, J.; Van Oirschot, B.; Van Houwelingen, J. C.; Rijksen, G.; Neyt, J. P.; Van Unnik, J. A. M.; Staal, G. E. J., Glycolytic enzymes in breast cancer, benign breast disease and normal breast tissue. *Tumour Biol.* **1987,** 8, (5), 251-263.
246. Gatenby, R. A.; Gawlinski, E. T., The glycolytic phenotype in carcinogenesis and tumor invasion: insights through mathematical models. *Cancer Res.* **2003,** 63, (14), 3847-3854.
247. Shen, M. R.; Hsu, Y. M.; Hsu, K. F.; Chen, Y. F.; Tang, M. J.; Chou, C. Y., Insulin-like growth factor 1 is a potent stimulator of cervical cancer cell invasiveness and proliferation that is modulated by $\alpha_v\beta_3$ integrin signalling. *Carcinogenesis* **2006,** 27, (5), 962-971.
248. Lopez, T.; Hanahan, D., Elevated levels of IGF-1 receptor convey invasive and metastatic capability in a mouse model of pancreatic islet tumorigenesis. *Cancer Cell* **2002,** 1, (4), 339-353.

249. Hollestelle, A.; Elstrodt, F.; Nagel, J. H. A.; Kallemeijn, W. W.; Schutte, M., Phosphatidylinositol-3-OH kinase or RAS pathway mutations in human breast cancer cell lines. *Mol. Cancer Res.* **2007,** 5, (2), 195-201.
250. Dreyfuss, G.; Matunis, M. J.; Pinol-Roma, S.; Burd, C. G., hnRNP proteins and the biogenesis of mRNA. *Annu. Rev. Biochem.* **1993,** 62, (1), 289-321.
251. Carpenter, B.; MacKay, C.; Alnabulsi, A.; MacKay, M.; Telfer, C.; Melvin, W. T.; Murray, G. I., The roles of heterogeneous nuclear ribonucleoproteins in tumour development and progression. *Biochim. Biophys. Acta* **2006,** 1765, (2), 85-100.
252. Iervolino, A.; Santilli, G.; Trotta, R.; Guerzoni, C.; Cesi, V.; Bergamaschi, A.; Gambacorti-Passerini, C.; Calabretta, B.; Perrotti, D., hnRNP A1 nucleocytoplasmic shuttling activity is required for normal myelopoiesis and BCR/ABL leukemogenesis. *Mol. Cell. Biol.* **2002,** 22, (7), 2255-2266.
253. Pino, I.; PÌo, R.; Toledo, G.; Zabalegui, N.; Vicent, S.; Rey, N.; Lozano, M.; Torre, W.; GarcÌa-Foncillas, J.; Montuenga, L., Altered patterns of expression of members of the heterogeneous nuclear ribonucleoprotein (hnRNP) family in lung cancer. *Lung Cancer* **2003,** 41, (2), 131-143.
254. Zhou, J.; Nong, L.; Wloch, M.; Cantor, A.; Mulshine, J.; Tockman, M., Expression of early lung cancer detection marker: hnRNP-A2/B1 and its relation to microsatellite alteration in non-small cell lung cancer. *Lung Cancer* **2001,** 34, (3), 341-350.
255. Zhou, J.; Allred, D. C.; Avis, I.; Martínez, A.; Vos, M. D.; Smith, L.; Treston, A. M.; Mulshine, J. L., Differential expression of the early lung cancer detection marker, heterogeneous nuclear ribonucleoprotein-A2/B1 (hnRNP-A2/B1) in normal breast and neoplastic breast cancer. *Breast Cancer Res. Treat.* **2001,** 66, (3), 217-224.
256. Zhou, R.; Shanas, R.; Nelson, M. A.; Bhattacharyya, A.; Shi, J., Increased expression of the heterogeneous nuclear ribonucleoprotein K in pancreatic cancer and its association with the mutant p53. *Int. J. Cancer* 126, (2), 395-404.
257. Albrethsen, J.; Knol, J.; Piersma, S.; Pham, T.; de Wit, M.; Mongera, S.; Carvalho, B.; Verheul, H.; Fijneman, R.; Meijer, G., Subnuclear proteomics in colorectal cancer. *Mol. Cell. Proteomics* **2010,** 9, (5), 988-1005.
258. Vander Heiden, M.; Cantley, L.; Thompson, C., Understanding the Warburg effect: the metabolic requirements of cell proliferation. *Sci. Signal.* **2009,** 324, (5930), 1029-1033.
259. Planck, S. R.; Listerud, M. D.; Buckley, S. D., Modulation of hnRNP A1 protein gene expression by epidermal growth factor in Rat-1 cells. *Nucleic Acids Res.* **1988,** 16, (24), 11663-11673.
260. Matrisian, L.; Rautmann, G.; Magun, B.; Breathnach, R., Epidermal growth factor or serum stimulation of rat fibroblasts induces an elevation in mRNA levels for lactate dehydrogenase and other glycolytic enzymes. *Nucleic Acids Res.* **1985,** 13, (3), 711-726.
261. Campisi, J.; Gray, H.; Pardee, A.; Dean, M.; Sonenshein, G., Cell-cycle control of c-myc but not c-ras expression is lost following chemical transformation. *Cell* **1984,** 36, (2), 241-247.
262. Mandal, M.; Vadlamudi, R.; Nguyen, D.; Wang, R. A.; Costa, L.; Bagheri-Yarmand, R.; Mendelsohn, J.; Kumar, R., Growth factors regulate heterogeneous nuclear ribonucleoprotein K expression and function. *J. Biol. Chem.* **2001,** 276, (13), 9699-9704.
263. Chen, Y.; Zhou, X.; Liu, N.; Wang, C.; Zhang, L.; Mo, W.; Hu, G., Arginine methylation of hnRNP K enhances p53 transcriptional activity. *FEBS Lett.* **2008,** 582, (12), 1761-1765.

264. Murphy, J. P.; Pinto, D. M., Targeted proteomic analysis of glycolysis in cancer cells. *J. Proteome Res.* **2010,** 10, (2), 604-613.
265. Bomsztyk, K.; Denisenko, O.; Ostrowski, J., hnRNP K: one protein multiple processes. *Bioessays* **2004,** 26, (6), 629-638.
266. Ostareck-Lederer, A.; Ostareck, D. H.; Cans, C.; Neubauer, G.; Bomsztyk, K.; Superti-Furga, G.; Hentze, M. W., c-Src-mediated phosphorylation of hnRNP K drives translational activation of specifically silenced mRNAs. *Mol. Cell. Biol.* **2002,** 22, (13), 4535-4543.
267. Kimura, Y.; Nagata, K.; Suzuki, N.; Yokoyama, R.; Yamanaka, Y.; Kitamura, H.; Hirano, H.; Ohara, O., Characterization of multiple alternative forms of heterogeneous nuclear ribonucleoprotein K by phosphate affinity electrophoresis. *Proteomics* **2010,** 10, (21), 3884-3895.
268. Klimek-Tomczak, K.; Wyrwicz, L. S.; Jain, S.; Bomsztyk, K.; Ostrowski, J., Characterization of hnRNP K protein-RNA interactions. *J. Mol. Biol.* **2004,** 342, (4), 1131-1141.
269. Mehta, A.; Driscoll, D. M., A sequence-specific RNA-binding protein complements apobec-1 to edit apolipoprotein B mRNA. *Mol. Cell. Biol.* **1998,** 18, (8), 4426-4432.
270. Fukuda, A.; Nakadai, T.; Shimada, M.; Hisatake, K., Heterogeneous nuclear ribonucleoprotein R enhances transcription from the naturally configured c-fos promoter in vitro. *J. Biol. Chem.* **2009,** 284, (35), 23472-23480.
271. Glinka, M.; Herrmann, T.; Funk, N.; Havlicek, S.; Rossoll, W.; Winkler, C.; Sendtner, M., The heterogeneous nuclear ribonucleoprotein R is necessary for axonal β-actin mRNA translocation in spinal motor neurons. *Hum. Mol. Genet.* **2010,** 19, (10), 1951-1966.
272. Lau, P. P.; Chang, B. H. J.; Chan, L., Two-hybrid cloning identifies an RNA-binding protein, GRY-RBP, as a component of apobec-1 editosome. *Biochem. Biophys. Res. Commun.* **2001,** 282, (4), 977-983.
273. Landthaler, M.; Gaidatzis, D.; Rothballer, A.; Chen, P.; Soll, S.; Dinic, L.; Ojo, T.; Hafner, M.; Zavolan, M.; Tuschl, T., Molecular characterization of human Argonaute-containing ribonucleoprotein complexes and their bound target mRNAs. *RNA* **2008,** 14, (12), 2580-2596.
274. Freibaum, B.; Chitta, R.; High, A.; Taylor, J., Global analysis of TDP-43 interacting proteins reveals strong association with RNA splicing and translation machinery. *J. Proteome Res.* **2010,** 9, (2), 1104-1120.
275. DeSouza, L. V.; Taylor, A. M.; Li, W.; Minkoff, M. S.; Romaschin, A. D.; Colgan, T. J.; Siu, K. W. M., Multiple reaction monitoring of mTRAQ-labeled peptides enables absolute quantification of endogenous levels of a potential cancer marker in cancerous and normal endometrial tissues. *J. Proteome Res.* **2008,** 7, (8), 3525-3534.
276. Zhuang, Z.; Huang, S.; Kowalak, J.; Shi, Y.; Lei, J.; Furata, M.; Lee, Y.; Lubensky, I.; Rodgers, G.; Cornelius, A., From tissue phenotype to proteotype: Sensitive protein identification in microdissected tumor tissue. *Int. J. Oncol.* **2006,** 28, (1), 103-110.
277. Hitosugi, T.; Kang, S.; Vander Heiden, M. G.; Chung, T. W.; Elf, S.; Lythgoe, K.; Dong, S.; Lonial, S.; Wang, X.; Chen, G. Z., Tyrosine phosphorylation inhibits PKM2 to promote the Warburg effect and tumor growth. *Sci. STKE* **2009,** 2, (97), ra73.
278. Dombrauckas, J. D.; Santarsiero, B. D.; Mesecar, A. D., Structural basis for tumor pyruvate kinase M2 allosteric regulation and catalysis. *Biochemistry* **2005,** 44, (27), 9417-9429.

279. Dang, C., PKM2 tyrosine phosphorylation and glutamine metabolism signal a different view of the Warburg effect. *Sci. STKE* **2009,** 2, (97), pe75.
280. Aleksic, T.; Chitnis, M. M.; Perestenko, O. V.; Gao, S.; Thomas, P. H.; Turner, G. D.; Protheroe, A. S.; Howarth, M.; Macaulay, V. M., Type 1 insulin-like growth factor receptor translocates to the nucleus of human tumor cells. *Cancer Res.* **2010,** 70, (16), 6412-6419.

Appendices

Appendix A. *Transitions for Glycolysis Peptides (M+28 and M+32) Uploadable to Analyst (v1.4+) Software.*

Q1	Q3	Dwell (msec)	Identifier (Protein Peptide Fragment Label)	CE
Method 1				
502.7	701.3	5	ACTAB AGFAGDDAPR y7 M+28	28
504.7	701.3	5	ACTAB AGFAGDDAPR y7 M+32	28
502.7	848.4	5	ACTAB AGFAGDDAPR y8 M+28	28
504.7	848.4	5	ACTAB AGFAGDDAPR y8 M+32	28
502.7	905.4	5	ACTAB AGFAGDDAPR y9 M+28	30
504.7	905.4	5	ACTAB AGFAGDDAPR y9 M+32	30
609.3	1060.6	100	ACTAB EITALAPSTMK y10 M+28	32
613.3	1064.6	100	ACTAB EITALAPSTMK y10 M+32	32
609.3	846.5	100	ACTAB EITALAPSTMK y8 M+28	32
613.3	850.5	100	ACTAB EITALAPSTMK y8 M+32	32
609.3	947.5	21	ACTAB EITALAPSTMK y9 M+28	32
613.3	951.5	21	ACTAB EITALAPSTMK y9 M+32	32
580.8	825.4	15	ACTAB GYSFTTTAER y7 M+28	31
582.8	825.4	15	ACTAB GYSFTTTAER y7 M+32	31
580.8	912.4	6	ACTAB GYSFTTTAER y8 M+28	29
582.8	912.4	6	ACTAB GYSFTTTAER y8 M+32	29
580.8	1075.5	5	ACTAB GYSFTTTAER y9 M+28	33
582.8	1075.5	5	ACTAB GYSFTTTAER y9 M+32	33
614.3	1062.5	100	ACTAB HQGVMVGMGQK y10 M+28	36
618.3	1066.5	100	ACTAB HQGVMVGMGQK y10 M+32	36
614.3	877.5	96	ACTAB HQGVMVGMGQK y8 M+28	38
618.3	881.5	96	ACTAB HQGVMVGMGQK y8 M+32	38
614.3	934.5	43	ACTAB HQGVMVGMGQK y9 M+28	34
618.3	938.5	43	ACTAB HQGVMVGMGQK y9 M+32	34
772.9	1259.6	28	ACTAB QEYDESGPSIVHR y11 M+28	49
774.9	1259.6	28	ACTAB QEYDESGPSIVHR y11 M+32	49
772.9	1388.6	10	ACTAB QEYDESGPSIVHR y12 M+28	49
774.9	1388.6	10	ACTAB QEYDESGPSIVHR y12 M+32	49
772.9	852.5	9	ACTAB QEYDESGPSIVHR y8 M+28	49
774.9	852.5	9	ACTAB QEYDESGPSIVHR y8 M+32	49
594.8	791.4	12	ALDO ALANSLACQGK y7 M+28	35
598.8	795.4	12	ALDO ALANSLACQGK y7 M+32	35
594.8	905.5	11	ALDO ALANSLACQGK y8 M+28	31
598.8	909.5	11	ALDO ALANSLACQGK y8 M+32	31
594.8	976.5	5	ALDO ALANSLACQGK y9 M+28	31
598.8	980.5	5	ALDO ALANSLACQGK y9 M+32	31
536.8	690.3	8	ALDO QLLLTADDR y6 M+28	35
538.8	690.3	8	ALDO QLLLTADDR y6 M+32	35
536.8	803.4	7	ALDO QLLLTADDR y7 M+28	31
538.8	803.4	7	ALDO QLLLTADDR y7 M+32	31
536.8	916.5	5	ALDO QLLLTADDR y8 M+28	33
538.8	916.5	5	ALDO QLLLTADDR y8 M+32	33
484.8	496.3	5	ALDOA ELSDIAHR y4 M+28	36
486.8	496.3	5	ALDOA ELSDIAHR y4 M+32	36
484.8	698.4	10	ALDOA ELSDIAHR y6 M+28	24

486.8	698.4	10	ALDOA ELSDIAHR y6 M+32	24
484.8	811.4	5	ALDOA ELSDIAHR y7 M+28	28
486.8	811.4	5	ALDOA ELSDIAHR y7 M+32	28
694.9	1006.5	5	ALDOA GILAADESTGSIAK y10 M+28	34
698.9	1010.5	5	ALDOA GILAADESTGSIAK y10 M+32	34
694.9	1077.5	5	ALDOA GILAADESTGSIAK y11 M+28	34
698.9	1081.5	5	ALDOA GILAADESTGSIAK y11 M+32	34
694.9	935.5	5	ALDOA GILAADESTGSIAK y9 M+28	34
698.9	939.5	5	ALDOA GILAADESTGSIAK y9 M+32	34
759.9	1249.6	24	ALDOA LQSIGTENTEENR y11 M+28	42
761.9	1249.6	24	ALDOA LQSIGTENTEENR y11 M+32	42
759.9	1377.6	9	ALDOA LQSIGTENTEENR y12 M+28	38
761.9	1377.6	9	ALDOA LQSIGTENTEENR y12 M+32	38
759.9	1049.5	41	ALDOA LQSIGTENTEENR y9 M+28	38
761.9	1049.5	41	ALDOA LQSIGTENTEENR y9 M+32	38
478.3	642.4	5	ENO TIAPALVSK y6 M+28	32
482.3	646.4	5	ENO TIAPALVSK y6 M+32	32
478.3	713.5	5	ENO TIAPALVSK y7 M+28	24
482.3	717.5	5	ENO TIAPALVSK y7 M+32	24
478.3	826.5	5	ENO TIAPALVSK y8 M+28	26
482.3	830.5	5	ENO TIAPALVSK y8 M+32	26
784.9	1342.7	100	ENO VVIGMDVAASEFFR y12 M+28	40
786.9	1342.7	100	ENO VVIGMDVAASEFFR y12 M+32	40
784.9	926.5	100	ENO VVIGMDVAASEFFR y8 M+28	48
786.9	926.5	100	ENO VVIGMDVAASEFFR y8 M+32	48
784.9	1041.5	100	ENO VVIGMDVAASEFFR y9 M+28	40
786.9	1041.5	100	ENO VVIGMDVAASEFFR y9 M+32	40
917	1251.7	100	ENO1 AAVPSGASTGIYEALELR y11 M+28	51
919	1251.7	100	ENO1 AAVPSGASTGIYEALELR y11 M+32	51
917	1563.8	63	ENO1 AAVPSGASTGIYEALELR y15 M+28	47
919	1563.8	63	ENO1 AAVPSGASTGIYEALELR y15 M+32	47
917	1063.6	100	ENO1 AAVPSGASTGIYEALELR y9 M+28	53
919	1063.6	100	ENO1 AAVPSGASTGIYEALELR y9 M+32	53
668.8	1195.5	100	ENO1 LMIEMDGTENK y10 M+28	36
672.8	1199.5	100	ENO1 LMIEMDGTENK y10 M+32	36
668.8	951.4	100	ENO1 LMIEMDGTENK y8 M+28	34
672.8	955.4	100	ENO1 LMIEMDGTENK y8 M+32	34
668.8	1064.5	100	ENO1 LMIEMDGTENK y9 M+28	36
672.8	1068.5	100	ENO1 LMIEMDGTENK y9 M+32	36
845.9	1207.6	31	ENO1 VNQIGSVTESLQACK y11 M+28	42
849.9	1211.6	31	ENO1 VNQIGSVTESLQACK y11 M+32	42
845.9	1562.8	23	ENO1 VNQIGSVTESLQACK y14 M+28	42
849.9	1566.8	23	ENO1 VNQIGSVTESLQACK y14 M+32	42
845.9	964.5	17	ENO1 VNQIGSVTESLQACK y8 M+28	42
849.9	968.5	17	ENO1 VNQIGSVTESLQACK y8 M+32	42
741.4	1177.6	6	ENO1 YISPDQLADLYK y10 M+28	40
745.4	1181.6	6	ENO1 YISPDQLADLYK y10 M+32	40
741.4	1290.7	5	ENO1 YISPDQLADLYK y11 M+28	40
745.4	1294.7	5	ENO1 YISPDQLADLYK y11 M+32	40
741.4	1090.6	8	ENO1 YISPDQLADLYK y9 M+28	38
745.4	1094.6	8	ENO1 YISPDQLADLYK y9 M+32	38
679.9	1259.7	100	FASN AALQEELQLCK y10 M+28	37
683.9	1263.7	100	FASN AALQEELQLCK y10 M+32	37
679.9	818.4	100	FASN AALQEELQLCK y6 M+28	37
683.9	822.4	100	FASN AALQEELQLCK y6 M+32	37
679.9	947.5	100	FASN AALQEELQLCK y7 M+28	39
683.9	951.5	100	FASN AALQEELQLCK y7 M+32	39
802.9	1117.6	100	FASN ACLDTAVENMPSLK y10 M+28	42

806.9	1121.6	100	FASN ACLDTAVENMPSLK y10 M+32	42
802.9	1505.7	100	FASN ACLDTAVENMPSLK y13 M+28	42
806.9	1509.7	100	FASN ACLDTAVENMPSLK y13 M+32	42
802.9	846.4	100	FASN ACLDTAVENMPSLK y7 M+28	42
806.9	850.4	100	FASN ACLDTAVENMPSLK y7 M+32	42
536.3	745.4	24	FASN AQVADVVVSR y7 M+28	29
538.3	745.4	24	FASN AQVADVVVSR y7 M+32	29
536.3	844.5	14	FASN AQVADVVVSR y8 M+28	29
538.3	844.5	14	FASN AQVADVVVSR y8 M+32	29
536.3	972.6	5	FASN AQVADVVVSR y9 M+28	29
538.3	972.6	5	FASN AQVADVVVSR y9 M+32	29
727.9	1339.7	100	FASN SLLVNPEGPTLMR y12 M+28	41
729.9	1339.7	100	FASN SLLVNPEGPTLMR y12 M+32	41
727.9	900.5	100	FASN SLLVNPEGPTLMR y8 M+28	33
729.9	900.5	100	FASN SLLVNPEGPTLMR y8 M+32	33
727.9	1014.5	100	FASN SLLVNPEGPTLMR y9 M+28	33
729.9	1014.5	100	FASN SLLVNPEGPTLMR y9 M+32	33

Method 2

526.4	682.5	100	FASN VLEALLPLK y6 M+28	32
530.4	686.5	100	FASN VLEALLPLK y6 M+32	32
526.4	811.5	18	FASN VLEALLPLK y7 M+28	28
530.4	815.5	18	FASN VLEALLPLK y7 M+32	28
526.4	924.6	5	FASN VLEALLPLK y8 M+28	30
530.4	928.6	5	FASN VLEALLPLK y8 M+32	30
817.5	1476.8	100	FBP1 EAVLDVIPTDIHQR y13 M+28	37
819.5	1476.8	100	FBP1 EAVLDVIPTDIHQR y13 M+32	37
817.5	866.5	20	FBP1 EAVLDVIPTDIHQR y7 M+28	37
819.5	866.5	20	FBP1 EAVLDVIPTDIHQR y7 M+32	37
817.5	1078.6	100	FBP1 EAVLDVIPTDIHQR y9 M+28	37
819.5	1078.6	100	FBP1 EAVLDVIPTDIHQR y9 M+32	37
931	1488.8	100	FBP1 GTGELTQLLNSLCTAVK y13 M+28	42
935	1492.8	100	FBP1 GTGELTQLLNSLCTAVK y13 M+32	42
931	1776	100	FBP1 GTGELTQLLNSLCTAVK y16 M+28	50
935	1780	100	FBP1 GTGELTQLLNSLCTAVK y16 M+32	50
931	1033.6	100	FBP1 GTGELTQLLNSLCTAVK y9 M+28	38
935	1037.6	100	FBP1 GTGELTQLLNSLCTAVK y9 M+32	38
607.3	822.4	100	FBP1 IYSLNEGYAK y7 M+28	40
611.3	826.4	100	FBP1 IYSLNEGYAK y7 M+32	40
607.3	909.5	70	FBP1 IYSLNEGYAK y8 M+28	34
611.3	913.5	70	FBP1 IYSLNEGYAK y8 M+32	34
607.3	1072.5	12	FBP1 IYSLNEGYAK y9 M+28	34
611.3	1076.5	12	FBP1 IYSLNEGYAK y9 M+32	34
651.3	734.4	100	G6PD GGYFDEFGIIR y6 M+28	40
653.3	734.4	100	G6PD GGYFDEFGIIR y6 M+32	40
651.3	849.5	100	G6PD GGYFDEFGIIR y7 M+28	34
653.3	849.5	100	G6PD GGYFDEFGIIR y7 M+32	34
651.3	996.5	100	G6PD GGYFDEFGIIR y8 M+28	36
653.3	996.5	100	G6PD GGYFDEFGIIR y8 M+32	36
573.8	599.3	100	G6PD GPTEADELMK b6 M+28	30
577.8	603.3	100	G6PD GPTEADELMK b6 M+32	30
573.8	734.4	12	G6PD GPTEADELMK y6 M+28	36
577.8	738.4	12	G6PD GPTEADELMK y6 M+32	36
573.8	1061.5	100	G6PD GPTEADELMK y9 M+28	32
577.8	1065.5	100	G6PD GPTEADELMK y9 M+32	32
580.8	592.3	8	G6PD GYLDDPTVPR b5 M+28	29
582.8	592.3	8	G6PD GYLDDPTVPR b5 M+32	29

580.8	684.4	15	G6PD GYLDDPTVPR y6 M+28	35
582.8	684.4	15	G6PD GYLDDPTVPR y6 M+32	35
580.8	1075.5	9	G6PD GYLDDPTVPR y9 M+28	33
582.8	1075.5	9	G6PD GYLDDPTVPR y9 M+32	33
515.8	742.4	18	G6PD IFGPIWNR b6 M+28	28
517.8	742.4	18	G6PD IFGPIWNR b6 M+32	28
515.8	685.4	67	G6PD IFGPIWNR y5 M+28	34
517.8	685.4	67	G6PD IFGPIWNR y5 M+32	34
515.8	889.5	5	G6PD IFGPIWNR y7 M+28	30
517.8	889.5	5	G6PD IFGPIWNR y7 M+32	30
463.2	540.3	19	G6PD LEDFFAR y4 M+28	31
465.2	540.3	19	G6PD LEDFFAR y4 M+32	31
463.2	655.3	64	G6PD LEDFFAR y5 M+28	27
465.2	655.3	64	G6PD LEDFFAR y5 M+32	27
463.2	784.4	100	G6PD LEDFFAR y6 M+28	27
465.2	784.4	100	G6PD LEDFFAR y6 M+32	27
945.5	1250.6	100	GAPDH IISNASCTTNCLAPLAK b11 M+28	47
949.5	1254.6	100	GAPDH IISNASCTTNCLAPLAK b11 M+32	47
945.5	1116.6	46	GAPDH IISNASCTTNCLAPLAK y10 M+28	47
949.5	1120.6	46	GAPDH IISNASCTTNCLAPLAK y10 M+32	47
945.5	1748.9	7	GAPDH IISNASCTTNCLAPLAK y16 M+28	47
949.5	1752.9	7	GAPDH IISNASCTTNCLAPLAK y16 M+32	47
779.9	1334.7	100	GAPDH VPTANVSVVDLTCR y12 M+28	41
781.9	1334.7	100	GAPDH VPTANVSVVDLTCR y12 M+32	41
779.9	1431.7	8	GAPDH VPTANVSVVDLTCR y13 M+28	41
781.9	1431.7	8	GAPDH VPTANVSVVDLTCR y13 M+32	41
779.9	949.5	100	GAPDH VPTANVSVVDLTCR y8 M+28	41
781.9	949.5	100	GAPDH VPTANVSVVDLTCR y8 M+32	41
552.8	750.4	100	GPI NLVTEDVMR y6 M+28	31
554.8	750.4	100	GPI NLVTEDVMR y6 M+32	31
552.8	849.4	52	GPI NLVTEDVMR y7 M+28	31
554.8	849.4	52	GPI NLVTEDVMR y7 M+32	31
552.8	962.5	15	GPI NLVTEDVMR y8 M+28	35
554.8	962.5	15	GPI NLVTEDVMR y8 M+32	35
550.3	769.5	14	GPI SNTPILVDGK y7 M+28	29
554.3	773.5	14	GPI SNTPILVDGK y7 M+32	29
550.3	870.5	29	GPI SNTPILVDGK y8 M+28	29
554.3	874.5	29	GPI SNTPILVDGK y8 M+32	29
550.3	984.6	13	GPI SNTPILVDGK y9 M+28	29
554.3	988.6	13	GPI SNTPILVDGK y9 M+32	29
856.5	1334.7	100	GPI TFTTQETITNAETAK y12 M+28	45
860.5	1338.7	100	GPI TFTTQETITNAETAK y12 M+32	45
856.5	1582.8	100	GPI TFTTQETITNAETAK y14 M+28	45
860.5	1586.8	100	GPI TFTTQETITNAETAK y14 M+32	45
856.5	976.5	61	GPI TFTTQETITNAETAK y9 M+28	41
860.5	980.5	61	GPI TFTTQETITNAETAK y9 M+32	41
493.3	584.4	43	LDHA FIIPNVVK y5 M+28	35
497.3	588.4	43	LDHA FIIPNVVK y5 M+32	35
493.3	697.5	100	LDHA FIIPNVVK y6 M+28	31
497.3	701.5	100	LDHA FIIPNVVK y6 M+32	31
493.3	810.5	11	LDHA FIIPNVVK y7 M+28	29
497.3	814.5	11	LDHA FIIPNVVK y7 M+32	29

Method 3

471.3	588.3	17	LDHA LVIITAGAR y6 M+28	30
473.3	588.3	17	LDHA LVIITAGAR y6 M+32	30
471.3	701.4	100	LDHA LVIITAGAR y7 M+28	26

473.3	701.4	100	LDHA LVIITAGAR y7 M+32	26
471.3	800.5	20	LDHA LVIITAGAR y8 M+28	28
473.3	800.5	20	LDHA LVIITAGAR y8 M+32	28
660.9	1164.7	37	LDHA QVVESAYEVIK y10 M+28	36
664.9	1168.7	37	LDHA QVVESAYEVIK y10 M+32	36
660.9	837.5	100	LDHA QVVESAYEVIK y7 M+28	38
664.9	841.5	100	LDHA QVVESAYEVIK y7 M+32	38
660.9	1065.6	100	LDHA QVVESAYEVIK y9 M+28	36
664.9	1069.6	100	LDHA QVVESAYEVIK y9 M+32	36
843.5	1142.7	100	LDHA SLADELALVDVLEDK y10 M+28	44
847.5	1146.7	100	LDHA SLADELALVDVLEDK y10 M+32	44
843.5	958.5	100	LDHA SLADELALVDVLEDK y8 M+28	44
847.5	962.5	100	LDHA SLADELALVDVLEDK y8 M+32	44
843.5	1029.6	100	LDHA SLADELALVDVLEDK y9 M+28	48
847.5	1033.6	100	LDHA SLADELALVDVLEDK y9 M+32	48
534.3	706.4	19	LDHA VHPVSTMIK y6 M+28	33
538.3	710.4	19	LDHA VHPVSTMIK y6 M+32	33
534.3	803.5	100	LDHA VHPVSTMIK y7 M+28	29
538.3	807.5	100	LDHA VHPVSTMIK y7 M+32	29
534.3	940.5	100	LDHA VHPVSTMIK y8 M+28	33
538.3	944.5	100	LDHA VHPVSTMIK y8 M+32	33
638.8	1036.4	46	LDHA VIGSGCNLDSAR y10 M+28	33
640.8	1036.4	46	LDHA VIGSGCNLDSAR y10 M+32	33
638.8	1149.5	10	LDHA VIGSGCNLDSAR y11 M+28	37
640.8	1149.5	10	LDHA VIGSGCNLDSAR y11 M+32	37
638.8	892.4	100	LDHA VIGSGCNLDSAR y8 M+28	33
640.8	892.4	100	LDHA VIGSGCNLDSAR y8 M+32	33
711.4	1246.6	100	MDH1 FVEGLPINDFSR y11 M+28	38
713.4	1246.6	100	MDH1 FVEGLPINDFSR y11 M+32	38
711.4	848.4	100	MDH1 FVEGLPINDFSR y7 M+28	36
713.4	848.4	100	MDH1 FVEGLPINDFSR y7 M+32	36
711.4	1018.5	100	MDH1 FVEGLPINDFSR y9 M+28	40
713.4	1018.5	100	MDH1 FVEGLPINDFSR y9 M+32	40
596.8	732.4	10	MDH1 GEFVTTVQQR y6 M+28	31
598.8	732.4	10	MDH1 GEFVTTVQQR y6 M+32	31
596.8	831.5	20	MDH1 GEFVTTVQQR y7 M+28	35
598.8	831.5	20	MDH1 GEFVTTVQQR y7 M+32	35
596.8	978.5	15	MDH1 GEFVTTVQQR y8 M+28	31
598.8	978.5	15	MDH1 GEFVTTVQQR y8 M+32	31
643.4	1200.6	100	PFKL GQLESIVENIR y10 M+28	34
645.4	1200.6	100	PFKL GQLESIVENIR y10 M+32	34
643.4	830.5	100	PFKL GQLESIVENIR y7 M+28	38
645.4	830.5	100	PFKL GQLESIVENIR y7 M+32	38
643.4	1072.6	100	PFKL GQLESIVENIR y9 M+28	38
645.4	1072.6	100	PFKL GQLESIVENIR y9 M+32	38
665.9	1173.6	100	PFKP EWSGLLEELAR y10 M+28	38
667.9	1173.6	100	PFKP EWSGLLEELAR y10 M+32	38
665.9	900.5	100	PFKP EWSGLLEELAR y8 M+28	32
667.9	900.5	100	PFKP EWSGLLEELAR y8 M+32	32
665.9	987.6	100	PFKP EWSGLLEELAR y9 M+28	40
667.9	987.6	100	PFKP EWSGLLEELAR y9 M+32	40
540.3	704.4	100	PFKP TFVLEVMGR y6 M+28	31
542.3	704.4	100	PFKP TFVLEVMGR y6 M+32	31
540.3	803.4	100	PFKP TFVLEVMGR y7 M+28	31
542.3	803.4	100	PFKP TFVLEVMGR y7 M+32	31
540.3	950.5	30	PFKP TFVLEVMGR y8 M+28	31
542.3	950.5	30	PFKP TFVLEVMGR y8 M+32	31
641.3	719.4	100	PFKP YLEEIATQMR y6 M+28	37

643.3	719.4	100	PFKP YLEEIATQMR y6 M+32	37
641.3	977.5	100	PFKP YLEEIATQMR y8 M+28	33
643.3	977.5	100	PFKP YLEEIATQMR y8 M+32	33
641.3	1090.6	17	PFKP YLEEIATQMR y9 M+28	37
643.3	1090.6	17	PFKP YLEEIATQMR y9 M+32	37
870.5	1527.8	100	PGAM ALPFWNEEIVPQIK y12 M+28	39
874.5	1531.8	100	PGAM ALPFWNEEIVPQIK y12 M+32	39
870.5	725.5	100	PGAM ALPFWNEEIVPQIK y6 M+28	45
874.5	729.5	100	PGAM ALPFWNEEIVPQIK y6 M+32	45
870.5	1097.6	100	PGAM ALPFWNEEIVPQIK y9 M+28	45
874.5	1101.6	100	PGAM ALPFWNEEIVPQIK y9 M+32	45

Method 4

558.3	730.5	100	PGAM HYGGLTGLNK y7 M+28	26
562.3	734.5	100	PGAM HYGGLTGLNK y7 M+32	26
558.3	787.5	47	PGAM HYGGLTGLNK y8 M+28	34
562.3	791.5	47	PGAM HYGGLTGLNK y8 M+32	34
558.3	950.5	16	PGAM HYGGLTGLNK y9 M+28	34
562.3	954.5	16	PGAM HYGGLTGLNK y9 M+32	34
963	1750.8	100	PGAM1 YADLTEDQLPSCESLK b15 M+28	43
967	1754.8	100	PGAM1 YADLTEDQLPSCESLK b15 M+32	43
963	1204.6	100	PGAM1 YADLTEDQLPSCESLK y10 M+28	49
967	1208.6	100	PGAM1 YADLTEDQLPSCESLK y10 M+32	49
963	1333.6	100	PGAM1 YADLTEDQLPSCESLK y11 M+28	53
967	1337.6	100	PGAM1 YADLTEDQLPSCESLK y11 M+32	53
480.8	617.4	100	PGK1 ALMDEVVK y5 M+28	30
484.8	621.4	100	PGK1 ALMDEVVK y5 M+32	30
480.8	748.4	100	PGK1 ALMDEVVK y6 M+28	30
484.8	752.4	100	PGK1 ALMDEVVK y6 M+32	30
480.8	861.5	100	PGK1 ALMDEVVK y7 M+28	30
484.8	865.5	100	PGK1 ALMDEVVK y7 M+32	30
470.8	556.3	34	PGK1 ELNYFAK y4 M+28	34
474.8	560.3	34	PGK1 ELNYFAK y4 M+32	34
470.8	670.4	100	PGK1 ELNYFAK y5 M+28	28
474.8	674.4	100	PGK1 ELNYFAK y5 M+32	28
470.8	783.4	37	PGK1 ELNYFAK y6 M+28	28
474.8	787.4	37	PGK1 ELNYFAK y6 M+32	28
831.9	1250.6	67	PGK1 LGDVYVNDAFGTAHR y11 M+28	42
833.9	1250.6	67	PGK1 LGDVYVNDAFGTAHR y11 M+32	42
831.9	1349.7	82	PGK1 LGDVYVNDAFGTAHR y12 M+28	48
833.9	1349.7	82	PGK1 LGDVYVNDAFGTAHR y12 M+32	48
831.9	1521.7	21	PGK1 LGDVYVNDAFGTAHR y14 M+28	42
833.9	1521.7	21	PGK1 LGDVYVNDAFGTAHR y14 M+32	42
503.3	502.3	100	PGK1 VDFNVPMK y4 M+28	35
507.3	506.3	100	PGK1 VDFNVPMK y4 M+32	35
503.3	763.4	100	PGK1 VDFNVPMK y6 M+28	29
507.3	767.4	100	PGK1 VDFNVPMK y6 M+32	29
503.3	878.4	100	PGK1 VDFNVPMK y7 M+28	25
507.3	882.4	100	PGK1 VDFNVPMK y7 M+32	25
899	1259.7	100	PGK1 VSHVSTGGGASLELLEGK y13 M+28	45
903	1263.7	100	PGK1 VSHVSTGGGASLELLEGK y13 M+32	45
899	1346.7	58	PGK1 VSHVSTGGGASLELLEGK y14 M+28	45
903	1350.7	58	PGK1 VSHVSTGGGASLELLEGK y14 M+32	45
899	1669.9	30	PGK1 VSHVSTGGGASLELLEGK y17 M+28	49
903	1673.9	30	PGK1 VSHVSTGGGASLELLEGK y17 M+32	49
712.4	1187.7	100	PGK1 AHSSMVGVNLPQK y11 M+28	36
716.4	1191.7	100	PGK1 AHSSMVGVNLPQK y11 M+32	36

712.4	1324.7	100	PGK1 AHSSMVGVNLPQK y12 M+28	36
716.4	1328.7	100	PGK1 AHSSMVGVNLPQK y12 M+32	36
712.4	783.5	100	PGK1 AHSSMVGVNLPQK y7 M+28	36
716.4	787.5	100	PGK1 AHSSMVGVNLPQK y7 M+32	36
639.4	1089.7	55	PKM2 CCSGAIIVLTK y10 M+28	35
643.4	1093.7	55	PKM2 CCSGAIIVLTK y10 M+32	35
639.4	842.6	18	PKM2 CCSGAIIVLTK y8 M+28	39
643.4	846.6	18	PKM2 CCSGAIIVLTK y8 M+32	39
639.4	929.6	100	PKM2 CCSGAIIVLTK y9 M+28	35
643.4	933.6	100	PKM2 CCSGAIIVLTK y9 M+32	35
599.4	585.4	5	PKM2 GDLGIEIPAEK y5 M+28	35
603.4	589.4	5	PKM2 GDLGIEIPAEK y5 M+32	35
599.4	714.4	5	PKM2 GDLGIEIPAEK y6 M+28	31
603.4	718.4	5	PKM2 GDLGIEIPAEK y6 M+32	31
599.4	884.5	5	PKM2 GDLGIEIPAEK y8 M+28	31
603.4	888.5	5	PKM2 GDLGIEIPAEK y8 M+32	31
524.3	684.4	5	PKM2 GDYPLEAVR y6 M+28	32
526.3	684.4	5	PKM2 GDYPLEAVR y6 M+32	32
524.3	847.5	5	PKM2 GDYPLEAVR y7 M+28	32
526.3	847.5	5	PKM2 GDYPLEAVR y7 M+32	32
524.3	962.5	5	PKM2 GDYPLEAVR y8 M+28	32
526.3	962.5	5	PKM2 GDYPLEAVR y8 M+32	32
495.3	644.4	9	PKM2 GIFPVLCK y5 M+28	31
499.3	648.4	9	PKM2 GIFPVLCK y5 M+32	31
495.3	791.5	23	PKM2 GIFPVLCK y6 M+28	31
499.3	795.5	23	PKM2 GIFPVLCK y6 M+32	31
495.3	904.5	53	PKM2 GIFPVLCK y7 M+28	27
499.3	908.5	53	PKM2 GIFPVLCK y7 M+32	27
523.8	645.4	9	PKM2 GSGTAEVELK y5 M+28	36
527.8	649.4	9	PKM2 GSGTAEVELK y5 M+32	36
523.8	874.5	5	PKM2 GSGTAEVELK y8 M+28	32
527.8	878.5	5	PKM2 GSGTAEVELK y8 M+32	32
523.8	961.5	5	PKM2 GSGTAEVELK y9 M+28	32
527.8	965.5	5	PKM2 GSGTAEVELK y9 M+32	32
627.3	783.4	34	PKM2 ITLDNAYMEK y6 M+28	39
631.3	787.4	34	PKM2 ITLDNAYMEK y6 M+32	39
627.3	898.4	100	PKM2 ITLDNAYMEK y7 M+28	37
631.3	902.4	100	PKM2 ITLDNAYMEK y7 M+32	37
627.3	1112.5	5	PKM2 ITLDNAYMEK y9 M+28	31
631.3	1116.5	5	PKM2 ITLDNAYMEK y9 M+32	31
759.9	1214.7	100	PKM2 IYVDDGLISLQVK y11 M+28	38
763.9	1218.7	100	PKM2 IYVDDGLISLQVK y11 M+32	38
759.9	1377.8	89	PKM2 IYVDDGLISLQVK y12 M+28	38
763.9	1381.8	89	PKM2 IYVDDGLISLQVK y12 M+32	38
759.9	885.6	100	PKM2 IYVDDGLISLQVK y8 M+28	42
763.9	889.6	100	PKM2 IYVDDGLISLQVK y8 M+32	42

Method 5

613.3	1084.6	5	PKM2 LDIDSPPITAR y10 M+28	34
615.3	1084.6	5	PKM2 LDIDSPPITAR y10 M+32	34
613.3	741.4	5	PKM2 LDIDSPPITAR y7 M+28	42
615.3	741.4	5	PKM2 LDIDSPPITAR y7 M+32	42
613.3	969.5	6	PKM2 LDIDSPPITAR y9 M+28	34
615.3	969.5	6	PKM2 LDIDSPPITAR y9 M+32	34
694.4	1245.7	5	PKM2 NTGIICTIGPASR y12 M+28	40
696.4	1245.7	5	PKM2 NTGIICTIGPASR y12 M+32	40
694.4	861.4	5	PKM2 NTGIICTIGPASR y8 M+28	40

696.4	861.4	5	PKM2 NTGIICTIGPASR y8 M+32	40
694.4	974.5	5	PKM2 NTGIICTIGPASR y9 M+28	40
696.4	974.5	5	PKM2 NTGIICTIGPASR y9 M+32	40
653.8	1149.5	73	PPIA EGMNIVEAMER y10 M+28	33
655.8	1149.5	73	PPIA EGMNIVEAMER y10 M+32	33
653.8	734.35	73	PPIA EGMNIVEAMER y6 M+28	33
655.8	734.35	73	PPIA EGMNIVEAMER y6 M+32	33
653.8	961.5	64	PPIA EGMNIVEAMER y8 M+28	33
655.8	961.5	64	PPIA EGMNIVEAMER y8 M+32	33
605.8	791.5	100	PPIA FEDENFILK y6 M+28	30
609.8	795.5	100	PPIA FEDENFILK y6 M+32	30
605.8	906.5	32	PPIA FEDENFILK y7 M+28	30
609.8	910.5	32	PPIA FEDENFILK y7 M+32	30
605.8	1035.5	5	PPIA FEDENFILK y8 M+28	30
609.8	1039.5	5	PPIA FEDENFILK y8 M+32	30
813.9	1372.6	40	PPIA IIPGFMCQGGDFTR y12 M+28	41
815.9	1372.6	40	PPIA IIPGFMCQGGDFTR y12 M+32	41
813.9	1485.7	94	PPIA IIPGFMCQGGDFTR y13 M+28	41
815.9	1485.7	94	PPIA IIPGFMCQGGDFTR y13 M+32	41
813.9	940.4	100	PPIA IIPGFMCQGGDFTR y8 M+28	41
815.9	940.4	100	PPIA IIPGFMCQGGDFTR y8 M+32	41
637.4	891.5	100	RLPL0 IIQLLDDYPK y7 M+28	32
641.4	895.5	100	RLPL0 IIQLLDDYPK y7 M+32	32
637.4	1019.5	95	RLPL0 IIQLLDDYPK y8 M+28	32
641.4	1023.5	95	RLPL0 IIQLLDDYPK y8 M+32	32
637.4	1132.6	14	RLPL0 IIQLLDDYPK y9 M+28	32
641.4	1136.6	14	RLPL0 IIQLLDDYPK y9 M+32	32
517.8	644.4	100	TKT HQPTAIIAK y6 M+28	35
521.8	648.4	100	TKT HQPTAIIAK y6 M+32	35
517.8	741.5	22	TKT HQPTAIIAK y7 M+28	31
521.8	745.5	22	TKT HQPTAIIAK y7 M+32	31
517.8	869.5	40	TKT HQPTAIIAK y8 M+28	31
521.8	873.5	40	TKT HQPTAIIAK y8 M+32	31
564.8	651.4	100	TKT NSTFSEIFK y5 M+28	40
568.8	655.4	100	TKT NSTFSEIFK y5 M+32	40
564.8	798.4	40	TKT NSTFSEIFK y6 M+28	30
568.8	802.4	40	TKT NSTFSEIFK y6 M+32	30
564.8	986.5	52	TKT NSTFSEIFK y8 M+28	30
568.8	990.5	52	TKT NSTFSEIFK y8 M+32	30
757.9	1250.6	26	TP1 HVFGESDELIGQK y11 M+28	40
761.9	1254.6	26	TP1 HVFGESDELIGQK y11 M+32	40
757.9	1349.7	15	TP1 HVFGESDELIGQK y12 M+28	40
761.9	1353.7	15	TP1 HVFGESDELIGQK y12 M+32	40
757.9	917.5	57	TP1 HVFGESDELIGQK y8 M+28	40
761.9	921.5	57	TP1 HVFGESDELIGQK y8 M+32	40
691.9	965.5	7	TP1 IIYGGSVTGATCK y10 M+28	41
695.9	969.5	7	TP1 IIYGGSVTGATCK y10 M+32	41
691.9	1128.5	5	TP1 IIYGGSVTGATCK y11 M+28	39
695.9	1132.5	5	TP1 IIYGGSVTGATCK y11 M+32	39
691.9	1241.6	5	TP1 IIYGGSVTGATCK y12 M+28	31
695.9	1245.6	5	TP1 IIYGGSVTGATCK y12 M+32	31
830	1248.7	100	TP1 VVLAYEPVWAIGTGK y11 M+28	42
834	1252.7	100	TP1 VVLAYEPVWAIGTGK y11 M+32	42
830	1531.9	89	TP1 VVLAYEPVWAIGTGK y14 M+28	42
834	1535.9	89	TP1 VVLAYEPVWAIGTGK y14 M+32	42
830	956.6	61	TP1 VVLAYEPVWAIGTGK y9 M+28	34
834	960.6	61	TP1 VVLAYEPVWAIGTGK y9 M+32	34
505.8	589.3	23	TPI FFVGGNWK y5 M+28	35

509.8	593.3	23	TPI	FFVGGNWK y5 M+32	35
505.8	688.4	34	TPI	FFVGGNWK y6 M+28	29
509.8	692.4	34	TPI	FFVGGNWK y6 M+32	29
505.8	835.5	12	TPI	FFVGGNWK y7 M+28	29
509.8	839.5	12	TPI	FFVGGNWK y7 M+32	29
597.4	882.4	13	TPI	IAVAAQNCYK y7 M+28	35
601.4	886.4	13	TPI	IAVAAQNCYK y7 M+32	35
597.4	981.5	12	TPI	IAVAAQNCYK y8 M+28	35
601.4	985.5	12	TPI	IAVAAQNCYK y8 M+32	35
597.4	1052.5	5	TPI	IAVAAQNCYK y9 M+28	33
601.4	1056.5	5	TPI	IAVAAQNCYK y9 M+32	33
735.9	1314.8	100	TPI	QSLGELIGTLNAAK y13 M+28	39
739.9	1318.8	100	TPI	QSLGELIGTLNAAK y13 M+32	39
735.9	815.5	100	TPI	QSLGELIGTLNAAK y8 M+28	39
739.9	819.5	100	TPI	QSLGELIGTLNAAK y8 M+32	39
735.9	928.6	100	TPI	QSLGELIGTLNAAK y9 M+28	39
739.9	932.6	100	TPI	QSLGELIGTLNAAK y9 M+32	39
631.8	1147.6	5	TPI	SNVSDAVAQSTR y11 M+28	37
633.8	1147.6	5	TPI	SNVSDAVAQSTR y11 M+32	37
631.8	732.4	7	TPI	SNVSDAVAQSTR y7 M+28	39
633.8	732.4	7	TPI	SNVSDAVAQSTR y7 M+32	39
631.8	934.5	7	TPI	SNVSDAVAQSTR y9 M+28	35
633.8	934.5	7	TPI	SNVSDAVAQSTR y9 M+32	35
761.9	1221.6	14	TPI	TATPQQAQEVHEK y10 M+28	43
765.9	1225.6	14	TPI	TATPQQAQEVHEK y10 M+32	43
761.9	1393.7	25	TPI	TATPQQAQEVHEK y12 M+28	39
765.9	1397.7	25	TPI	TATPQQAQEVHEK y12 M+32	39
761.9	868.5	12	TPI	TATPQQAQEVHEK y7 M+28	45
765.9	872.5	12	TPI	TATPQQAQEVHEK y7 M+32	45
453.8	533.3	5	TPI	VVFEQTK y4 M+28	33
457.8	537.3	5	TPI	VVFEQTK y4 M+32	33
453.8	680.4	5	TPI	VVFEQTK y5 M+28	27
457.8	684.4	5	TPI	VVFEQTK y5 M+32	27
453.8	779.4	5	TPI	VVFEQTK y6 M+28	27
457.8	783.4	5	TPI	VVFEQTK y6 M+32	27
680.5	1072.6	5	YWHAZ	FLIPNASQAESK y10 M+28	34
680.5	1185.6	5	YWHAZ	FLIPNASQAESK y11 M+28	34
684.5	1076.6	5	YWHAZ	FLIPNASQAESK y10 M+32	34
684.5	1189.6	5	YWHAZ	FLIPNASQAESK y11 M+32	34
680.5	959.5	5	YWHAZ	FLIPNASQAESK y9 M+28	34
684.5	963.5	5	YWHAZ	FLIPNASQAESK y9 M+32	34

Appendix B. *Transitions for hnRNP Peptides (M+28 and M+32) Uploadable to Analyst (v1.4+) Software.*

Q1	Q3	Dwell (msec)	Identifier (hnRNP Peptide Fragment Label)	CE
Method 1				
660.9	746.4	32	M AFITNIPFDVK y6 M+28	33
664.9	750.4	32	M AFITNIPFDVK y6 M+32	33
660.9	860.5	38	M AFITNIPFDVK y7 M+28	33
664.9	864.5	38	M AFITNIPFDVK y7 M+32	33
660.9	961.5	32	M AFITNIPFDVK y8 M+28	33
664.9	965.5	32	M AFITNIPFDVK y8 M+32	33
660.9	1074.6	10	M AFITNIPFDVK y9 M+28	33
664.9	1078.6	10	M AFITNIPFDVK y9 M+32	33
702.8	1105.5	56	A1 ATVEEVDAAMNAR y10 M+28	35
704.8	1105.5	56	A1 ATVEEVDAAMNAR y10 M+32	35
702.8	748.3	100	A1 ATVEEVDAAMNAR y7 M+28	35
704.8	748.3	100	A1 ATVEEVDAAMNAR y7 M+32	35
702.8	847.4	10	A1 ATVEEVDAAMNAR y8 M+28	35
704.8	847.4	10	A1 ATVEEVDAAMNAR y8 M+32	35
702.8	976.5	10	A1 ATVEEVDAAMNAR y9 M+28	35
704.8	976.5	10	A1 ATVEEVDAAMNAR y9 M+32	35
553.7	583.2	11	A2 DYFEEYGK b4 M+28	28
557.7	587.2	11	A2 DYFEEYGK b4 M+32	28
553.7	653.3	10	A2 DYFEEYGK y5 M+28	28
557.7	657.3	10	A2 DYFEEYGK y5 M+32	28
553.7	800.4	10	A2 DYFEEYGK y6 M+28	28
557.7	804.4	10	A2 DYFEEYGK y6 M+32	28
553.7	963.4	10	A2 DYFEEYGK y7 M+28	28
557.7	967.4	10	A2 DYFEEYGK y7 M+32	28
553.2	875.4	10	A1 DYFEQYGK b6 M+28	28
557.2	879.4	10	A1 DYFEQYGK b6 M+32	28
553.2	652.3	10	A1 DYFEQYGK y5 M+28	28
557.2	656.3	10	A1 DYFEQYGK y5 M+32	28
553.2	799.4	10	A1 DYFEQYGK y6 M+28	28
557.2	803.4	10	A1 DYFEQYGK y6 M+32	28
553.2	962.4	10	A1 DYFEQYGK y7 M+28	28
557.2	966.4	10	A1 DYFEQYGK y7 M+32	28
561.8	855.5	100	M FEPYANPTK y8 M+28	28
565.8	859.5	100	M FEPYANPTK y8 M+32	28
561.8	558.3	100	M FEPYANPTK y5 M+28	28
565.8	562.3	100	M FEPYANPTK y5 M+32	28
561.8	721.4	93	M FEPYANPTK y6 M+28	28
565.8	725.4	93	M FEPYANPTK y6 M+32	28
561.8	818.4	100	M FEPYANPTK y7 M+28	28
565.8	822.4	100	M FEPYANPTK y7 M+32	28
546.3	603.3	100	M FESPEVAER y5 M+28	28
548.3	603.3	100	M FESPEVAER y5 M+32	28
546.3	700.4	10	M FESPEVAER y6 M+28	28
548.3	700.4	10	M FESPEVAER y6 M+32	28
546.3	787.4	10	M FESPEVAER y7 M+28	28

548.3	787.4	10	M FESPEVAER y7 M+32	28
546.3	916.4	10	M FESPEVAER y8 M+28	28
548.3	916.4	10	M FESPEVAER y8 M+32	28
424.2	317.2	10	U FIEIAAR y3 M+28	23
426.2	317.2	10	U FIEIAAR y3 M+32	23
424.2	430.3	10	U FIEIAAR y4 M+28	23
426.2	430.3	10	U FIEIAAR y4 M+32	23
424.2	559.3	10	U FIEIAAR y5 M+28	23
426.2	559.3	10	U FIEIAAR y5 M+32	23
424.2	672.4	10	U FIEIAAR y6 M+28	23
426.2	672.4	10	U FIEIAAR y6 M+32	23
698.9	1142.6	10	K IILDLISESPIK y10 M+28	35
702.9	1146.6	10	K IILDLISESPIK y10 M+32	35
698.9	801.4	58	K IILDLISESPIK y7 M+28	35
702.9	805.4	58	K IILDLISESPIK y7 M+32	35
698.9	914.5	10	K IILDLISESPIK y8 M+28	35
702.9	918.5	10	K IILDLISESPIK y8 M+32	35
698.9	1029.6	100	K IILDLISESPIK y9 M+28	35
702.9	1033.6	100	K IILDLISESPIK y9 M+32	35
860	1090.6	10	A0 LFIGGLNVQTSESGLR y10 M+28	42
862	1090.6	10	A0 LFIGGLNVQTSESGLR y10 M+32	42
860	1317.7	10	A0 LFIGGLNVQTSESGLR y13 M+28	42
862	1317.7	10	A0 LFIGGLNVQTSESGLR y13 M+32	42
860	1430.8	100	A0 LFIGGLNVQTSESGLR y14 M+28	42
862	1430.8	100	A0 LFIGGLNVQTSESGLR y14 M+32	42
860	877.4	61	A0 LFIGGLNVQTSESGLR y8 M+28	42
862	877.4	61	A0 LFIGGLNVQTSESGLR y8 M+32	42
552.8	662.4	10	U NGQDLGVAFK y6 M+28	28
556.8	666.4	10	U NGQDLGVAFK y6 M+32	28
552.8	777.4	10	U NGQDLGVAFK y7 M+28	28
556.8	781.4	10	U NGQDLGVAFK y7 M+32	28
552.8	905.5	27	U NGQDLGVAFK y8 M+28	28
556.8	909.5	27	U NGQDLGVAFK y8 M+32	28
552.8	962.5	10	U NGQDLGVAFK y9 M+28	28
556.8	966.5	10	U NGQDLGVAFK y9 M+32	28
612.3	1049.5	10	M NLPFDFTWK b8 M+28	31
616.3	1053.5	10	M NLPFDFTWK b8 M+32	31
612.3	724.3	45	M NLPFDFTWK y5 M+28	31
616.3	728.3	45	M NLPFDFTWK y5 M+32	31
612.3	871.4	19	M NLPFDFTWK y6 M+28	31
616.3	875.4	19	M NLPFDFTWK y6 M+32	31
612.3	968.5	10	M NLPFDFTWK y7 M+28	31
616.3	972.5	10	M NLPFDFTWK y7 M+32	31
572.2	546.3	20	A2 NYYEQWGK y4 M+28	29
576.2	550.3	20	A2 NYYEQWGK y4 M+32	29
572.2	675.3	11	A2 NYYEQWGK y5 M+28	29
576.2	679.3	11	A2 NYYEQWGK y5 M+32	29
572.2	838.4	10	A2 NYYEQWGK y6 M+28	29
576.2	842.4	10	A2 NYYEQWGK y6 M+32	29
572.2	1001.4	10	A2 NYYEQWGK y7 M+28	29
576.2	1005.4	10	A2 NYYEQWGK y7 M+32	29
883.4	1118.5	41	F QSGEAFVELGSEDDVK y10 M+28	43
887.4	1122.5	41	F QSGEAFVELGSEDDVK y10 M+32	43
883.4	1265.6	10	F QSGEAFVELGSEDDVK y11 M+28	43

887.4	1269.6	10	F QSGEAFVELGSEDDVK y11 M+32	43
883.4	890.4	10	F QSGEAFVELGSEDDVK y8 M+28	43
887.4	894.4	10	F QSGEAFVELGSEDDVK y8 M+32	43
883.4	1019.5	10	F QSGEAFVELGSEDDVK y9 M+28	43
887.4	1023.5	10	F QSGEAFVELGSEDDVK y9 M+32	43
872.5	938.5	33	U SSGPTSLFAVTVAPPGAR y10 M+28	43
874.5	938.5	33	U SSGPTSLFAVTVAPPGAR y10 M+32	43
872.5	1085.6	10	U SSGPTSLFAVTVAPPGAR y11 M+28	43
874.5	1085.6	10	U SSGPTSLFAVTVAPPGAR y11 M+32	43
872.5	1198.7	61	U SSGPTSLFAVTVAPPGAR y12 M+28	43
874.5	1198.7	61	U SSGPTSLFAVTVAPPGAR y12 M+32	43
872.5	867.5	100	U SSGPTSLFAVTVAPPGAR y9 M+28	43
874.5	867.5	100	U SSGPTSLFAVTVAPPGAR y9 M+32	43
716.8	1075.5	10	A1 SSGPYGGGGQYFAK y10 M+28	35
720.8	1079.5	10	A1 SSGPYGGGGQYFAK y10 M+32	35
716.8	1172.5	16	A1 SSGPYGGGGQYFAK y11 M+28	35
720.8	1176.5	16	A1 SSGPYGGGGQYFAK y11 M+32	35
716.8	855.4	10	A1 SSGPYGGGGQYFAK y8 M+28	35
720.8	859.4	10	A1 SSGPYGGGGQYFAK y8 M+32	35
716.8	912.4	19	A1 SSGPYGGGGQYFAK y9 M+28	35
720.8	916.4	19	A1 SSGPYGGGGQYFAK y9 M+32	35
600.9	603.3	58	R STAYEDYYYHPPPR y5 M+28	33
602.9	603.3	58	R STAYEDYYYHPPPR y5 M+32	33
600.9	766.4	10	R STAYEDYYYHPPPR y6 M+28	33
602.9	766.4	10	R STAYEDYYYHPPPR y6 M+32	33
600.9	929.5	10	R STAYEDYYYHPPPR y7 M+28	33
602.9	929.5	10	R STAYEDYYYHPPPR y7 M+32	33
600.9	1092.5	10	R STAYEDYYYHPPPR y8 M+28	33
602.9	1092.5	10	R STAYEDYYYHPPPR y8 M+32	33

Method 2

465.3	545.4	10	K DLAGSIIGK y5 M+28	35
469.3	549.4	10	K DLAGSIIGK y5 M+32	35
465.3	602.4	36	K DLAGSIIGK y6 M+28	29
469.3	606.4	36	K DLAGSIIGK y6 M+32	29
465.3	673.4	38	K DLAGSIIGK y7 M+28	25
469.3	677.4	38	K DLAGSIIGK y7 M+32	25
465.3	786.5	50	K DLAGSIIGK y8 M+28	25
469.3	790.5	50	K DLAGSIIGK y8 M+32	25
620.3	854.4	10	A0 EDIYSGGGGGGSR y10 M+28	38
622.3	854.4	10	A0 EDIYSGGGGGGSR y10 M+32	38
620.3	967.5	10	A0 EDIYSGGGGGGSR y11 M+28	38
622.3	967.5	10	A0 EDIYSGGGGGGSR y11 M+32	38
620.3	1082.5	80	A0 EDIYSGGGGGGSR y12 M+28	36
622.3	1082.5	80	A0 EDIYSGGGGGGSR y12 M+32	36
620.3	691.3	10	A0 EDIYSGGGGGGSR y9 M+28	40
622.3	691.3	10	A0 EDIYSGGGGGGSR y9 M+32	40
500.8	585.3	100	H3 EIAENALGK b5 M+28	25
504.8	589.3	100	H3 EIAENALGK b5 M+32	25
500.8	659.4	100	H3 EIAENALGK y6 M+28	33
504.8	663.4	100	H3 EIAENALGK y6 M+32	33
500.8	730.4	39	H3 EIAENALGK y7 M+28	29
504.8	734.4	39	H3 EIAENALGK y7 M+32	29

500.8	843.5	39	H3 EIAENALGK y8 M+28	29
504.8	847.5	39	H3 EIAENALGK y8 M+32	29
764.4	804.4	100	A/B EVYQQQQYGSGGR b6 M+28	41
766.4	804.4	100	A/B EVYQQQQYGSGGR b6 M+32	41
764.4	1370.6	10	A/B EVYQQQQYGSGGR y12 M+28	41
766.4	1370.6	10	A/B EVYQQQQYGSGGR y12 M+32	41
764.4	1108.9	10	A/B EVYQQQQYGSGGR y10 M+28	43
766.4	1108.9	10	A/B EVYQQQQYGSGGR y10 M+32	43
764.4	980.3	10	A/B EVYQQQQYGSGGR y9 M+28	41
766.4	980.3	10	A/B EVYQQQQYGSGGR y9 M+32	41
612.3	664.3	100	D FGEVVDCTIK y5 M+28	42
616.3	668.3	100	D FGEVVDCTIK y5 M+32	42
612.3	763.4	100	D FGEVVDCTIK y6 M+28	38
616.3	767.4	100	D FGEVVDCTIK y6 M+32	38
612.3	991.5	10	D FGEVVDCTIK y8 M+28	28
616.3	995.5	10	D FGEVVDCTIK y8 M+32	28
612.3	1048.5	25	D FGEVVDCTIK y9 M+28	32
616.3	1052.5	25	D FGEVVDCTIK y9 M+32	32
483.3	550.3	37	M GCAVVEFK y4 M+28	32
487.3	554.3	37	M GCAVVEFK y4 M+32	32
483.3	649.4	86	M GCAVVEFK y5 M+28	30
487.3	653.4	86	M GCAVVEFK y5 M+32	30
483.3	720.4	16	M GCAVVEFK y6 M+28	28
487.3	724.4	16	M GCAVVEFK y6 M+32	28
483.3	880.5	13	M GCAVVEFK y7 M+28	28
487.3	884.5	13	M GCAVVEFK y7 M+32	28
679.3	1272.6	10	C GFAFVQYVNER y10 M+28	29
681.3	1272.6	10	C GFAFVQYVNER y10 M+32	29
679.3	808.4	100	C GFAFVQYVNER y6 M+28	37
681.3	808.4	100	C GFAFVQYVNER y6 M+32	37
679.3	907.5	10	C GFAFVQYVNER y7 M+28	37
681.3	907.5	10	C GFAFVQYVNER y7 M+32	37
679.3	1125.6	10	C GFAFVQYVNER y9 M+28	35
681.3	1125.6	10	C GFAFVQYVNER y9 M+32	35
500.8	719.3	44	R&Q GFCFLEYEDHK y5 M+28	23
504.8	723.3	44	R&Q GFCFLEYEDHK y5 M+32	23
500.8	848.4	10	R&Q GFCFLEYEDHK y6 M+28	27
504.8	852.4	10	R&Q GFCFLEYEDHK y6 M+32	27
500.8	540.2	100	R&Q GFCFLEYEDHK b4 M+28	27
504.8	544.2	100	R&Q GFCFLEYEDHK b4 M+32	27
500.8	556.3	100	R&Q GFCFLEYEDHK y4 M+28	27
504.8	560.3	100	R&Q GFCFLEYEDHK y4 M+32	27
703.3	1035.5	10	A2 GGGGNFGPGPGSNFR y10 M+28	42
705.3	1035.5	10	A2 GGGGNFGPGPGSNFR y10 M+32	42
703.3	1206.6	14	A2 GGGGNFGPGPGSNFR y12 M+28	42
705.3	1206.6	14	A2 GGGGNFGPGPGSNFR y12 M+32	42
703.3	1263.6	32	A2 GGGGNFGPGPGSNFR y13 M+28	42
705.3	1263.6	32	A2 GGGGNFGPGPGSNFR y13 M+32	42
703.3	888.4	10	A2 GGGGNFGPGPGSNFR y9 M+28	42
705.3	888.4	10	A2 GGGGNFGPGPGSNFR y9 M+32	42
521.2	780.3	10	A2 GGNFGFGDSR b8 M+28	26
523.2	780.3	10	A2 GGNFGFGDSR b8 M+32	26
521.2	785.4	11	A2 GGNFGFGDSR y7 M+28	30
523.2	785.4	11	A2 GGNFGFGDSR y7 M+32	30

521.2	899.4	53	A2 GGNFGFGDSR y8 M+28	30
523.2	899.4	53	A2 GGNFGFGDSR y8 M+32	30
521.2	956.4	10	A2 GGNFGFGDSR y9 M+28	34
523.2	956.4	10	A2 GGNFGFGDSR y9 M+32	34
766.9	1334.6	10	H1 GLPWSCSADEVQR y11 M+28	39
768.9	1334.6	10	H1 GLPWSCSADEVQR y11 M+32	39
766.9	1447.7	11	H1 GLPWSCSADEVQR y12 M+28	39
768.9	1447.7	11	H1 GLPWSCSADEVQR y12 M+32	39
766.9	804.4	100	H1 GLPWSCSADEVQR y7 M+28	45
768.9	804.4	100	H1 GLPWSCSADEVQR y7 M+32	45
766.9	1051.5	10	H1 GLPWSCSADEVQR y9 M+28	45
768.9	1051.5	10	H1 GLPWSCSADEVQR y9 M+32	45
563.7	577.3	20	K GSDFDCELR y4 M+28	40
565.7	577.3	20	K GSDFDCELR y4 M+32	40
563.7	692.3	10	K GSDFDCELR y5 M+28	32
565.7	692.3	10	K GSDFDCELR y5 M+32	32
563.7	839.4	10	K GSDFDCELR y6 M+28	36
565.7	839.4	10	K GSDFDCELR y6 M+32	36
563.7	1041.4	10	K GSDFDCELR y8 M+28	36
565.7	1041.4	10	K GSDFDCELR y8 M+32	36
674.3	688.3	93	U GYFEYIEENK b5 M+28	35
678.3	692.3	93	U GYFEYIEENK b5 M+32	35
674.3	823.4	10	U GYFEYIEENK y6 M+28	35
678.3	827.4	10	U GYFEYIEENK y6 M+32	35
674.3	1099.5	13	U GYFEYIEENK y8 M+28	35
678.3	1103.5	13	U GYFEYIEENK y8 M+32	35
674.3	1262.6	10	U GYFEYIEENK y9 M+28	39
678.3	1266.6	10	U GYFEYIEENK y9 M+32	39
486.3	553.4	59	C VPPPPPIAR y5 M+28	26
488.3	553.4	59	C VPPPPPIAR y5 M+32	26
486.3	650.4	10	C VPPPPPIAR y6 M+28	26
488.3	650.4	10	C VPPPPPIAR y6 M+32	26
486.3	747.5	10	C VPPPPPIAR y7 M+28	26
488.3	747.5	10	C VPPPPPIAR y7 M+32	26
486.3	844.5	10	C VPPPPPIAR y8 M+28	26
488.3	844.5	10	C VPPPPPIAR y8 M+32	26
434.7	322.2	10	H3 YIEIFR y2 M+28	24
436.7	322.2	10	H3 YIEIFR y2 M+32	24
434.7	435.3	10	H3 YIEIFR y3 M+28	24
436.7	435.3	10	H3 YIEIFR y3 M+32	24
434.7	564.3	100	H3 YIEIFR y4 M+28	24
436.7	564.3	100	H3 YIEIFR y4 M+32	24
434.7	677.4	100	H3 YIEIFR y5 M+28	24
436.7	677.4	100	H3 YIEIFR y5 M+32	24

Method 3

644.3	1146.5	10	K IDEPLEGSEDR y10 M+28	43
646.3	1146.5	10	K IDEPLEGSEDR y10 M+32	43
644.3	805.4	100	K IDEPLEGSEDR y7 M+28	43
646.3	805.4	100	K IDEPLEGSEDR y7 M+32	43
644.3	902.4	53	K IDEPLEGSEDR y8 M+28	43
646.3	902.4	53	K IDEPLEGSEDR y8 M+32	43
644.3	1031.5	10	K IDEPLEGSEDR y9 M+28	37

646.3	1031.5	10	K IDEPLEGSEDR y9 M+32	37
608.8	746.8	27	A2 IDTIEIITDR y6 M+28	34
610.8	746.8	27	A2 IDTIEIITDR y6 M+32	34
608.8	859.5	81	A2 IDTIEIITDR y7 M+28	36
610.8	859.5	81	A2 IDTIEIITDR y7 M+32	36
608.8	960.5	60	A2 IDTIEIITDR y8 M+28	36
610.8	960.5	60	A2 IDTIEIITDR y8 M+32	36
608.8	1075.6	49	A2 IDTIEIITDR y9 M+28	32
610.8	1075.6	49	A2 IDTIEIITDR y9 M+32	32
780.4	1172.6	25	A/B IFVGGLNPEATEEK y11 M+28	45
784.4	1176.6	25	A/B IFVGGLNPEATEEK y11 M+32	45
780.4	1271.7	10	A/B IFVGGLNPEATEEK y12 M+28	43
784.4	1275.7	10	A/B IFVGGLNPEATEEK y12 M+32	43
780.4	1418.7	10	A/B IFVGGLNPEATEEK y13 M+28	39
784.4	1422.7	10	A/B IFVGGLNPEATEEK y13 M+32	39
780.4	945.5	37	A/B IFVGGLNPEATEEK y8 M+28	39
784.4	949.5	37	A/B IFVGGLNPEATEEK y8 M+32	39
772.9	1157.6	10	D IFVGGLSPDTPEEK y11 M+28	39
776.9	1161.6	10	D IFVGGLSPDTPEEK y11 M+32	39
772.9	1403.7	10	D IFVGGLSPDTPEEK y13 M+28	39
776.9	1407.7	10	D IFVGGLSPDTPEEK y13 M+32	39
772.9	843.4	10	D IFVGGLSPDTPEEK y7 M+28	43
776.9	847.4	10	D IFVGGLSPDTPEEK y7 M+32	43
772.9	930.4	10	D IFVGGLSPDTPEEK y8 M+28	37
776.9	934.4	10	D IFVGGLSPDTPEEK y8 M+32	37
838.4	1045.5	10	U NFILDQTNVSAAAQR y10 M+28	42
840.4	1045.5	10	U NFILDQTNVSAAAQR y10 M+32	42
838.4	1273.7	10	U NFILDQTNVSAAAQR y12 M+28	42
840.4	1273.7	10	U NFILDQTNVSAAAQR y12 M+32	42
838.4	1386.7	10	U NFILDQTNVSAAAQR y13 M+28	40
840.4	1386.7	10	U NFILDQTNVSAAAQR y13 M+32	40
838.4	1533.8	100	U NFILDQTNVSAAAQR y14 M+28	42
840.4	1533.8	100	U NFILDQTNVSAAAQR y14 M+32	42
611.9	757.5	10	K NLPLPPPPPPR b7 M+28	34
613.9	757.5	10	K NLPLPPPPPPR b7 M+32	34
611.9	1080.7	100	K NLPLPPPPPPR y10 M+28	36
613.9	1080.7	100	K NLPLPPPPPPR y10 M+32	36
611.9	870.5	100	K NLPLPPPPPPR y8 M+28	36
613.9	870.5	100	K NLPLPPPPPPR y8 M+32	36
611.9	967.6	21	K NLPLPPPPPPR y9 M+28	36
613.9	967.6	21	K NLPLPPPPPPR y9 M+32	36
861.8	1118.5	10	A1 NQGGYGGSSSSSSYGSGR y12 M+28	49
863.8	1118.5	10	A1 NQGGYGGSSSSSSYGSGR y12 M+32	49
861.8	1175.5	10	A1 NQGGYGGSSSSSSYGSGR y13 M+28	53
863.8	1175.5	10	A1 NQGGYGGSSSSSSYGSGR y13 M+32	53
861.8	1452.6	10	A1 NQGGYGGSSSSSSYGSGR y16 M+28	47
863.8	1452.6	10	A1 NQGGYGGSSSSSSYGSGR y16 M+32	47
861.8	887.4	100	A1 NQGGYGGSSSSSSYGSGR y9 M+28	53
863.8	887.4	100	A1 NQGGYGGSSSSSSYGSGR y9 M+32	53
526.3	643.3	17	C SDVEAIFSK b6 M+28	32
530.3	647.3	17	C SDVEAIFSK b6 M+32	32
526.3	722.8	10	C SDVEAIFSK y6 M+28	34
530.3	726.8	10	C SDVEAIFSK y6 M+32	34
526.3	821.5	84	C SDVEAIFSK y7 M+28	32

530.3	825.5	84	C SDVEAIFSK y7 M+32	32
526.3	936.5	39	C SDVEAIFSK y8 M+28	32
530.3	940.5	39	C SDVEAIFSK y8 M+32	32
970	1218.5	10	A3 SSGSPYGGGYGSGGGSGGYGSR y14 M+28	48
972	1218.5	10	A3 SSGSPYGGGYGSGGGSGGYGSR y14 M+32	48
970	1275.5	37	A3 SSGSPYGGGYGSGGGSGGYGSR y15 M+28	54
972	1275.5	37	A3 SSGSPYGGGYGSGGGSGGYGSR y15 M+32	54
970	1332.6	10	A3 SSGSPYGGGYGSGGGSGGYGSR y16 M+28	54
972	1332.6	10	A3 SSGSPYGGGYGSGGGSGGYGSR y16 M+32	54
970	1592.7	10	A3 SSGSPYGGGYGSGGGSGGYGSR y18 M+28	54
972	1592.7	10	A3 SSGSPYGGGYGSGGGSGGYGSR y18 M+32	54
639.8	1017.5	100	L SSSGLLEWESK b9 M+28	31
643.8	1021.5	100	L SSSGLLEWESK b9 M+32	31
639.8	1163.6	28	L SSSGLLEWESK y10 M+28	35
643.8	1167.6	28	L SSSGLLEWESK y10 M+32	35
639.8	819.4	10	L SSSGLLEWESK y6 M+28	41
643.8	823.4	10	L SSSGLLEWESK y6 M+32	41
639.8	932.5	10	L SSSGLLEWESK y7 M+28	33
643.8	936.5	10	L SSSGLLEWESK y7 M+32	33
664.3	1212.6	20	H3 STGEAFVQFASK y11 M+28	40
668.3	1216.6	20	H3 STGEAFVQFASK y11 M+32	40
664.3	707.4	10	H3 STGEAFVQFASK y6 M+28	42
668.3	711.4	10	H3 STGEAFVQFASK y6 M+32	42
664.3	854.5	24	H3 STGEAFVQFASK y7 M+28	34
668.3	858.5	24	H3 STGEAFVQFASK y7 M+32	34
664.3	925.5	100	H3 STGEAFVQFASK y8 M+28	34
668.3	929.5	100	H3 STGEAFVQFASK y8 M+32	34
670.3	679.3	10	R&Q TGYTLDVTTGQR b6 M+28	40
672.3	679.3	10	R&Q TGYTLDVTTGQR b6 M+32	40
670.3	1210.6	10	R&Q TGYTLDVTTGQR y11 M+28	40
672.3	1210.6	10	R&Q TGYTLDVTTGQR y11 M+32	40
670.3	776.4	10	R&Q TGYTLDVTTGQR y7 M+28	44
672.3	776.4	10	R&Q TGYTLDVTTGQR y7 M+32	44
670.3	889.5	10	R&Q TGYTLDVTTGQR y8 M+28	38
672.3	889.5	10	R&Q TGYTLDVTTGQR y8 M+32	38
543.3	613.4	100	A2 TLETVPLER y5 M+28	35
545.3	613.4	100	A2 TLETVPLER y5 M+32	35
543.3	714.4	10	A2 TLETVPLER y6 M+28	35
545.3	714.4	10	A2 TLETVPLER y6 M+32	35
543.3	843.5	40	A2 TLETVPLER y7 M+28	29
545.3	843.5	40	A2 TLETVPLER y7 M+32	29
543.3	956.5	38	A2 TLETVPLER y8 M+28	35
545.3	956.5	38	A2 TLETVPLER y8 M+32	35
563.3	570.4	10	R TLIEAGLPQK y5 M+28	34
567.3	574.4	10	R TLIEAGLPQK y5 M+32	34
563.3	770.4	10	R TLIEAGLPQK y7 M+28	32
567.3	774.4	10	R TLIEAGLPQK y7 M+32	32
563.3	883.5	10	R TLIEAGLPQK y8 M+28	30
567.3	887.5	10	R TLIEAGLPQK y8 M+32	30
563.3	996.6	94	R TLIEAGLPQK y9 M+28	30
567.3	1000.6	94	R TLIEAGLPQK y9 M+32	30
904.9	1030.5	10	K TDYNASVSVPDSSGPER y10 M+28	44
906.9	1030.5	10	K TDYNASVSVPDSSGPER y10 M+32	44
904.9	1216.6	10	K TDYNASVSVPDSSGPER y12 M+28	44

906.9	1216.6	10	K TDYNASVSVPDSSGPER y12 M+32	44
904.9	632.3	10	K TDYNASVSVPDSSGPER y6 M+28	44
906.9	632.3	10	K TDYNASVSVPDSSGPER y6 M+32	44
904.9	844.4	10	K TDYNASVSVPDSSGPER y8 M+28	44
906.9	844.4	10	K TDYNASVSVPDSSGPER y8 M+32	44

Appendix C. *Transitions for Pyruvate Kinase Splice Variant Peptides (M+28 and M+36) Uploadable to Analyst (v1.4+) Software.*

Q1	Q3	Dwell (msec)	Identifier (Protein Peptide Fragment Label)	CE
645.4	1095.6	50	PKM2 CCSGAIIVLTK y10 M+36	33
645.4	791.6	50	PKM2 CCSGAIIVLTK y7 M+36	33
645.4	848.6	50	PKM2 CCSGAIIVLTK y8 M+36	33
645.4	935.6	50	PKM2 CCSGAIIVLTK y9 M+36	33
548.3	661.3	50	PKM1 EAEAAMFHR y5 M+36	29
548.3	732.4	50	PKM1 EAEAAMFHR y6 M+36	29
548.3	861.4	50	PKM1 EAEAAMFHR y7 M+36	29
548.3	932.4	50	PKM1 EAEAAMFHR y8 M+36	29
527.3	587.4	50	PKM1M2 GDYPLEAVR y5 M+36	28
527.3	684.4	50	PKM1M2 GDYPLEAVR y6 M+36	28
527.3	847.5	50	PKM1M2 GDYPLEAVR y7 M+36	28
527.3	962.5	50	PKM1M2 GDYPLEAVR y8 M+36	28
556.3	669.3	50	PKM1 OxyEAE y5 M+36	30
556.3	740.4	50	PKM1 OxyEAE y6 M+36	30
556.3	869.4	50	PKM1 OxyEAE y7 M+36	30
556.3	940.4	50	PKM1 OxyEAE y8 M+36	30
553.3	669.3	50	PKM1 OxyEAE y5 M+36	30
553.3	740.4	50	PKM1 OxyEAE y6 M+36	30
553.3	869.4	50	PKM1 OxyEAE y7 M+36	30
553.3	940.4	50	PKM1 OxyEAE y8 M+36	30
639.4	785.6	50	PKM2 CCSGAIIVLTK y7 M+28	33
639.4	842.6	50	PKM2 CCSGAIIVLTK y8 M+28	33
639.4	929.6	50	PKM2 CCSGAIIVLTK y9 M+28	33
639.4	1089.6	50	PKM2 CCSGAIIVLTK y10 M+28	33
545.3	661.3	50	PKM1 EAEAAMFHR y5 M+28	29
545.3	732.4	50	PKM1 EAEAAMFHR y6 M+28	29
545.3	861.4	50	PKM1 EAEAAMFHR y7 M+28	29
545.3	932.4	50	PKM1 EAEAAMFHR y8 M+28	29
524.3	587.4	50	PKM1M2 GDYPLEAVR y5 M+28	30
524.3	684.4	50	PKM1M2 GDYPLEAVR y6 M+28	30
524.3	847.5	50	PKM1M2 GDYPLEAVR y7 M+28	30
524.3	962.5	50	PKM1M2 GDYPLEAVR y8 M+28	30
502.7	701.3	50	ACTAB AGFAGDDAPR y7 M+28	28
502.7	848.4	50	ACTAB AGFAGDDAPR y8 M+28	28
502.7	905.4	50	ACTAB AGFAGDDAPR y9 M+28	30
609.3	1060.6	50	ACTAB EITALAPSTMK y10 M+28	32
609.3	846.5	50	ACTAB EITALAPSTMK y8 M+28	32
609.3	947.5	50	ACTAB EITALAPSTMK y9 M+28	32
580.8	825.4	50	ACTAB GYSFTTTAER y7 M+28	31
580.8	912.4	50	ACTAB GYSFTTTAER y8 M+28	29
580.8	1075.5	50	ACTAB GYSFTTTAER y9 M+28	33
614.3	1062.5	50	ACTAB HQGVMVGMGQK y10 M+28	36
614.3	877.5	50	ACTAB HQGVMVGMGQK y8 M+28	38
614.3	934.5	50	ACTAB HQGVMVGMGQK y9 M+28	34
772.9	1259.6	50	ACTAB QEYDESGPSIVHR y11 M+28	49
772.9	1388.6	50	ACTAB QEYDESGPSIVHR y12 M+28	49
772.9	852.5	50	ACTAB QEYDESGPSIVHR y8 M+28	49
653.8	672.3	50	PPIA EGMNIVEAMER b6 M+28	34

653.8	1149.5	50	PPIA EGMNIVEAMER y10 M+28	34
653.8	961.5	50	PPIA EGMNIVEAMER y8 M+28	34
605.8	663.3	50	PPIA FEDENFILK b5 M+28	32
605.8	906.5	50	PPIA FEDENFILK y7 M+28	32
605.8	1035.5	50	PPIA FEDENFILK y8 M+28	32
813.9	1372.6	50	PPIA IIPGFMCQGGDFTR y12 M+28	41
813.9	1485.7	50	PPIA IIPGFMCQGGDFTR y13 M+28	41
813.9	940.4	50	PPIA IIPGFMCQGGDFTR y8 M+28	41

.

Appendix D. Copyright Agreements

Chapter 1 Copyright Agreement

Dear Dr. Murphy:

Thank you for your interest in our copyrighted material, and for requesting permission for its use.

Permission is granted for the following subject to the conditions outlined below:

Murphy, J. P.; Cote, P.D; Pinto, D. M., Monitoring the Switch: The Warburg Effect and Targeted Proteomic Analysis of Cancer Metabolism, Current Proteomics

To be used in the following manner:

1. Bentham Science Publishers grants you the right to reproduce the material indicated above on a one-time, non-exclusive basis, solely for the purpose described. Permission must be requested separately for any future or additional use.

2. For an article, the copyright notice must be printed on the first page of article or book chapter. For figures, photographs, covers, or tables, the notice may appear with the material, in a footnote, or in the reference list.

Thank you for your patience while your request was being processed. If you wish to contact us further, please use the address below.

Sincerely,

AMBREEN IRSHAD

Permissions & Rights **Manager**
Bentham Science Publishers Ltd
Email: permission@bentham.org
URL: www.bentham.org

Chapter 2 Copyright Agreement

Dear Dr. Murphy,

We hereby grant permission for the requested use expected that due credit is given to the original source.

Please note that we only grant rights for a printed version, but not the rights for an electronic/ online/ web/ microfiche publication, but you are free to create a link to the article in question which is posted on our website (http://www3.interscience.wiley.com)

- ***You may use the version of the contribution as originally submitted for publication for an electronic presentation of the thesis. The contribution may not be updated or replaced with the published version. The version posted must contain a legend as follows: This is the pre-peer reviewed version of the following article: FULL CITE.***

With kind regards

Bettina Loycke
****

Bettina Loycke
Senior Rights Manager
Wiley-VCH Verlag GmbH & Co. KGaA
Boschstr. 12
69469 Weinheim
Germany

Phone: +49 (0) 62 01- 606 - 280
Fax: +49 (0) 62 01 - 606 - 332
Email: rights@wiley-vch.de

Chapter 3 Copyright Agreement

November 17, 2010

Proteomics
WILEY-VCH Verlag GmbH & Co. KGaA
P. O. Box 10 11 61
D-69451 Weinheim
Germany

I am preparing my PhD thesis for submission to the Faculty of Graduate Studies at Dalhousie University, Halifax, Nova Scotia, Canada. I am seeking your permission to include a manuscript version of the following paper(s) as a chapter in the thesis:

Murphy, J. P.; Pinto, D. M., Temporal proteomic analysis of IGF-1R signalling in MCF-7 breast adenocarcinoma cells. *Proteomics* **2010,** *10* (9), 1847-1860

Canadian graduate theses are reproduced by the Library and Archives of Canada (formerly National
Library of Canada) through a non-exclusive, world-wide license to reproduce, loan, distribute, or sell theses. I am also seeking your permission for the material described above to be reproduced and distributed by the LAC(NLC). Further details about the LAC(NLC) thesis program are available on the LAC(NLC) website (www.nlc-bnc.ca).

Full publication details and a copy of this permission letter will be included in the thesis.

Yours sincerely,

J. Patrick Murphy

Permission is granted for:

a) the inclusion of the material described above in your thesis.

b) for the material described above to be included in the copy of your thesis that is sent to the Library and Archives of Canada (formerly National Library of Canada) for reproduction and distribution.

Name: _____
Title:_____

Signature: _____
Date:_____